CONTROLLING SIDESLIP ANGLE TO REDUCE THE RADAR EXPOSURE OF A TACTICAL, ROTARY WINGED UAV

THESIS

Jonathan D. Bulseco, Major, USA
AFIT/GAE/ENY/05-M26

DEPARTMENT OF THE AIR FORCE
AIR UNIVERSITY

AIR FORCE INSTITUTE OF TECHNOLOGY

Wright-Patterson Air Force Base, Ohio

The views expressed in this thesis are those of the author and do not reflect the official policy or position of the United States Army, United States Air Force, Department of Defense, or the United States Government.

AFIT/GAE/ENY/05-M26

CONTROLLING SIDESLIP ANGLE TO REDUCE THE RADAR EXPOSURE OF A TACTICAL, ROTARY WINGED UAV

THESIS

Presented to the Faculty

Department of Aeronautics & Astronautics

Graduate School of Engineering and Management

Air Force Institute of Technology

Air University

Air Education and Training Command

In Partial Fulfillment of the Requirements for the

Degree of Master of Science in Aeronautical Engineering

Jonathan D. Bulseco, BS

Major, USA

March 2005

AFIT/GAE/ENY/05-M26

CONTROLLING SIDESLIP ANGLE TO REDUCE THE RADAR EXPOSURE OF A TACTICAL, ROTARY WINGED UAV

Jonathan D. Bulseco, BS

Major, USA

Approved:

_____/signed/_____	9 Mar 2005
Richard G. Cobb (Chairman)	Date
_____/signed/_____	9 Mar 2005
Donald L. Kunz (Member)	Date
_____/signed/_____	9 Mar 2005
Paul A. Blue, Major, USAF (Member)	Date

Abstract

This work investigates another way of contributing to the radar minimization solution for air vehicles in a threat environment. While much research has been conducted on structural solutions to radar exposure minimization, not much work has been done in the area of using control to continuously assess and present the smallest radar cross section of an air vehicle to oncoming threat radar systems by changing the aircraft's orientation. This work looks at the application of sideslip/beta angle feedback control of an unmanned helicopter to minimize radar cross section exposure in a hostile radar environment. A new way of controlling aircraft trajectory is introduced that incorporates both path and orientation optimization feedback; the aircraft's heading is controlled to orient the vehicle in a way that reduces its radar cross section, while sideslip angle is used to control the aircraft's path. A representative hostile environment is created and results show that a substantial reduction in radar cross section exposure can be achieved with beta feedback control. A linear state space model is derived for the OH-6A helicopter with the JANRAD software program. Eigenstructure assignment is used to shape the response of the helicopter into desired response modes. A Matlab based flight control system is developed around the derived helicopter model with altitude, heading, and beta angle command signals that drive four conventional helicopter control inputs.

Acknowledgments

I would like to first acknowledge the inspiration from Heavenly Father, the absence of which would have caused me to produce just a fraction of this work. I must also acknowledge my sponsor, Dr. Bill Lewis at the U.S. Army Research, Development, and Engineering Command (RDECOM), with whom the discussions of exploiting the unique capabilities of rotary-winged flight for radar-signature reduction began. My advisor, Dr. Richard Cobb, allowed me the freedom to explore this topic in the way that I saw fit. He provided crucial feedback at critical points of this study, and served as a sounding board for thought throughout. Also, this topic could not have been explored without my committee members, Dr. Donald Kunz and Major Paul Blue. Both served as instructors to me in the areas of dynamics, rotary-wing aerodynamics, optimization, and control. Without their instruction in these areas, and input throughout the course of this study, this work would not have come to pass. Finally, I want to thank my family: my wife and my two kids. You keep me grounded with constant reminders of what matters most.

Table of Contents

Page

Page

Page

List of Figures

Figure Page

Figure Page

List of Tables

Table Page

List of Notations and Symbols

Symbol	*Definition*	*Unit*
*	Hermitian Transpose	-
a	Lift Curve Slope	rad^{-1}
a	Flat Plate Length	m
α	Angle of Attack	deg
α_{L0}	Zero Lift Angle of Attack	deg
A	State Space A Matrix	-
AC	Aerodynamic Center	-
AR_H	Horizontal Stabilizer Aspect Ratio	-
AR_{Vu}	Upper Vertical Fin Aspect Ratio	-
A_{Vu}	Upper Vertical Fin Area	ft^2
b	Span	ft
b_{Vu}	Span of the Upper Vertical Fin	in
B	State Space B Matrix	-
β	Sideslip Angle	deg
C	State Space C Matrix	-
C_D	Coefficient of Drag	-
C_L	Coefficient of Lift	-
C_{Lmax}	Maximum Coefficient of Lift	-
c	Chord	in
c_r	Root Chord	in
c_t	Tip Chord	in
c_{vlr}	Lower Vertical Fin Root Chord	in
c_{vlt}	Lower Vertical Fin Tip Chord	in
c_{vur}	Upper vertical fin root chord	in
c_{vut}	Upper vertical fin tip chord	in
CG	Center of Gravity	-
D	State Space D Matrix	-

Symbol	*Definition*	*Unit*
δ	Generic Input Vector	-
dB	Decibel	dB
F	Vector Function of the Non-Linear Aircraft Dynamics	-
G_t	Antenna Gain	-
$\Lambda_{c/2}$	Mid Chord Sweep Angle	deg
$\Lambda_{c/2H}$	Mid Chord Sweep Angle of the Horizontal Stabilizer	deg
$\Lambda_{c/2u}$	Mid Chord Sweep Angle of the Upper Vertical Fin	deg
h	Altitude	ft
I_{xx}	Roll Moment of Inertia	slug-ft^2
I_{yy}	Pitch Moment of Inertia	slug-ft^2
I_{zz}	Yaw Moment of Inertia	slug-ft^2
I_{xz}	Total XZ Moment of Inertia	slug-ft^2
JANRAD	Joint Army/Navy Rotorcraft Analysis and Design Software	-
K	Gain Matrix	-
Kh_LonCyc	Altitude Gain on the Longitudinal Cyclic Input	-
Kh_Col	Altitude Gain on the Collective Input	-
Kpsi_LatCyc	Heading/Psi Gain on the Lateral Cyclic Input	-
Kpsi_TR	Heading/Psi Gain on the Tail Rotor Input	-
Kbeta_LatCyc	Sideslip/Beta Gain on the Lateral Cyclic Input	-
Kbeta_TR	Sideslip/Beta Gain on the Tail Rotor Input	-
L	Length of the Mean Aerodynamic Chord	ft
L	External Moment in the x Direction	N-m
λ	Wavelength of the Radar Energy	m
λ	Eigenvalue	-
M	External Moment in the y Direction	N-m
M.A.C	Mean Aerodynamic Chord	-
μ	Air Viscosity	lb/ft/s
N	Square Matrix Consisting of the υ Column Vectors	-

Symbol	*Definition*	*Unit*
N	External Moment in the z Direction	N-m
NACA	National Advisory Committee for Aeronautics	-
υ	Column Vector	-
p	Roll Rate	rad/s
P_t	Transporting Power of the Antenna	watts
P_i	Square Weighting Matrix	-
φ	Roll Angle	deg
q	Pitch Rate	rad/s
r	Yaw Rate	rad/s
RCS	Radar Cross Section	dB or m^2
Re	Reynold's Number	-
ρ	Density of the Air at Sea Level	lb/ft^3
S_{min}	Minimum detectable signal	-
σ	Target radar cross section	dB
ψ	Yaw Angle	deg
R_{max}	Maximum detection range	m
t	Airfoil Thickness	in
θ	Pitch Angle	deg
θ_0	Main Rotor Collective Input	-
θ_{1c}	Lateral Cyclic Input	-
θ_{1s}	Longitudinal Cyclic Input	-
θ_{TR}	Tail Rotor Collective Input	-
u	Control Input Vector	-
u	Body Fixed Forward Velocity	ft/s
UAV	Unmanned Aerial Vehicle	-
UCAR	Uninhabited Combat Aerial Vehicle	-
v	Body Fixed Side Velocity	ft/s
v	Eigenvector	-

Symbol	*Definition*	*Unit*
v_i^d	Desired Eigenvector	-
V	Magnitude of the Aircraft Total Velocity Vector	ft/s
V_∞	Free stream Velocity	ft/s
w	Body Fixed Up/Down Velocity (Positive Down)	ft/s
w	Eigenvector	-
W	Square Matrix Consisting of the w Column Eigenvectors	-
x	State Vector	-
x	Body Fixed Axis Out the Nose of the Aircraft	-
X	External Force in the x Direction	N
y	Output Vector	-
y	Body Fixed Axis from the Aircraft CG Out the Right Wing	-
Y	External Force in the y Direction	N
z	Body Fixed Axis From Aircraft CG Out the Bottom	-
z_l	Location of the MAC of the Lower Vertical Fin in z Direction	in
z_u	Location of the MAC of the Upper Vertical Fin in z Direction	in
Z	External Force in the z Direction	N

CONTROLLING SIDESLIP ANGLE TO REDUCE THE RADAR EXPOSURE OF A TACTICAL, ROTARY WINGED UAV

I. Introduction

Overview

The value of unmanned aerial vehicles and uninhabited combat aerial vehicles to front-line military units has been realized. They are no longer additional nice-to-have assets for military units. They are and will be an integral part of the force structure, whose role in front-line tactical units will only grow. The recent "Final Report of the Defense Science Board Task Force on Unmanned Aerial Vehicles (UAVs) and Uninhabited Combat Aerial Vehicles (UCAVs)" (1) cited as its "single most important recommendation" the accelerating of UAVs into the force structure. This report and the "Unmanned Aerial Vehicles Roadmap" from the Office of the Secretary of Defense (2) guarantee that UAVs/UCAVs will continue to play important roles in fighting America's wars.

The unique benefits of rotorcraft flight (i.e. vertical take-off and landing, hover, and the ability to operate without a runway) make rotorcraft UAVs/UCAVs an important component of the Department of Defense (DOD) total UAV inventory. This is evidenced by the numerous rotorcraft UAV programs currently in use and in development. Among them are Boeing's A160 Hummingbird, Dragonfly and Unmanned Little Bird, Sikorsky's

Fire Scout, Bell and Lockheed Martin's Unmanned Combat Armed Rotorcraft (UCAR), and Bell's Eagle Eye.

Figure 1. Left: Sikorsky's Firescout (www.news.navy.mil). Right: Boeing's Unmanned Little Bird (www.boeingmedia.com).

The doctrine for how these platforms will be utilized, and in what configuration, is still being written, but, it is safe to assume that these unmanned aircraft will be called upon to perform critical missions in hostile environments. This work investigates another way to make these aircraft more survivable in the high threat environment: sideslip (or sideward) flight that orients the aircraft in a way that minimizes its radar cross section (RCS) to threat radar. Sustained sideward flight and continuously changing sideslip angles, acting within the directional control limits of the aircraft, could cause pilot disorientation in a piloted aircraft, but this would not be an issue in an unmanned aircraft. This flight control technique, working in conjunction with other low-observable technologies, can help to decrease the likelihood of these aircraft being detected, thereby improving their survivability. Improving the aircraft's survivability means increasing the probability of mission success, and as the Department of Defense becomes more

dependent on these types of aircraft for reconnaissance, attack, and security missions, tactical and operational success.

Preview

The rest of this chapter will briefly discuss aircraft survivability as it pertains to reducing the vehicle's radar cross section. Radar theory is a large research area and the reader is invited to read Skolnik (3) for more details on this subject. The radar theory presented in this work is meant to be an introduction to the effects that orientation changes can have on an aircraft's radar cross section.

Chapter 2 presents the helicopter model used in the flight control simulations involved in this study. The existing helicopter models in the literature were of aircraft that were too large when compared to the rotorcraft UAVs being developed today. In the absence of an acceptable plant model, a suitable model representative of current rotorcraft UAVs was created herein.

Chapters 3 and 4 consist of the experimental setup for the simulations necessary to conduct an investigation into the new way of conducting path following and radar exposure minimization theorized in this study. The bare aircraft dynamics are evaluated and improved upon with an automatic flight controller. The sideslip/beta angle feedback loop is introduced and discussed as a new way to control an air vehicle's trajectory.

Chapter 5 presents the results of the simulations and shows how an aircraft's radar cross section exposure can be reduced, and even eliminated, when a sideslip angle (beta) feedback loop is incorporated into the flight control system. It also presents a new concept for path following; one that differs from the way traditional navigation

controller's function that allows the exploitation of the helicopter's unique capability to head in one direction and fly in another.

Chapter 6 gives final conclusions of the work, offers the significance of the study, and recommends areas that this work can be continued and improved upon with further research.

Aircraft Survivability and Susceptibility

Combat survivability is defined here as "the capability of an aircraft to avoid or withstand a man-made hostile environment (4: Sec 1.1.1)." Ball also breaks down the estimation of an aircraft's survivability into two sub-categories: susceptibility and vulnerability. Susceptibility is defined as "the inability of an aircraft to avoid the guns, approaching missiles, exploding warheads, air interceptors, radars, and all of the other elements of an enemy's air defense that make up the man-made hostile mission environment (4:Sec 1.1.1)."

Reducing an aircraft's susceptibility increases its capability to avoid the hostile environment. Susceptibility reduction, also known as threat avoidance, is achieved by reducing the probability the aircraft is detected, tracked, engaged, and hit. There are six survivability enhancements in the area of aircraft susceptibility, one of which is signature reduction. An aircraft's signature comes from its "observables" including radar, thermal/infrared, visible light, aural, and electromagnetic transmissions (like radios and on-board radar which emit signals).

Some operational techniques that reduce an aircraft's susceptibility include flying as fast as possible, as high as possible, utilizing terrain to mask the aircraft as much as

possible (such as nap of the earth flight), and by optimizing an aircraft's path trajectory to its target by avoiding known threat radar systems or minimizing exposure time along the route.

The type of rotary winged vehicle focused on in this research is the type used in support of front line ground forces. Some of the missions that modern day piloted reconnaissance helicopters perform were the focus of the type of missions that the sideslip angle controller discussed in this work would benefit from. These missions include zone, route, and objective reconnaissance, and ordnance delivery in a deliberate attack in the most hostile and dangerous environment. The reconnaissance missions can confirm or deny enemy locations for immediate follow-on action by ground forces. These extremely dangerous missions could be performed by unmanned aerial vehicles, and thus safeguard piloted vehicles for other roles like front line troop close air support. With these types of roles in mind, a UAV performing in this capacity cannot fly high and fast and still accomplish its mission. Other ways of reducing its susceptibility, and increasing survivability, must be explored. This is the impetus of the development of the sideslip controller - reducing the vehicles signature by taking advantage of RCS variations with respect to aircraft orientation. This will result in an uncoordinated flight condition – also known as asymmetric flight – which for a piloted aircraft may be a problem, but not so in the case of a UAV. The reduction in RCS exposed to hostile radars through asymmetric flight can be significant, even along an optimized path trajectory. This is the focus of this research - exploring how sideslip control can change

the orientation of the aircraft to produce the smallest RCS signature of a rotary winged UAV, making it less susceptible, and hence, more survivable.

How Radar Cross Section (RCS) is Calculated

The term radar cross section describes the effective size of a target as it seen by a radar system (5:2-7). Units of RCS are given in square meters, m^2, or decibels (dB). The conversion from square meters to decibels is:

$$RCS(dB) = 10 * \log_{10}[RCS(m^2)] \quad (1)$$

A target's RCS is derived by measuring the amount of total energy reflected to a receiver and then determining the reflective sphere size that would return the same amount of energy. The cross-sectional area of the sphere would be the target's RCS.

Changes in Aircraft Signature as a Function of Azimuth Angle

An aircraft's RCS changes dramatically as its orientation to the radar receiver changes. This is illustrated in Figure 2, which shows how the magnitude of the radar return varies, based on a flat plate reflector, with small changes in the flat plate's angle of incidence (4:Sec 4.3.2). Note that a 6 degree angle of incidence change reduces the RCS by 25%.

Figure 3 shows how RCS varies with azimuth angle for an example aircraft, the A-7 Corsair (4:Sec 4.3.2). The majority of the A-7's RCS values fall on the 10 dB line – 10 dB is equivalent to 10 m^2. However, on the sides of the aircraft (profile view), the aircraft's RCS jumps beyond the 30 dB line. Thirty dB is equivalent to 1000 m^2 - see Equation (1). This means that a change in orientation from either the front or rear to the

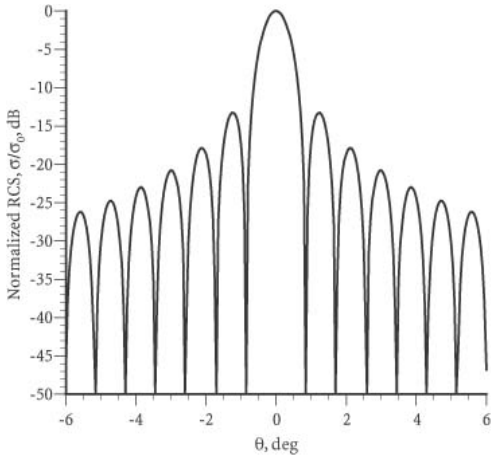

Figure 2. Backscattering from a square flat plate of length a vs. the angle of incidence, θ, for a/λ = 100/3, where λ ≡ signal wavelength.

sides results in a 100-fold increase in radar cross section exposure. This increase is significant, and such large RCS exposures should, and can, be minimized or eliminated along an air vehicle's route. This concept, changing the aircraft's orientation to minimize or eliminate its radar exposure along a route, is the focus of this study.

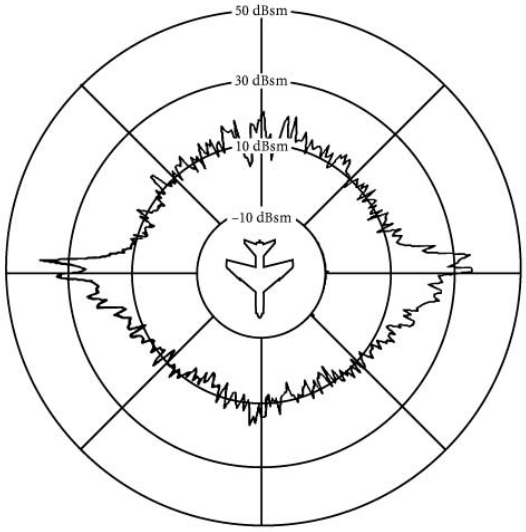

Figure 3. Polar plot of the A-7 Corsair II - median RCS.

Ball supports the idea that almost all aircraft reflect its largest RCS when its profile is to the radar receiver: “Relatively flat surfaces usually occur on the sides of some fuselages, on the vertical tail, and on the upper and lower surfaces of the wing and horizontal tail. Consequently, the RCS of many aircraft are largest when the aircraft is viewed from the sides and from directly above and below” (4:Sec 4.3.2).

An aircraft’s thermal/IR signature is similar to an aircraft’s radar signature in that certain orientations present a much larger IR signature than others. Figure 4 shows this for an example helicopter. Clearly, reducing or eliminating the exposure of those aircraft orientations that present the airframes largest radar or IR signature to hostile radars would increase its survivability.

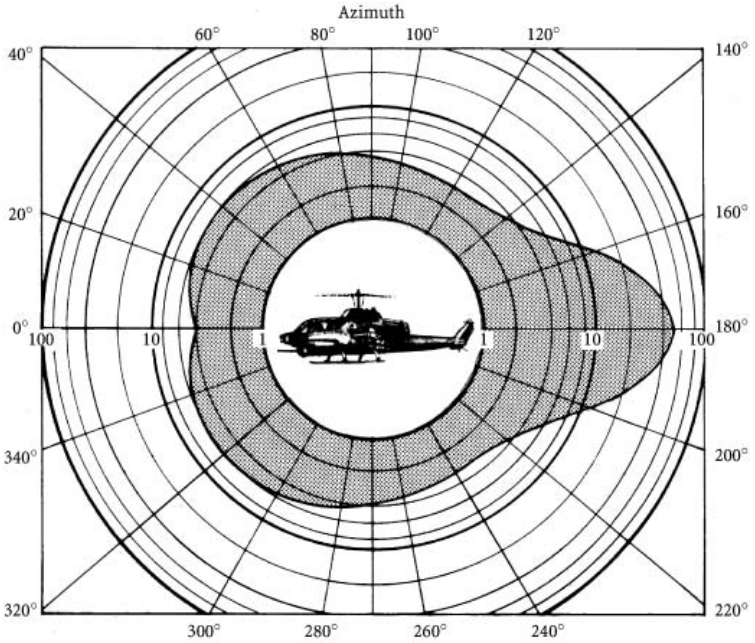

Figure 4. Polar plot of the radiant intensity (watts/steradian) from a helicopter in a given wavelength band.

Reducing Aircraft Signature with Control

Signature reduction, or the reduction of the observables of the aircraft, makes the aircraft more difficult to detect and track. Aircraft whose signatures have been reduced to low levels are sometimes referred to as stealth or stealthy aircraft. There are many ways of reducing an aircraft's signature. Two ways which have received considerable interest are radar and thermal absorbing structural materials on the aircraft, and through the use of structural shaping. Each of the major services in the Department of Defense has researchers and labs dedicated to making their vehicles less observable and therefore, more survivable. This study proposes an additional way to make rotary winged aircraft less observable to a set of hostile radar detectors – orient the aircraft in a way that presents the smallest possible radar cross section through control.

One of the first papers presented on control-based observability minimization for aerial vehicles was one by McFarland, Zachery, and Taylor of the U.S. Air Force Research Laboratory Munitions Directorate in 1999. In their paper titled "Motion Planning for Reduced Observability of Autonomous Vehicles," they "propose a novel solution based on coordinated vehicle orientation control and trajectory shaping techniques borrowed from robot motion planning" to significantly reduce the RCS projection of cruise missiles and autonomous aerial vehicles (6:231). They conclude that searching for the six-degree-of-freedom minimal solution of aircraft RCS exposure to threat radar would be computationally intensive, but, that limiting the computational process to one variable that may have a greater influence on RCS is possible. "The motion planner could simply search for a continuous sequence of φ [roll angle, for

example] commands that minimizes the probability of detection. This requires searching in only one dimension of the configuration space (6:234)."

Asymmetric Flight in Sideslip

This research takes the idea of orientation optimization presented by McFarland, Zachery, and Taylor (6), and further researched by Pendleton (5) as he applied it to aircraft roll, and applies it to sideslip angle for a helicopter. The idea being that there exists an optimal sideslip angle command that minimizes the aircraft's signature to hostile radar in a threat environment. This technology, working together with radar absorbing composites, particularly in the rotor blades, and structural designs that minimize radar returns, can have a significant effect in increasing the survivability of stealth UAVs gathering intelligence for ground forces.

Route Optimization

Route optimization is an area that has seen considerable interest in recent years. Succinctly said, it is "the desire for an optimal set of vehicle waypoints to navigate through to meet a desired objective" (7:1.3). In the context of this work, the desired objective is to minimize an aircraft's signature during ingress and egress to a target objective. Pachter (8) developed an analytic solution to the problem of minimizing the radar exposure of an air vehicle. Novy (7) and Hebert (9) continued his work and found numerical solutions to the single and two radar scenarios. Misovec (10) offers a solution to the same problem through the use of the Nonlinear Trajectory Generation (NTG) software package developed at Caltech. All of the numerical solutions use a gradient descent optimization method to minimize a defined cost model.

Route optimization works hand-in-hand with low-observable aircraft technologies to reduce the signature of the aircraft in a threat sensor environment. Working in conjunction with the aforementioned low-observable technology and tactical flight techniques like nap-of-the-earth flight and military crest flying, Department of Defense UAVs can be made extremely difficult to detect.

Having defined the potential benefits of finding an optimal sideslip command for a helicopter that changes its orientation in a threat environment, and provided background information, the effectiveness of this technology will be based on a numerical solution. Before this can be done, an analytical model is required and is developed in Chapter II.

II. Development of the Helicopter Model

Figure 5. OH-6A "Cayuse" (www.redstone.army.mil/history/aviation)

Introduction of the Plant, the OH-6A "Cayuse"

With no suitable helicopter models available for use in this study, the author decided to create his own. The helicopter used as the plant in the simulations in this work is the OH-6A, a militarized version of McDonnell Douglas Helicopter Inc. (MDHI) MD500 model 369H. This helicopter was designed for use as a military scout during the Vietnam War to meet the U.S. Army's need for an extremely maneuverable light observation helicopter (LOH program). "Initially fielded in Vietnam in early 1968, the [former] Hughes OH-6A was used for command and control, observation, target acquisition, and reconnaissance. The Cayuse was a small, light, sturdy, maneuverable helicopter, with very low drag" (11). This helicopter's max gross weight is 2500 lbs, roughly the same weight of a reconnaissance UAV this work was oriented toward. For this, and the fact that a stealthy reconnaissance rotary winged UAV must have low-drag, the OH-6A was chosen. Parenthetically, while research for this study was being conducted, Boeing, who now owns MDHI, announced that they are developing an

"unmanned little bird," a modernized design of the very same aircraft that would be used for the same missions described in this work.

OH-6A Geometric and Aerodynamic Characteristics

In developing a linearized plant model for use in simulations, the stability derivates needed to derive the aircraft equations of motion require that much about the aircraft be known. The following is a discussion of how the aircraft's characteristics were either derived or determined.

OH-6A General Dimensions.

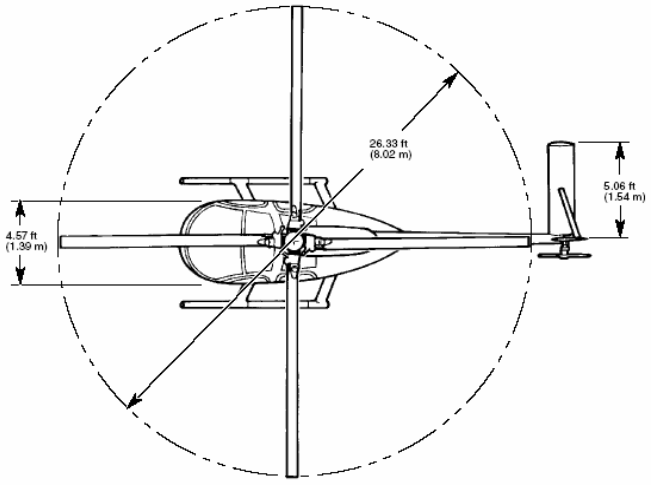

Figure 6. Top view OH-6A (12:1-13).

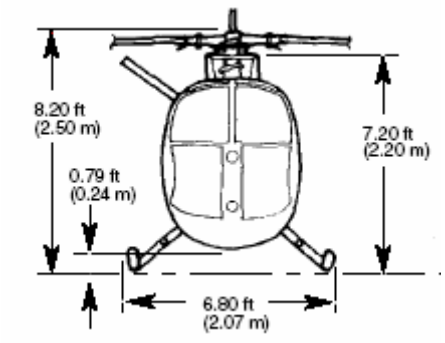

Figure 7. Front view OH-6A (12:1-13).

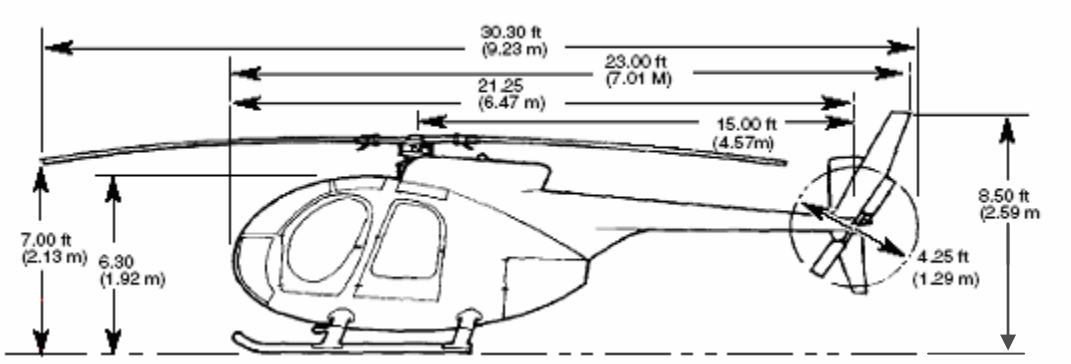

Figure 8. Profile view OH-6A (12:1-13).

When considering a coordinate axis system for the aircraft geometry, the x axis runs the length of the aircraft and is anchored, with the y and z axes, at the aircraft reference datum, a theoretical point far enough in front of and below the aircraft that every point has a coordinate in this axis system. The y direction is to the aircraft's right (when looking from the rear), and z is positive up. Figure 9 shows the x-axis.

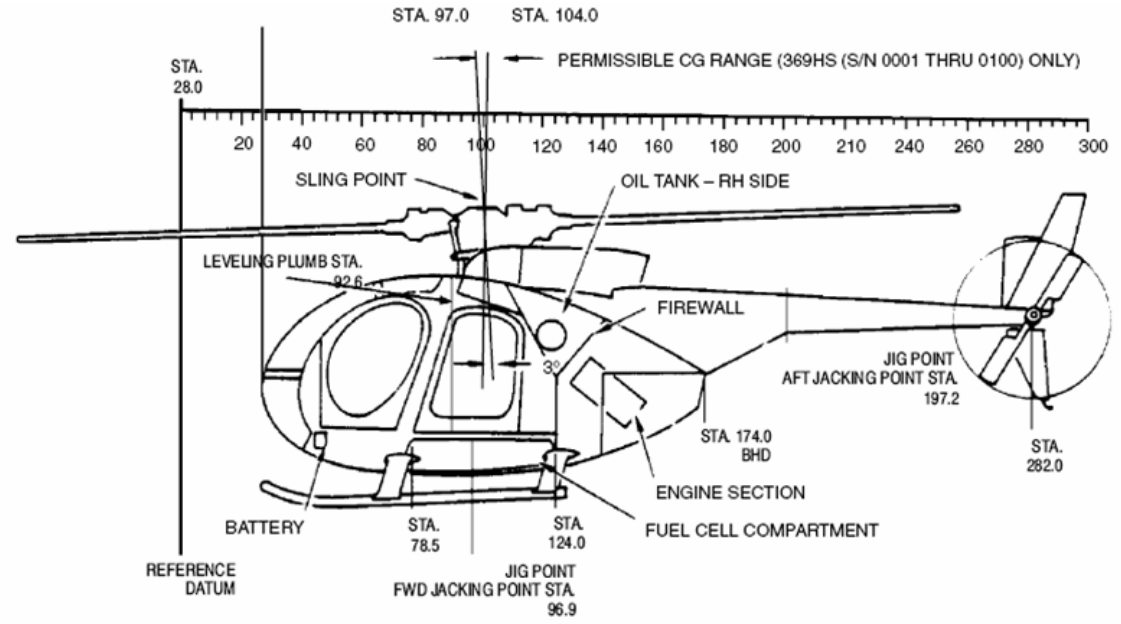

Figure 9. Station Diagram OH-6A (12:6-4)

Main Rotor Characteristics.

The aircraft stability derivatives needed to develop the linear state space model of this helicopter also required that the main rotor parameters were defined. Table 1 provides a summary of those characteristics, and the reference of how they were either derived or found.

Table 1. OH-6A Main Rotor Characteristics.

	Value	**Reference**
Number of Blades	4	(12:1-10)
Rotor Velocity (rpm and rad/s)	483 / 50.58	(13:App F)
Blade Twist (degrees)	-7	(13:App F)
Blade Radius (ft)	13.135	(13:App F)
Hinge Offset (ft)	0.4583	(13:App F)
Aerodynamic Root Cutout (ft)	1.72	(13:App F)
Blade Root Chord (ft)	0.56	(16:694)
Blade Taper Ratio	1	(12:1-13)
Blade Weight (lbs)	33.5	(14:26)
Blade Lift Curve Slope (rad)	5.73	NACA 0012
Flapping Moment of Inertia (slug-ft^2)	62.6	(15)
Hub Height Above CG (ft)	2.7833	(13:App F)
Hub Position aft of CG (ft)	-0.15	(13:App F)
Hub Position Right of Buttline (ft)	0	(13:App F)
Mast Incidence – negative forward (deg)	-3	(12:6-4)
Airfoil	NACA 0012	Chosen because NACA 0015 n/a in JANRAD

Tail Rotor Characteristics.

Similarly, the OH-6A tail rotor characteristics utilized to calculate the aircraft stability derivatives and generate the linear state-space model are presented in Table 2.

Table 2. OH-6A Tail Rotor Characteristics.

	Value	**Reference**
Number of Blades	2	(12:1-10)
Rotor Velocity (rpm and rad/s)	3018 / 316.04	(13:App F)
Blade Radius (ft)	2.125	(13:App F)
Blade Chord (ft)	0.44	(16:694)
Blade Coefficient of Drag, C_D	0.0087	(13:App F)
Location aft of CG (ft)	15.04	(12:6-4)
Height above CG (ft)	0.388	(12:6-5)
Right of Buttline (ft)	0	(12:1-10)
Lift Curve Slope (rad)	5.73	NACA 0012
Flap Moment of Inertia (slug-ft^2)	0.1	(16:694)
Delta 3 Angle (deg)	45	(13:App F)
Blade Twist (deg)	-7	(13:App F)
Airfoil	NACA 0012	Chosen because NACA 0015 n/a in JANRAD

Vertical Fin Geometry.

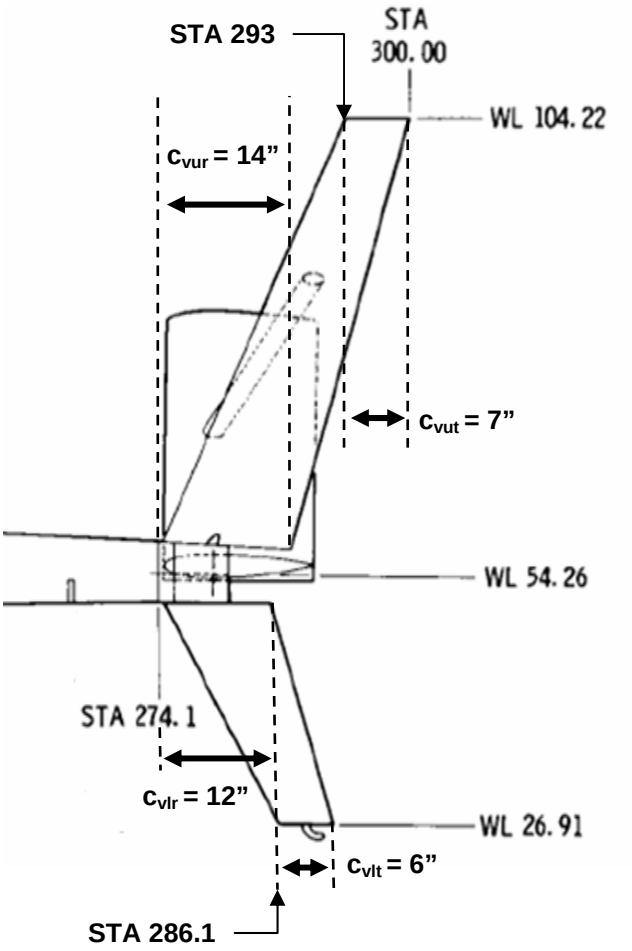

Figure 10. OH-6A Vertical Fin Geometry (12:6-5).

where:

c_{vur} ≡ upper vertical fin root chord (in)
c_{vut} ≡ upper vertical fin tip chord (in)
c_{vlr} ≡ lower vertical fin root chord (in)
c_{vlt} ≡ lower vertical fin tip chord (in)

Several aspects of the tail section of the OH-6A are unique to this aircraft and make it a little more challenging to work with. One unique aspect is having distinct upper and lower portions of the vertical fin. Conventional helicopters have one continuous vertical fin that sweeps back at one angle. The OH-6A has an upper vertical fin with its own root, tip, and sweep dimensions, and a lower vertical fin with its unique

root, tip, and sweep dimensions. Each section had to be considered independently, and then its aerodynamic effect considered as a ratio of the entire structure.

Vertical Fin Coefficient of Lift, C_{L_α}

In order to calculate the vertical fin's lift curve slope, the lift curve slope of both sections of the fin had to be found. To do this each section's aspect ratio had to be found with the following equation:

$$AR_{Vu} = \frac{b_{Vu}^{\ 2}}{A_{Vu}} \tag{2}$$

where:

AR_{Vu} ≡ Upper vertical fin aspect ratio
b_{Vu} ≡ Upper vertical fin span (in)
A_{Vu} ≡ Upper vertical fin Area = $\frac{1}{2}(c_r + c_t)b$ (in^2)
c_r ≡ root chord (in)
c_t ≡ tip chord (in)

With AR found, the following quantity was found:

$$AR_{Vu}[1 + \tan^2 \Lambda_{c/2_u}] \tag{3}$$

where: $\Lambda_{c/2u}$ ≡ Sweep angle at mid chord of the upper vertical fin (deg)

The same steps were taken for the lower vertical fin. With these quantities, the lift curve slope for each section of the vertical fin was found from Figure 8.6 in Prouty (16). The lift curve slope for the entire vertical fin was found by observing that the upper vertical fin makes up approximately 2/3rds of the entire vertical fin structure. A weighting of 2/3 and 1/3 was applied to the upper and lower sections respectively and a total value obtained. The results are summarized in Table 3.

Table 3. Vertical Fin Lift Values.

	Upper Vertical Fin	Lower Vertical Fin	Vertical Fin (Total)
Area (ft^2)	3.65	1.7	5.36
Span, b (ft)	4.17	2.28	6.45
Aspect Ratio	4.762	3.04	n/a
Mid-chord Sweep, $\Lambda_{c/2}$ (deg)	17.12	18.2	n/a
$AR_{Vu}[1+\tan^2\Lambda_{c/2_u}]$	5	3.2	n/a
a, Lift Curve Slope (1/rad) (16:Fig. 8.6)	4.14	3.34	3.89
C_L, Coefficient of Lift (2.5 deg α)	n/a	n/a	.17

Vertical Fin Coefficient of Drag, C_D.

In order to calculate the coefficient of drag for the vertical fin, the Reynolds number at the vertical fin must be found.

$$\mathrm{Re} = \frac{\rho V L}{\mu} \tag{4}$$

where:

ρ ≡ density of the air at sea level (lb/ft^3)
V ≡ Velocity of the air (ft/s)
L ≡ Length of the mean aerodynamic chord (ft)
μ ≡ Air viscosity (lb/ft/sec)

Using a NACA 0012 airfoil for all aerodynamic surfaces, and referring to Figure 4.15 in Prouty (16), gives the following vertical fin drag values, summarized in Table 4.

Table 4. Vertical Fin Drag Values.

	Vertical Fin
Airspeed (ft/s)	67.5
Reynold's Number	5.7×10^5
t/c, Airfoil Thickness to Chord Ratio	0.12
C_D, Coefficient of Drag (16:Fig 4.15)	0.01

Vertical Fin Aerodynamic Center.

Calculating the aerodynamic center (AC) of an aircraft surface is an important part of a vehicle's stability and control analysis, and is necessary in order to determine the moment arm of the aerodynamic surface to the aircraft CG. The procedure followed to calculate the vertical fin AC is located in Appendix A, the results of which are depicted in Figure 11.

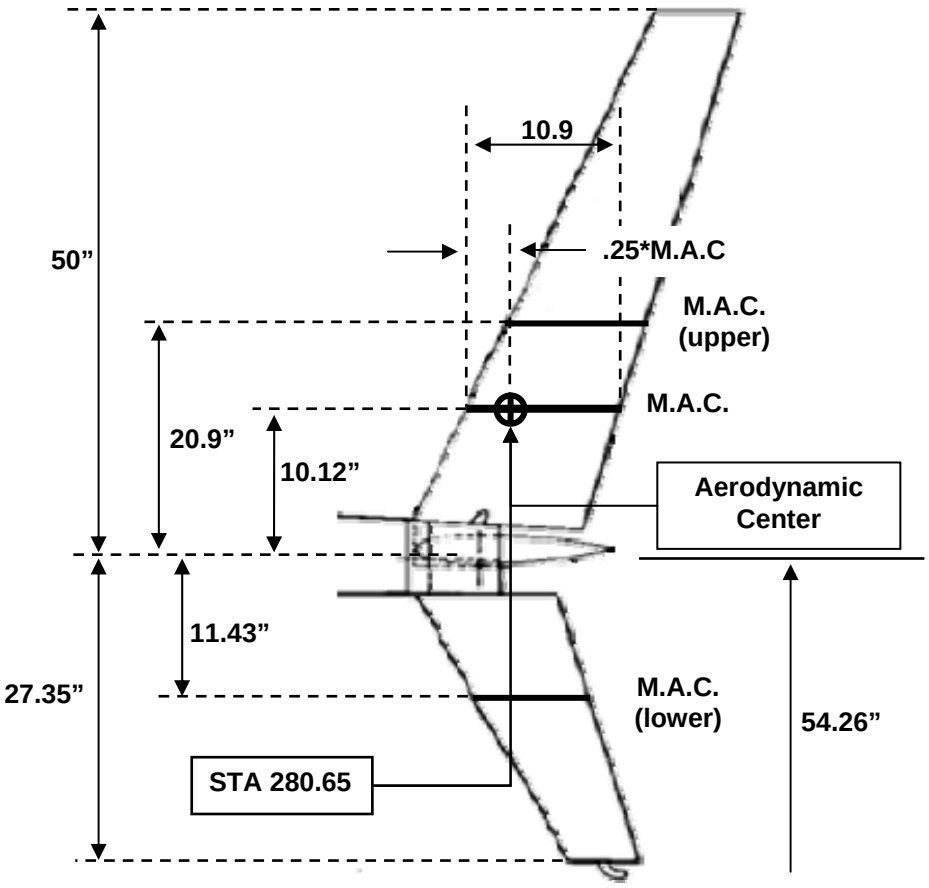

Figure 11. Vertical Fin Aerodynamic Center Location.

Other Characteristics of the Vertical Fin.

There were other parameters of the vertical fin needed to calculate the linear state space model of the OH-6A. These included the maximum coefficient of lift value, dynamic pressure ratio, and angle of attack for zero lift. The values of these characteristics are summarized in Table 5.

Table 5. Miscellaneous Vertical Fin Characteristics.

	Value	**Reference**
$\mathbf{C_{Lmax}}$	1.37	(16:Fig 6.43)
Dynamic Pressure Ratio	0.85	(16:Fig 8.9)
$\boldsymbol{\alpha_{L0}}$	0	NACA 0012

Horizontal Stabilizer Geometry.

The horizontal stabilizer for the OH-6A is very unique in that it is not horizontal like most conventional helicopters. The stabilizer is approximately 40 degrees off vertical (17:40) as shown in Figure 12.

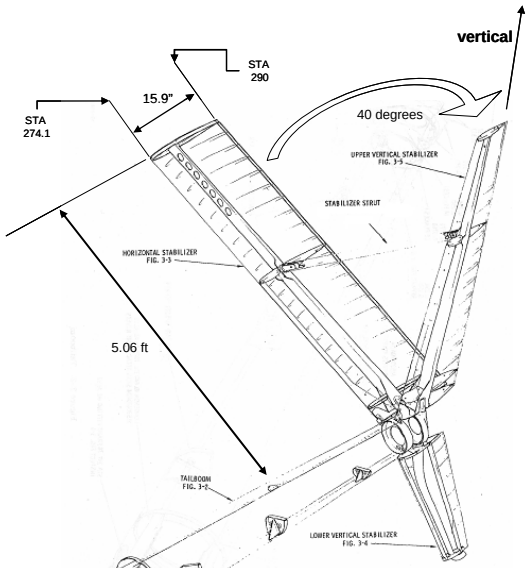

Figure 12. Horizontal Stabilizer Dimensions (18:3-3).

Horizontal Stabilizer Coefficient of Lift, C_L.

C_L for the horizontal stabilizer is found in a manner very similar to that of the vertical tail. Not having two separate components makes this task a little easier. The results of this are found in Table 6.

Table 6. Horizontal Stabilizer Lift Values.

	Horizontal Stabilizer
Area (ft^2)	6.7
Span, b (ft)	5.06
Aspect Ratio	3.82
$\Lambda_{c/2}$ (deg)	0
$AR_H[1+\tan^2\Lambda_{c/2_H}]$	3.82
a, Lift Curve Slope (1/rad) (16:Fig 8.6)	3.82
C_L, Coefficient of Lift (-3 deg α)	-0.2

Horizontal Stabilizer Coefficient of Drag, C_D.

Drag values were also found in a way that is very similar to the vertical fin calculations. These values are presented in Table 7.

Table 7. Horizontal Stabilizer Drag Values.

	Horizontal Stabilizer
Airspeed (ft/s)	67.5
Re	4.32×10^5
t/c, Airfoil Thickness to Chord Ratio	0.12
C_D, Coefficient of Drag (16:Fig 4.15)	0.01

Horizontal Stabilizer Aerodynamic Center.

With the dimensions from Figure 12, the horizontal stabilizer's AC was readily found and displayed in Figure 13. The aircraft center of gravity (CG) is located at (101.85, 0, 49.6) in the x, y, and z directions respectively, from the aircraft reference line. The horizontal stabilizer aerodynamic center then is located 176.25" (14.7') behind the cg (x direction), 19.52" (1.63') right of the cg (y direction), and 24.175" (2.01') above the cg (z direction). Figure 13 shows the aerodynamic center station coordinates.

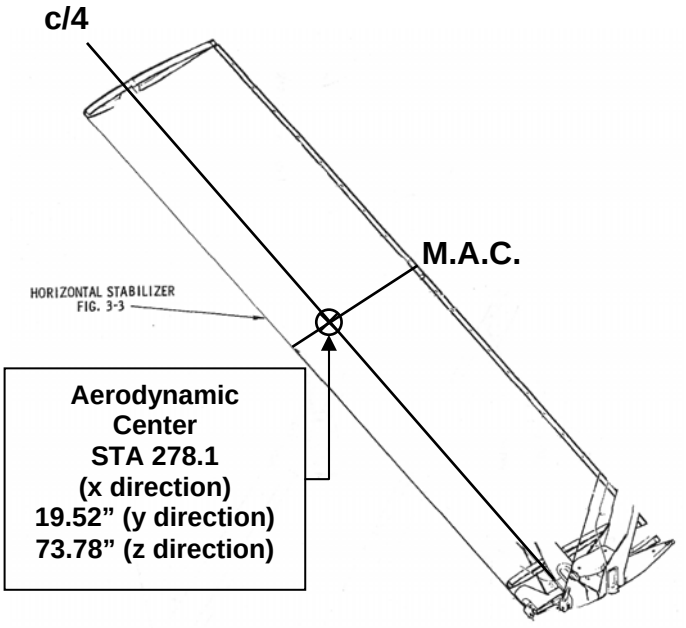

Figure 13. Horizontal Stabilizer Aerodynamic Center.

Other Characteristics of the Horizontal Stabilizer.

There were other parameters of the horizontal stabilizer needed to calculate the linear state space model of the OH-6A. These included the rotor downwash ratio, fuselage downwash ratio, dynamic pressure ratio, and angle of incidence. These values and their references are summarized in Table 8.

Table 8. Miscellaneous Horizontal Tail Characteristics.

	Value	Reference
Rotor Downwash Ratio	2.7	(16:Fig 8.11)
Fuselage Downwash Ratio	0.06	(16:Fig 8.15)
Dynamic Pressure Ratio	0.85	(16:Fig 8.9)
Angle of Incidence (degrees)	-3	From Prouty's Example Helicopter (16:App A)

OH-6A Fuselage Characteristics

Moments of inertia and fuselage areas are presented in Table 9.

Table 9. OH-6A Fuselage Characteristics.

	Value	Reference
Flat Plate Area (ft^2)	30	(12:1-10)
Vertical Projection Area (ft^2)	55	(12:1-10)
Roll Moment of Inertia, I_{xx} ($slug\text{-}ft^2$)	306	(13:App F)
Pitch Moment of Inertia, I_{yy} ($slug\text{-}ft^2$)	875	(13:App F)
Yaw Moment of Inertia, I_{zz} ($slug\text{-}ft^2$)	689	(13:App F)
Total XZ Moment of Inertia, I_{xz} ($slug\text{-}ft^2$)	-94	(13:App F)

III. Helicopter Stability

Linearization

The helicopter equations of motion described in non-linear form (19:207) are:

$$\dot{\mathbf{x}} = \mathbf{F}(\mathbf{x}, \mathbf{u}, t) \tag{5}$$

where: $\mathbf{F}(\mathbf{x}, \mathbf{u}, t) \equiv$ vector function that includes all of the aerodynamic loads, gravitational forces, and inertial forces and moments

In six degree-of-freedom form, the motion states are:

$$\mathbf{x} = \{u, w, q, \theta, v, p, \phi, r, \psi\} \tag{6}$$

where:

u, v, w ≡ translational velocities in the three orthogonal directions (see Figure 14)
p, q, r ≡ angular velocities about the x, y, and z axes
θ, φ, ψ ≡ Euler angles representing the aircraft's orientation of the body relative to the center of earth

The control vector **u** has four components:

$$\mathbf{u} = \{\theta_{1s}, \theta_o, \theta_{1c}, \theta_{TR}\} \tag{7}$$

where:

$\theta_{1s} \equiv$ longitudinal cyclic
$\theta_0 \equiv$ main rotor collective
$\theta_{1c} \equiv$ lateral cyclic
$\theta_{TR} \equiv$ tail rotor collective

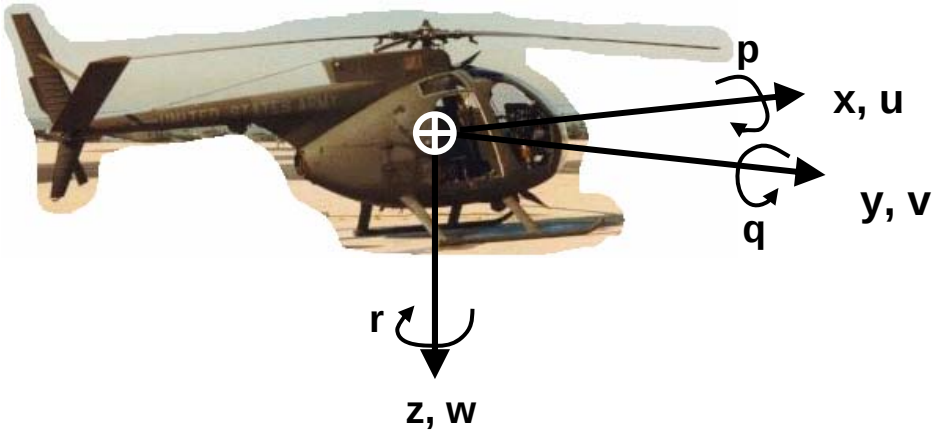

Figure 14. Helicopter Stability Axes.

Using small perturbation theory we assume that during disturbed motion, the helicopter can be described as a perturbation from the trim, written in the following form (19:208):

$$\mathbf{x} = \mathbf{X}_e + \delta\mathbf{x} \tag{8}$$

where:

$\mathbf{X}_e \equiv$ the equilibrium value of the state vector
$\delta\mathbf{x} \equiv$ the perturbation of the state vector

The external forces X, Y, and Z, and moments L, M, and N can then be written in the approximate form:

$$\mathbf{X} = \mathbf{X}_e + \frac{\partial \mathbf{X}}{\partial u}\delta u + \frac{\partial \mathbf{X}}{\partial w}\delta w + \ldots + \frac{\partial \mathbf{X}}{\partial \theta_{1s}}\partial\theta_{1s} + \text{etc.} \tag{9}$$

All six forces and moments can be expanded this way. The linearized equations of motion about a general trim condition can then be written as (19:209):

$$\begin{aligned} \dot{\mathbf{x}} - \mathbf{A}\mathbf{x} &= \mathbf{B}\mathbf{u}(t) \\ \mathbf{y} - \mathbf{C}\mathbf{x} &= \mathbf{D}\mathbf{u}(t) \end{aligned} \tag{10}$$

where:

$$\mathbf{A} = \left(\frac{\partial \mathbf{F}}{\partial \mathbf{x}}\right)_{\mathbf{x}=\mathrm{M}_e} \tag{11}$$

$$\mathbf{B} = \left(\frac{\partial \mathbf{F}}{\partial \mathbf{u}}\right)_{\mathbf{x}=\mathbf{x}_e} \tag{12}$$

It is assumed that the function $\mathbf{F}$ is differentiable with all first derivatives bounded for bounded values of flight trajectory $\mathbf{x}$ and time t (19:251). The initial value at $t = 0$ is:

$$\mathbf{x}(0) = \mathbf{x}_0 \tag{13}$$

Joint Army/Navy Rotorcraft Analysis and Design (JANRAD) Software

The software used to develop the linear state space model of the OH-6A was a Matlab based software program called Joint Army/Navy Rotorcraft Analysis and Design (JANRAD). JANRAD was originally written by Nicholson (20) as a rotorcraft performance tool at the Naval Post Graduate School to aid in a design contest for the American Helicopter Society. Wirth (21) developed a stability and control module for the software that creates the A and B matrices referred to in Equation (10). This software was validated by Eccles (22) when he compared JANRAD output results with NASA flight test data of the H-34 and UH-60A helicopters. Many other modifications and updates have been made to the software culminating into JANRAD version 6.0 written by Heathorn (23) which added several front-end GUIs to aid in user interface.

As research was conducted for this work, a few deficiencies in JANRAD's interface were identified and will be included in the recommendations for future work section of this study. Also, version 6.0 of the program was not compatible with Matlab release 14 due to some of the JANRAD files being named the same as other files in various Matlab toolboxes. This author updated the JANRAD program so that it is now compatible with Matlab release 14. The final JANRAD program is included on a CD attached to this work.

OH-6A State Space Representation

With all of the geometry, aerodynamic, and fuselage characteristics defined for the OH-6A, those values were entered into the JANRAD software program and the state

space A and B matrices were created. The JANRAD input/output screens are shown in Appendix B. The flight and atmospheric conditions chosen are shown in Table 10.

Table 10. Model Flight and Atmospheric Conditions.

Condition	Value
Forward Airspeed (knots & ft/s)	40 / 67.5
Atmospheric Temperature (F)	95
Altitude (ft)	0
Gross Weight (lbs)	2500

Forty knots was chosen for two reasons: first, the type of missions the target rotorcraft UAV would perform (i.e. reconnaissance, battle damage assessment, etc.) would necessitate flight at slower airspeeds in order to accomplish its mission. Second, most current helicopters have sideward flight limits of 35-40 knots that would preclude them from being able to sustain the type of orientation commands designed in this work if they were flying at faster speeds. Although, the now cancelled Comanche helicopter demonstrated controlled sideward flight up to 75 knots. The limiting factor would be tail rotor control authority.

The state space model output of JANRAD's stability and control module is presented in Table 11 and Table 12. The state variable ψ is generally not included in the helicopter linear dynamic model because the aerodynamic loads, gravitational forces, inertial forces and moments do not change with respect to heading in a no-wind condition. The heading angle ψ is obtained by integrating yaw rate, r.

Table 11. A Matrix for the OH-6A at 40 knots, S.L., 95º F.

1.06373	6.56344	-0.516079	-32.2	-0.00272007	-0.139593	0	0	**u**
-0.101738	-0.671477	67.4447	0	0	0	0	1.28755	**w**
-0.631604	-5.33766	-1.95648	0	-0.000928645	0.0787117	0	0	**q**
0	0	1	0	0	0	0	0	**θ**
0.0287491	0.015253	-0.164369	0	-0.294801	-2.64116	32.2	-66.9437	**v**
0.00762645	0.0454309	-0.428589	0	0.0179573	-7.51575	0	0.414223	**p**
0	0	0	0	0	1	0	0	**φ**
-0.0621721	-0.00967244	0.0584723	0	-0.0259588	1.06516	0	-0.973771	**r**

Table 12. B Matrix for the OH-6A at 40 knots, S.L., 95º F.

1.33115	0.291038	-0.120947	0	**----------**
-0.150704	-9.33149	0	0	**----------**
-1.35256	0.192282	0.122892	0	**Longitudinal Cyclic**
0	0	0	0	**Collective**
0.183277	0.274863	0.869456	-3.43421	**Lateral Cyclic**
0.532504	0.647642	2.52618	-2.12599	**Tail Rotor**
0	0	0	0	**----------**
-0.0726492	0.382478	-0.344645	5.86634	**----------**

The Analysis of Linear Dynamic Systems

Equation (10) is valid for calculating the perturbed responses from a trim point, but in the homogeneous form it can be used to quantify the stability characteristics for small motions of the nonlinear dynamic system described by Equation (5). This is a very important application and underpins most of the understanding of flight dynamics. The

free motion solutions of Equation (10) take the form of exponential functions; the signs of the real parts determine the stability with positive values indicating instability. The theory of the stability of motion for linear dynamic systems can be most succinctly expressed using linear algebra and the concepts of eigenvalues and eigenvectors.

Consider the free motion of the helicopter, described by the homogenous form of Equation (10):

$$\dot{\mathbf{x}} - \mathbf{A}\mathbf{x} = 0 \tag{14}$$

With the intention of simplifying the equations, the following transformation is introduced:

$$\mathbf{x} = \mathbf{W}\mathbf{y} \tag{15}$$

so that Equation (14) can be written as:

$$\dot{\mathbf{y}} - \mathbf{\Lambda}\mathbf{y} = 0 \tag{16}$$

where:

$$\mathbf{\Lambda} = \mathbf{W}^{-1}\mathbf{A}\mathbf{W} \tag{17}$$

For a given matrix **A**, there is a unique transformation matrix **W** that reduces **A** to a canonical form, **Λ**, most often diagonal, so that Equation (16) can usually be written as a series of uncoupled equations:

$$\dot{y}_i - \lambda_i y_i = 0, \quad i = 1,2,...n \tag{18}$$

with solutions:

$$y_i = y_{i_0} e^{\lambda_i t} \tag{19}$$

Collected together in vector form, the solution can be written as:

$$\mathbf{y} = \text{diag}[\exp(\lambda_i t)]\mathbf{y}_0 \tag{20}$$

Transforming back to the flight state vector **x**, the following is obtained:

$$\mathbf{x}(t) = \mathbf{W}\,\text{diag}[\exp(\lambda_i t)]\mathbf{W}^{-1}\mathbf{x_0} = \mathbf{Y}(t)\mathbf{x}_0 \equiv \exp(\mathbf{A}t)\mathbf{x}_0 \tag{21}$$

where the principal matrix solution **Y**(t) is defined by:

$$\begin{aligned} \mathbf{Y}(t) &= \mathbf{0}, \quad t < 0 \\ \mathbf{Y}(t) &= \mathbf{W}\,\text{diag}[\exp(\lambda_i t)]\mathbf{W}^{-1}, \quad t \geq 0 \end{aligned} \tag{22}$$

The transformation matrix **W** and the set of numbers λ have a special meaning in linear algebra; if $\mathbf{w_i}$ is a column of **W** then the pairs [$\mathbf{w_i}$, λ_i] are the eigenvectors and eigenvalues of the matrix **A**. The eigenvectors are special in that when they are transformed by the matrix **A**, all that happens is that they change in length, as given by the equation:

$$\mathbf{A}\mathbf{w}_i = \lambda_i \mathbf{w}_i \tag{23}$$

No other vectors in the space on which **A** operates are quite like the eigenvectors. Their special property makes them suitable as basis vectors for describing more general motion. The associated eigenvalues, λ, are the real or complex scalars given by the *n* solutions of the polynomial:

$$\det[\lambda\mathbf{I} - \mathbf{A}] = 0 \tag{24}$$

The free motion of a helicopter is therefore described by a linear combination of simple exponential functions, each with a mode shape (distribution among the states) defined by the eigenvector, and a trajectory envelope (exponential character in time) defined by the

eigenvalue. Each natural mode is linearly independent of the others, i.e., the motion in a mode is unique and cannot be made up from a combination of other modes (19:252).

Equation (21) can be written in the alternative form:

$$\mathbf{x}(t) = \sum_{i=1}^{n} (\mathbf{v}_i^{\mathrm{T}} \mathbf{x_0}) \exp(\lambda_i t) \mathbf{w}_i \tag{25}$$

where $\mathbf{v}$ is the eigenvector of the matrix $\mathbf{A^T}$, i.e. $\mathbf{v}_j^{\mathbf{T}}$ are the rows of $\mathbf{W}^{-1}$ ($\mathbf{V^T} = \mathbf{W}^{-1}$) so that:

$$\mathbf{A}^{\mathrm{T}} \mathbf{v}_j = \lambda_j \mathbf{v}_j \tag{26}$$

The dual vectors $\mathbf{w}$ and $\mathbf{v}$ satisfy the bi-orthogonality relationship:

$$\mathbf{v}_j^{\mathbf{T}} \mathbf{w}_k = 0, \quad \mathrm{j} \neq \mathrm{k} \tag{27}$$

Bare Airframe Stability

The stability of the bare airframe with no stability augmentation is determined entirely by the signs of the real parts of the eigenvalues. A positive eigenvalue will indicate instability; a negative real part indicates stability. A plot of the 8 eigenvalues of the helicopter model shown in Table 11, found from Equation (24), is shown in Figure 15.

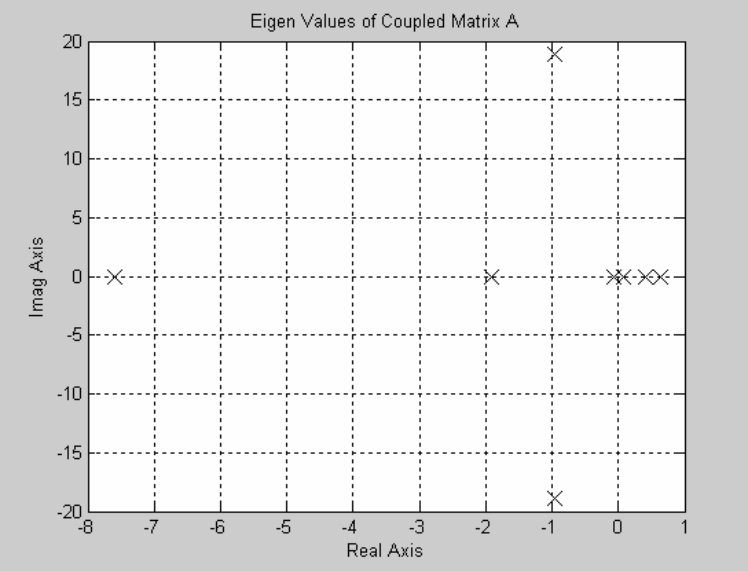

Figure 15. Eigenvalues of the Bare Helicopter Dynamics.

Figure 15 shows that the bare airframe has three unstable modes. Further analysis shows that 2 of them are in the pitch/longitudinal direction, and one is a lateral/ directional instability. With no stability augmentation, this helicopter would not be able to fly. Feedback control will be necessary to stabilize the aircraft.

Having created the linear helicopter model, established the bare airframe dynamics, and provided the background for helicopter stability analysis, an aircraft autopilot/flight controller can now be developed. The autopilot/flight controller will stabilize the aircraft and shape the aircraft response into desired response modes. The autopilot will also allow the aircraft to track altitude, heading, and sideslip commands that will orient the aircraft in a way that minimizes its radar cross section to hostile radar. This autopilot design is presented in Chapter IV.

IV. Control

Modes

Most helicopters have three modes of motion in the longitudinal axis, and three modes of motion in the lateral axis of the helicopter (24:157). The three longitudinal modes of motion are as follows:

(1) **Forward speed mode** – this is a stable, heavily damped subsistence in speed. The motion is coupled with pitch attitude and pitch rate. It has a short time constant of the order 0.5 second. Also known as the short period mode.

(2) **Pitching oscillation mode**– The oscillation couples with the forward speed mode and is mainly due to rotor flapping caused by speed changes. The stability of this mode is both speed and flight condition dependent.

(3) **Vertical velocity mode** – also known as heave mode. This is a stable, heavily damped subsistence in vertical velocity. The motion is decoupled from speed and pitch and has a time constant of the order 1 to 2 seconds.

The three modes associated with lateral/directional motion are as follows:

(1) **Yawing mode** - this is equivalent to the fixed wing spiral mode. It is independent of roll and lateral translation and is an exponential motion that can be either convergent or divergent. The time constant is moderately long, between 5 and 20 seconds.

(2) **Rolling mode** – this is damped subsistence in pure roll. The motion has a short time constant of the order 1 to 2 seconds.

(3) **Lateral/Directional oscillation** – also called dutch roll, is an oscillation in both roll and yaw, which like the pitching oscillation can be flight dependent. Typically the oscillation is unstable in the hover and in a climb.

The open loop modes of the OH-6A in the flight condition defined are examined. The open loop eigenvalues and eigenvectors are given in Table 13 and Table 14.

Table 13. Bare Airframe Eigenvalues.

1	-0.9537 ± 18.9377j
2	-7.5931
3	-1.9048
4	0.6455
5	0.4025
6	-0.0737
7	0.0824

Table 14. Bare Airframe Eigenvectors.

States	1	2	3	4	5	6	7
u	0.0373 ± 0.2919j	0.0027	-0.0049	-0.0536	-0.1993	-0.1912	0.4836
w	-0.9201 ± 0j	0.0138	0.0007	0.0060	0.0233	0.0224	-0.0572
q	0.0039 ± 0.2579j	0.0013	0.0004	0.0003	0.0002	0.0002	0.0003
θ	-0.0136 ± 0.0005j	-0.0002	-0.0002	0.0004	0.0006	-0.0023	0.0032
v	0.0037 ± 0.0045j	-0.4757	-0.9997	0.9985	0.9796	0.9810	-0.8729
p	0.0046 ± 0.0039j	0.8608	-0.0049	0.0015	0.0017	0.0015	-0.0024
φ	0.0002 ± 0.0003j	-0.1134	0.0026	0.0023	0.0043	-0.0210	-0.0294
r	-0.0015 ± 0.0006j	-0.1403	-0.0226	-0.0130	-0.0083	-0.0135	-0.0089

As noted earlier, there are 3 unstable modes in the open-loop aircraft. Inspection of Table 14 also reveals heavy sideward velocity state, v, coupling in all modes except the first, a very undesirable feature. Eigenstructure assignment is a modern control technique for multi-input, multi-output (MIMO) systems that can be used to re-shape the eigenvalues and eigenvectors to produce desirable response modes and to decouple the modes to the extent possible. The theory of eigenstructure assignment is discussed next.

Theory of Eigenstructure Assignment

The basic theory behind eigenstructure assignment is presented below. Detailed discussions can be found in the research presented by Liebst (25) and Andry (26).

According to Liebst (25:475), if the desired system is controllable and observable, and the matrices **B** and **C** from Equation (10) are full rank, the eigenstructure assignment design procedure consists of solving for the eigenvectors ($\mathbf{w}_i$) that satisfy:

$$(\lambda_i \mathbf{I} - \mathbf{A})\mathbf{v}_i^d = \mathbf{B}\mathbf{w}_i \tag{28}$$

where (λ_i, $\mathbf{v}_i^d$) are the desired eigenvalue-eigenvector pairs.

If $\mathbf{v}_i^d$ does not lie in the $(\lambda_i\mathbf{I}\text{-}\mathbf{A})^{-1}\mathbf{B}$ achievable vector space there is no solution. It may be possible, however, to find a vector in the achievable vector space that is close to the desired eigenvector. To do so, it is first necessary to define the following performance index:

$$J_i = (\mathbf{v}_i - \mathbf{v}_i^d) * \mathbf{P}_i (\mathbf{v}_i - \mathbf{v}_i^d) \tag{29}$$

where $\mathbf{v}_i$ is the attainable eigenvector.

The attainable $\mathbf{v}_i$ and corresponding $\mathbf{w}_i$ that will minimize the performance index J_i can be found by adjoining equations (28) and (29) with the Lagrange multipliers $\boldsymbol{\upsilon}_i$, taking the partial derivatives with respect to $\mathbf{v}_i$, $\mathbf{w}_i$, and $\boldsymbol{\upsilon}_i$, and setting the derivatives equal to zero. This is equivalent to finding $\mathbf{w}_i$ such that:

$$\begin{bmatrix} (\mathbf{I}\lambda_i - \mathbf{A}) & -\mathbf{B} & 0 \\ 0 & 0 & \mathbf{B}^{\mathrm{T}} \\ \mathbf{P}_i & 0 & (\mathbf{I}\lambda_i - \mathbf{A})^* \end{bmatrix} \begin{Bmatrix} \mathbf{v}_i \\ \mathbf{w}_i \\ \boldsymbol{\upsilon}_i \end{Bmatrix} = \begin{Bmatrix} 0 \\ 0 \\ \mathbf{P}_i \mathbf{v}_i^{\,d} \end{Bmatrix} \tag{30}$$

where:

$\mathbf{P}_i \equiv$ positive definite symmetric matrix whose elements can be chosen to weight the difference between the elements of the desired and attainable eigenvectors

$* \equiv$ hermitian transpose

The attainable $\mathbf{v}_i$ and $\mathbf{w}_i$ are then:

$$\begin{Bmatrix} \mathbf{v}_i \\ \mathbf{w}_i \\ \boldsymbol{\upsilon}_i \end{Bmatrix} = \mathbf{N}_i^{-1} \begin{Bmatrix} 0 \\ 0 \\ \mathbf{P}_i \mathbf{v}_i^{d} \end{Bmatrix} \tag{31}$$

where $\mathbf{N}_i \equiv$ the non-singular matrix from Equation (30).

Once the $\mathbf{w}_i$'s have been found, the gain matrix is calculated as:

$$\mathbf{K} = \mathbf{W}[\mathbf{CV}]^{-1} \tag{32}$$

when the inverse exists.

The Matlab file that performs this eigenstructure assignment technique and the accompanying code that uses it is located in Appendix G and D, respectively.

Inner-Loop Control – Desired and Achieved Eigenstructure

The desired eigenvalues are presented in Table 15 and the desired eigenvectors are presented in Table 16.

Table 15. Desired Eigenvalues.

Roll Mode	-3.5
Pitching Oscillation Mode	-2.9
Dutch Roll Mode	-0.802 ± 0.388j
Forward Speed Mode	-0.801 ± 0.387j
Heave Mode	-1.0
Yaw Mode	-1.5

Table 16. Desired Eigenvectors.

Modes/ States	**Roll Mode**	**Pitching Oscillation Mode**	**Dutch Roll Mode**	**Forward Speed Mode**	**Heave Mode**	**Yaw Mode**
u	0	0	0	1 ± 1j	0	0
w	0	0	0	0	1	0
q	0	1	0	-0.801 ± 0.387j	0	0
θ	0	-0.3448	0	0.801 ± 0.387j	0	0
v	0	0	1 ± 1j	0	0	0
p	1	0	0	0	0	0
φ	-.2857	0	0	0	0	0
r	0	0	0	0	0	1.5

The roll eigenvalue was selected to give a roll bandwidth of 3.5 rad/sec. Similarly, the pitching oscillation eigenvalue was selected to give a pitching oscillation

bandwidth of 2.9 rad/sec, a yaw bandwidth of 1.5 rad/sec, and a vertical velocity bandwidth of 1 rad/sec. The eigenvalues associated with the forward speed and dutch roll modes were selected to be complex with a natural frequency of 0.9 rad/sec and a damping factor of 0.9. This resulted in bandwidths of about 1 rad/sec for the forward speed and dutch roll modes as well as the heave mode (27:27). The values for bandwidth, damping factor, and natural frequency were chosen consistent with values in the literature addressing multivariable helicopter flight control such as Walker (28:788) and Garrard (27:27).

The roll mode eigenvector makes roll rate unity. Since the roll angle, φ is the integral of the roll rate, the element associated with the roll angle is the inverse of the roll eigenvalue. The rest of the eigenvectors are developed in similar fashion as described in the modes discussion earlier in this chapter. If this desired eigenstructure is achieved, the lateral modes, roll and sideslip, are decoupled from the longitudinal, vertical velocity and yaw rate modes. The desired eigenvectors associated with the pitching eigenvalue, -2.9, and the forward speed eigenvectors associated with $-0.801 \pm 0.387j$, are chosen in a similar manner to decouple the longitudinal modes from the lateral, vertical velocity, and yaw rate modes (27:27).

Applying this methodology with unity weighting on the squared error between all elements of the desired and attainable eigenvectors - the **P** matrix from Equation (29) - yields the following achievable eigenstructure, presented in Table 17 and Table 18.

Table 17. Achieved Eigenvalues, Unity Weighting.

Roll Mode	-3.5
Pitching Oscillation Mode	-2.9
Dutch Roll Mode	-0.802 ± 0.388j
Forward Speed Mode	-0.801 ± 0.387j
Heave Mode	-1.0
Yaw Mode	-1.5

Table 18. Achieved Eigenvectors, Unity Weighting.

Modes/ States	**Roll Mode**	**Pitching Oscillation Mode**	**Dutch Roll Mode**	**Forward Speed Mode**	**Heave Mode**	**Yaw Mode**
u	-0.0003	-0.8877	0 ± 0j	-0.9976 ± 0j	-0.0033	-0.0090
w	-0.0003	-0.3866	0 ± 0j	-0.0059 ± 0.0467j	0.9984	-0.0041
q	-0.0050	0.2356	0.0001 ± 0j	0.0267 ± 0.0213j	-0.0395	-0.0019
θ	0.0014	-0.0813	0.0001 ± 0j	-0.0375 ± 0.0085j	0.0395	0.0013
v	-0.0071	0.0001	1 ± 0j	0 ± 0.0001j	0	0.0627
p	-0.9510	0.0185	0.0009 ± 0.0018j	0.0005 ± 0.0011j	-0.0001	-0.8008
φ	0.2717	-0.0064	-0.0017 ± 0.0014j	0 ± 0.0013j	0.0001	0.5339
r	0.1471	0.0034	0.0064 ± 0.0051j	0.0009 ± 0.0013j	-0.0008	0.2640

As expected, all of the desired eigenvalues were achieved and the sideward velocity state, v, has been decoupled; however, there is vertical velocity coupling in the pitching eigenvector as well as heavy roll rate coupling in the yaw mode. Moreover, negative real parts in the forward speed mode and roll mode have the opposite desired response.

An attempt to fix these issues was made by weighting the error between the desired and attainable elements of the states deemed most important to get right. In other words, the weighting matrix **P** allows the engineer to weight some of the error more heavily than others. The weighted errors drive up the cost function unless the error for those weighted values is significantly reduced or eliminated. The values in the **P** matrix are important only in their relationship to the other weighting values. For these reasons, the forward speed element in the pitch mode was weighted by a factor of 10. Similarly, the vertical velocity element was weighted by a factor of 8 to reduce the error in the pitching mode, and the pitch rate element was weighted by a factor of 5 to reduce the error also found in the pitching eigenvector.

The final weighting **P** matrix is shown in Table 19:

Table 19. Final Weighting Matrix, P.

u	10	0	0	0	0	0	0	0
w	0	8	0	0	0	0	0	0
q	0	0	5	0	0	0	0	0
θ	0	0	0	1	0	0	0	0
v	0	0	0	0	1	0	0	0
p	0	0	0	0	0	1	0	0
φ	0	0	0	0	0	0	1	0
r	0	0	0	0	0	0	0	1

The final weighting was selected through an iteration process to achieve the best possible response. The final eigenstructure will still show less than ideal response, but, it

is the best response found through many iterations of the weighting matrix. For example a weighting that forced the yaw mode to decouple caused problems in several other modes. The final eigenstructure is in effect an optimization to achieve the closest response to the desired eigenstructure.

The final eigenstructure with the applied weighting matrix **P** in Table 19 is presented in Table 20 and Table 21.

Table 20. Achieved Eigenvalues, Final Weighting.

Roll Mode	-3.5
Pitching Oscillation Mode	-2.9
Dutch Roll Mode	-0.802 ± 0.388j
Forward Speed Mode	-0.801 ± 0.387j
Heave Mode	-1.0
Yaw Mode	-1.5

Table 21. Achieved Eigenvectors, Final Weighting.

Modes/ States	**Roll Mode**	**Pitching Oscillation Mode**	**Dutch Roll Mode**	**Forward Speed Mode**	**Heave Mode**	**Yaw Mode**
u	0.0006	0.8371	0 ± 0j	0.9985 ± 0j	-0.0010	-0.0010
w	0.0003	0.4557	0 ± 0j	-0.0010 ± 0.0173j	0.9984	-0.0006
q	0.0049	-0.2318	0.0001 ± 0j	-0.0261 ± 0.0222j	-0.0396	-0.0027
θ	-0.0014	0.0799	-0.0001 ± 0j	0.0373 ± 0.0097j	0.0396	0.0018
v	0.0071	-0.0035	1 ± 0j	0 ± 0.0003j	0	0.0627
p	0.9510	-0.1660	0.0009 ± 0.0018j	-0.0005 ± 0.0037j	0.0001	-0.8008
φ	-0.2717	0.0572	-0.0017 ± 0.0014j	-0.0013 ± 0.0040j	-0.0001	0.5339
r	-0.1471	0.0234	0.0064 ± 0.0051j	-0.0014 ± 0.0026j	-0.0009	0.2640

Upon examination of the final eigenvector structure, it is seen that the yaw mode is still coupled and that the vertical velocity element is still coupled in the pitching oscillation mode. Other feedback loops, altitude, heading, and sideslip, will help to correct this response.

The **K** matrix in Equation (32) calculated to achieve the final eigenstructure is shown in Table 22. Notice that none of these gains are excessively large. Large gain values can lead to actuator saturation which is not modeled in linearized dynamics, and hence, would lead to vehicle instability.

Table 22. K Matrix to Achieve Final Eigenstructure.

0.5703	3.9635	-2.5707	-4.9851	0.0007	-0.1468	0.1768	0.0239
-0.0390	-0.1329	-6.4521	1.6632	0.0001	-0.0013	-0.0066	-0.1454
-0.1143	-0.7793	2.4118	0.5575	0.0045	-0.9374	2.0411	0.2675
-0.0085	0.0096	0.5574	-0.1022	-0.0052	0.0316	0.0009	0.0788

Outer-Loop Control

In the previous section, the procedure to design the flight controller's inner-loop with eigenstructure assignment was presented. Full-state feedback was assumed for this vehicle (with the state vector defined in Equation (6)). This assumption is valid given the advanced sensors available to UAV engineers today. If full state feedback were not available or possible, then an estimator would have to be created in the flight control system to estimate the value of states that were not measurable. The following section addresses the flight controller's outer-loops.

Building the entire longitudinal and lateral motion autopilot with altitude, heading, ψ, and sideslip angle, β, feedback began with getting the uncoupled longitudinal model working first. The thought process was to get the individual pieces of the autopilot simulation working first before trying to bring the entire system together. The final autopilot simulation will have full state feedback, altitude feedback, heading feedback, ψ, and sideslip angle feedback, β.

Helicopters typically have four control inputs:

(1) Longitudinal cyclic - controls pitch attitude and longitudinal velocity.

(2) Collective – changes pitch angle on all main rotor blades simultaneously, or collectively, thereby controlling vertical velocity.

(3) Lateral cyclic – controls bank angle and lateral velocity.

(4) Tail rotor – changes pitch angle on all tail rotor blades simultaneously, thereby controlling the yaw attitude and rate of the helicopter.

The benefit of looking at the decoupled longitudinal and lateral responses separately, besides only having to work with half of the states, is that one doesn't have to deal with the off-diagonal coupling in the full 8X8 model. In other words, there are lateral responses to longitudinal inputs in the full 8X8 model, and conversely, there are longitudinal responses to lateral inputs. The off-diagonal terms in the full 8X8 model represent this off-axis coupling. Dealing with each motion separately to begin with eliminates the off-axis coupling, albeit at the expense of accuracy in the response. Nevertheless, setting up the autopilots in the longitudinal and lateral motions separately to start assures that the separate parts work before the full autopilot is combined.

Longitudinal-Pitch Model

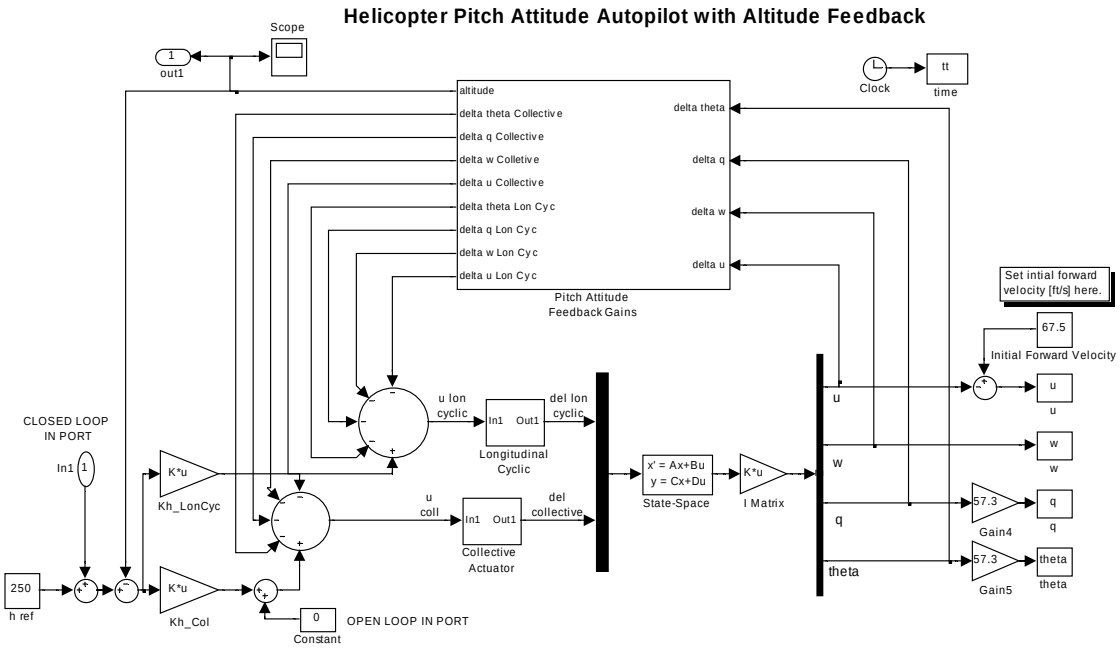

Figure 16. Longitudinal Autopilot with Altitude Feedback.

The longitudinal model with altitude feedback is shown in Figure 16. The helicopter plant model had only four states in this simulation, forward velocity, u, vertical velocity, w, pitch rate, q, and pitch angle, θ. The two longitudinal control inputs are represented, longitudinal cyclic, and collective.

The methodology of how the altitude outer loop gains (one per control input) were chosen will be discussed in the outer loop gain optimization section later in this chapter.

The aim of this simulation model was to ensure that the flight controller tracked the altitude inputs it was given. It did and so the lateral-directional controller was looked at next.

Lateral-Directional Model

The lateral-directional model developed is shown in Figure 17.

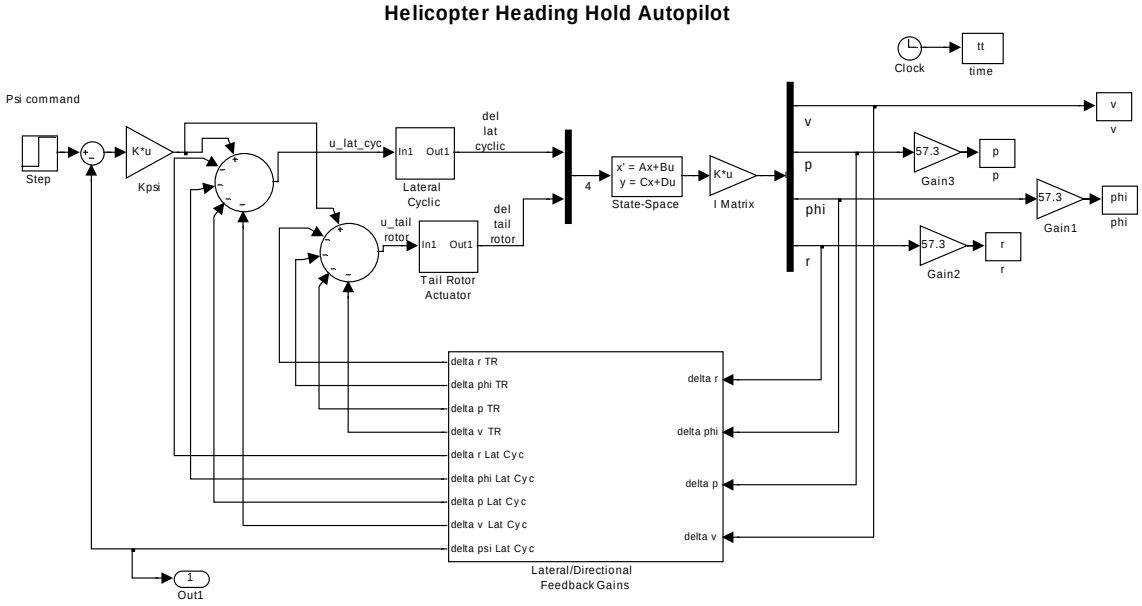

Figure 17. Lateral-Directional Autopilot.

The helicopter plant model in this autopilot consisted of the following states: sideslip velocity, v, roll rate, p, roll angle, φ, and yaw rate, r. The control inputs were lateral cyclic and tail rotor. Like the longitudinal model, the methodology of how the heading outer loop gain was chosen will be discussed in the outer loop gain optimization section later in this chapter.

The objective of this controller was to make sure the response tracked any heading command. It did, so the two halves were combined with the full 8 X 8 coupled plant.

Complete Lateral-Longitudinal Model

The complete autopilot system with altitude and heading feedback is shown in Figure 18. This autopilot shows the off-axis feedback to account for the off-axis coupling in the helicopter dynamics. The integration of both motions and the ability to track both heading and altitude commands was the objective end state of this controller. It successfully tracked all heading and altitude commands, so the beta feedback loop was developed next.

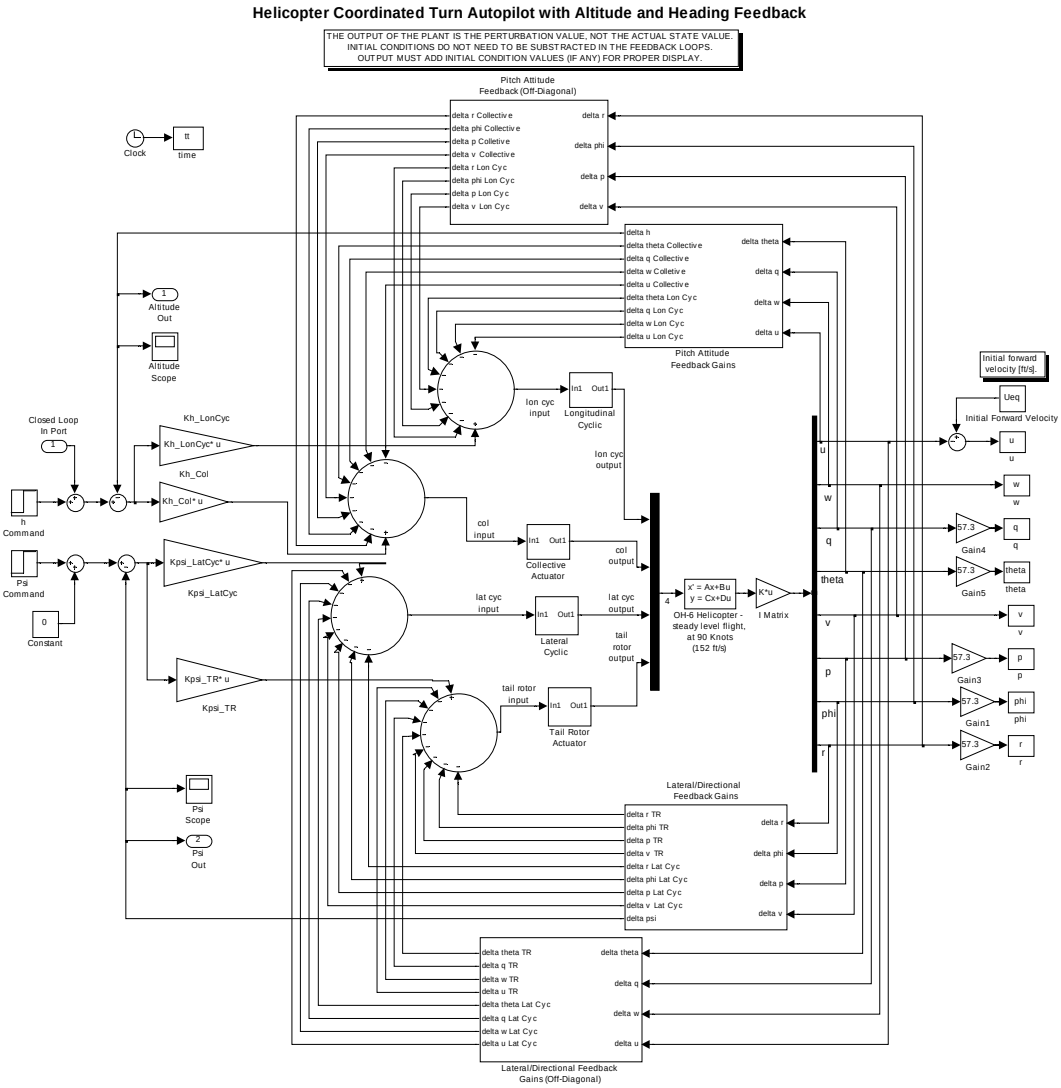

Figure 18. Lateral/Longitudinal Autopilot with Altitude and Heading Feedback.

Sideslip Control Model

Sideslip/beta angle is shown in Figure 19.

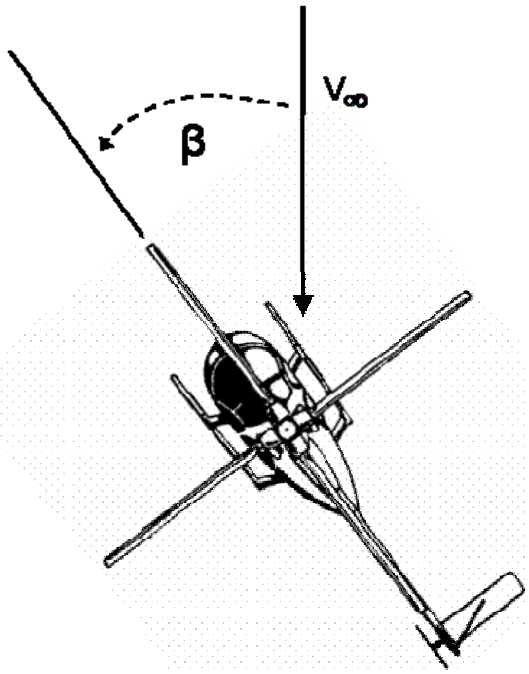

Figure 19. Sideslip/Beta Angle.

If an air vehicle has a positive v component, or positive sideslip velocity, positive defined as shown in Figure 14, then the aircraft will have a beta angle with its nose to the left as shown. Thus, positive beta angle is defined nose left as shown in Figure 19.

The value of the angle, β, is defined by the following:

$$\beta = \sin^{-1}\frac{v}{V} \tag{33}$$

where:

v ≡ sideslip velocity of the aircraft CG (ft/s)
V ≡ magnitude of the total velocity vector of the aircraft CG (ft/s)

This quantity is needed to control the direction of the helicopter while its nose is oriented in a different direction. This is the essence of the beta feedback control. Traditionally, heading, ψ, is commanded to steer the aircraft in a desired direction. In order to keep the aircraft on a given trajectory while its nose is oriented in a different direction, another degree of freedom is introduced, β. The new model is presented in Figure 20, with the diagram's sub-components displayed in Appendix C.

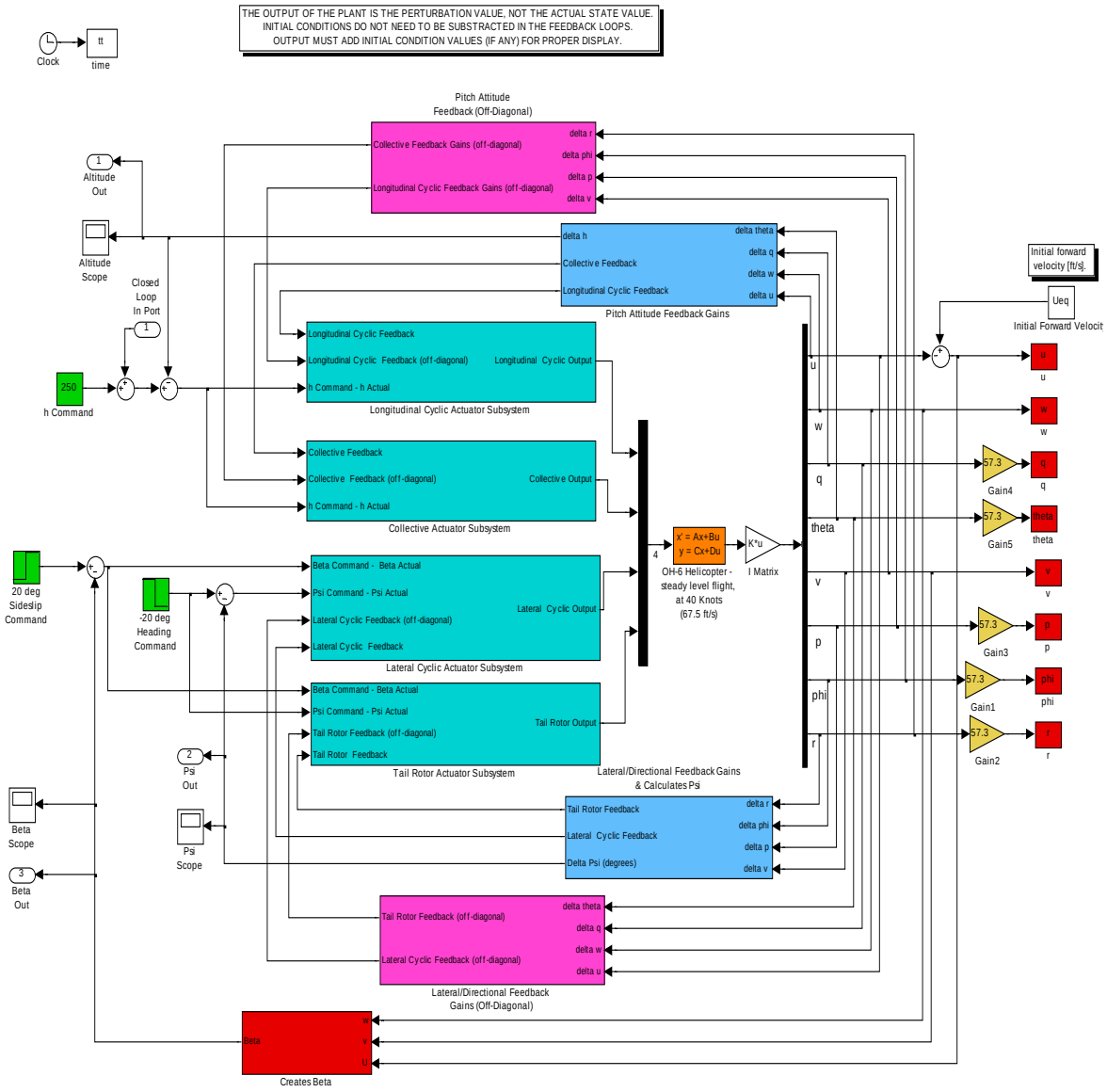

Figure 20. Complete Autopilot with Beta Feedback.

System Response

The system response to simultaneous step inputs of 250 ft altitude increase, -20 degree heading command and a 20 degree beta command is shown in Figure 21. This response does not include any actuator dynamics. Including actuator dynamics in this beta feedback simulation model will be left for follow-on work.

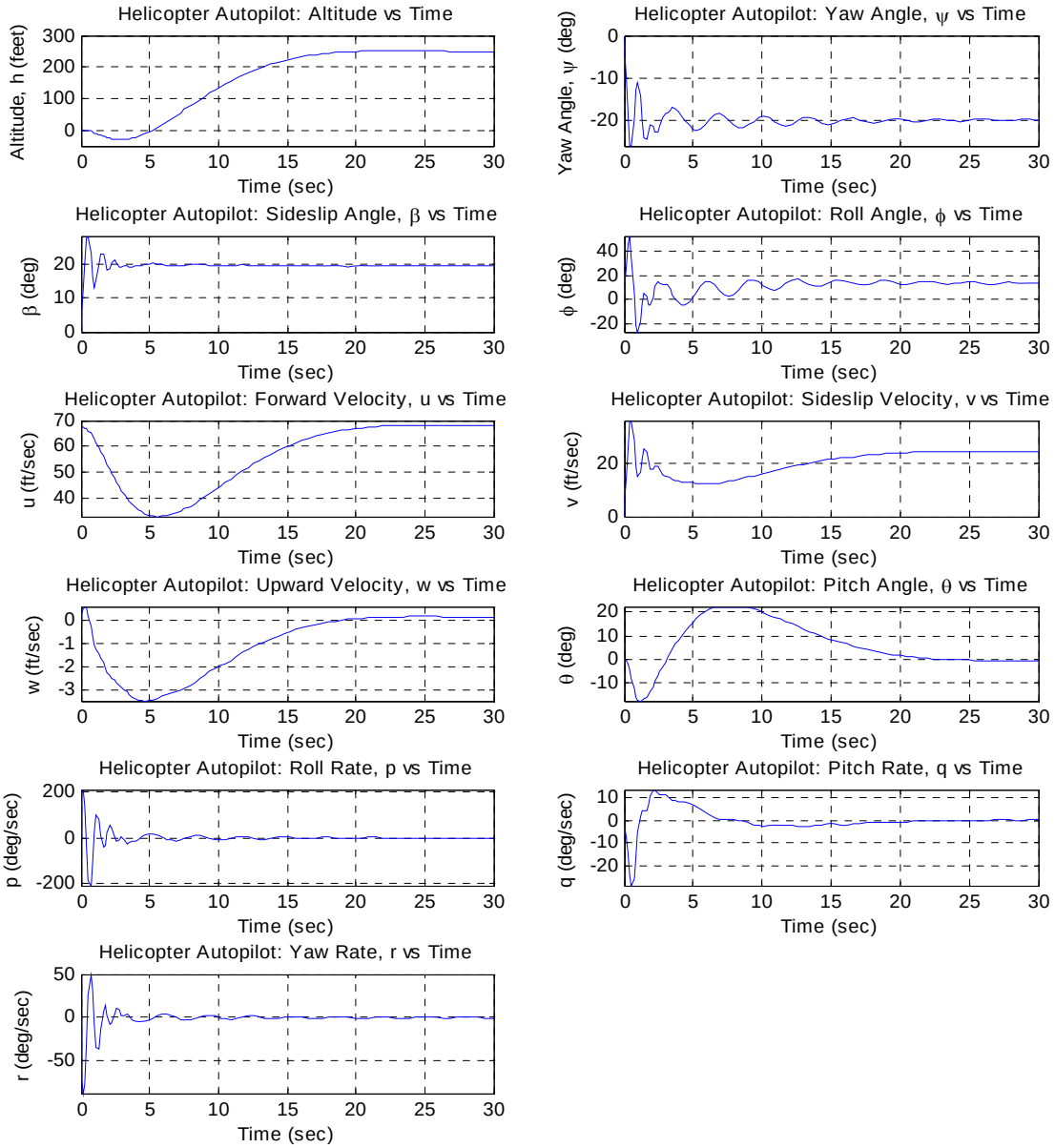

Figure 21. Controller Simulation to 20° Beta, -20° Heading, and 250 ft Altitude Step Commands, no Actuator Dynamics.

As shown, the controller tracks all commands well with good convergence. The immediate response of the helicopter in pitch angle and pitch rate seems counterintuitive. The response is in the negative direction when a positive step input in altitude is made. This response, while counterintuitive, is due to two factors: first, the pitch rate, q, component of the pitch oscillation eigenvector shown in Table 21, is negative. Second, the cross-coupling response in the yaw and roll axes. This is consistent with other published works showing cross-coupling helicopter response (28).

Outer Loop Gain Selection using Multi-Objective Optimization

Figure 20 includes gains on the differences between commanded altitude and actual altitude, commanded heading and actual heading, and commanded sideslip angle and actual sideslip angle. The gain on the altitude feedback has two components: one to the longitudinal cyclic input, and one to the collective input. The gain on the heading feedback is broken down into a gain for the lateral cyclic input and a gain for the tail rotor input. The same is true for individual gains on the sideslip angle feedback loops.

There are a couple of techniques that can be chosen to select the outer-loop gains. The original **A** matrix could be appended to include the additional states ψ, β, and h. Design variables could have been selected for these states and the desired eigenvalues and eigenvectors assigned with eigenstructure assignment, much the same way the inner-loop gains were selected. Another way to select these outer-loop gains is through multi-objective optimization. Multi-objective optimization was selected for this study.

Matlab's FMINCON command was at the core of the optimization process. It uses a gradient search technique to minimize a user-defined multi-objective cost function.

In this case, the cost function contained 2 objectives for the altitude output, 3 objectives for the heading output, and the same 3 objectives for the sideslip angle output. The simulation performance objectives and their associated cost functions and weighting values are shown in Table 23.

Table 23. Multi-Objective Optimization Cost Functions and Weights

Design Variable	Objective	Objective Cost Function	Weighting Value
Altitude, h	Final Track Ability	$cost1 = \lvert h_{last} - h_{command} \rvert$	2
Altitude, h	Max Difference from Command	$cost2 = \lvert \max(h - h_{command}) \rvert$	1
Heading Angle, ψ	Final Track Ability	$cost3 = \lvert \psi_{last} - \psi_{command} \rvert$	2
Heading Angle, ψ	Max Difference from Command	$cost4 = \lvert \max(\psi - \psi_{command}) \rvert$	3
Heading Angle, ψ	Convergence	$cost5 = \left\lvert \max(\psi_{last\frac{1}{3}} / \psi_{command}) \right\rvert$	2.5
Sideslip Angle, β	Final Track Ability	$cost6 = \lvert \beta_{last} - \beta_{command} \rvert$	2
Sideslip Angle, β	Max Difference from Command	$cost7 = \lvert \max(\beta - \beta_{command}) \rvert$	5
Sideslip Angle, β	Convergence	$cost8 = \left\lvert \max(\beta_{last\frac{1}{3}} / \beta_{command}) \right\rvert$	3

The overall cost function is then:

$$J = \sum_{i=1}^{n} W_i cost_i \tag{34}$$

The altitude parameters were final altitude and max deviation from the command, and the heading and sideslip parameters were final value, max deviation from command, and slope of the last third of the output vector to ensure convergence. The optimization program runs the flight controller for some designated time period and then looks at the results of the simulation. It then perturbs the gain values mentioned in some direction until it finds a gradient that minimizes the cost function. It continues searching to minimize the cost function until it reaches a defined gradient tolerance. The optimization call file contains initial values which the optimization function is very sensitive to due to the non-linear nature of the simulation. Although the plant is a linear helicopter dynamics model, the beta angle calculation shown in Appendix C makes the controller non-linear. Due to the initial condition sensitivity, the results of the output to the optimization have to be scrutinized carefully as the FMINCON function will find local minima solutions that may not give the researcher the simulation response he/she desires.

Initial conditions of zero for the gains were often a good starting point for the optimization routine as it did not put any bias on which way the program would search for a minimum solution. However, sometimes zero for the gain initial conditions produced a solution of all gains equal to zero, so a perturbation in either the positive or negative direction was necessary.

After an iterative process of solving for a solution vector and then re-initiating the optimization routine with the solution set found, a set of gains was found that produced the desired tracking response, final tracking value, and convergence. Those values are

presented in Table 24. Appendix E – Thesis8_optimize_call.m, and Appendix F – Thesis8_cost.m, contain the Matlab code created to select these gains.

Table 24. Controller Gains for Altitude, Heading, and Sideslip Angle Feedback.

Kh_LonCyc	0.0072
Kh_Col	-0.0016
Kpsi_LatCyc	0.5
Kpsi_TR	-2.6789e-04
Kbeta_LatCyc	1.372
Kbeta_TR	-0.0782

where:

K ≡ gain
h ≡ altitude
LonCyc ≡ Longitudinal Cyclic Input
Col ≡ Collective Input
LatCyc ≡ Lateral Cyclic Input
TR ≡ Tail Rotor Input

V. Path Following and Radar Exposure Minimization

Controlling Route Trajectory with Sideslip Angle, β vs. Heading Angle, ψ

It is important for the purpose of this work to clearly demonstrate how heading and sideslip angles are related for the purposes of route following and radar exposure minimization. If the β and ψ commands are equal and opposite in their magnitude, the vehicle will follow a straight path as shown in Figure 22.

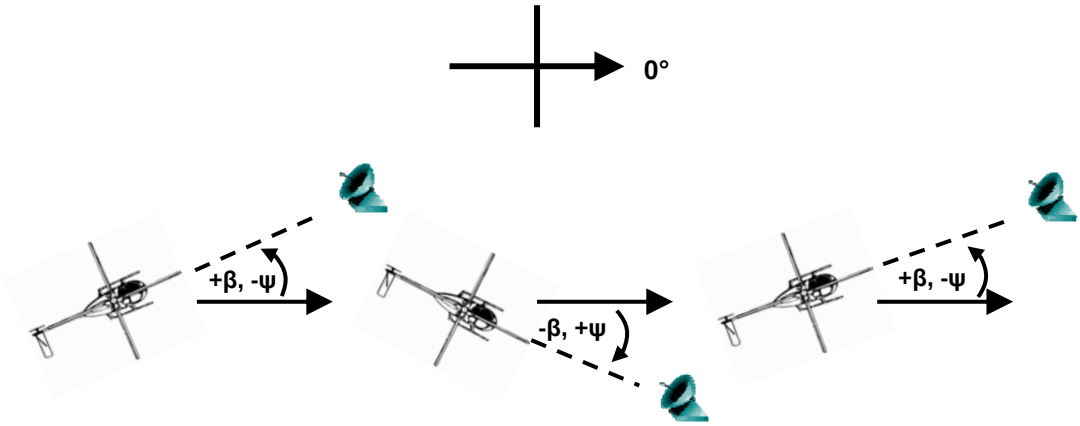

Figure 22. Changing β and ψ Angles, Straight Trajectory.

Example beta and heading angle commands necessary to generate the straight trajectory in Figure 22 is shown in Figure 23.

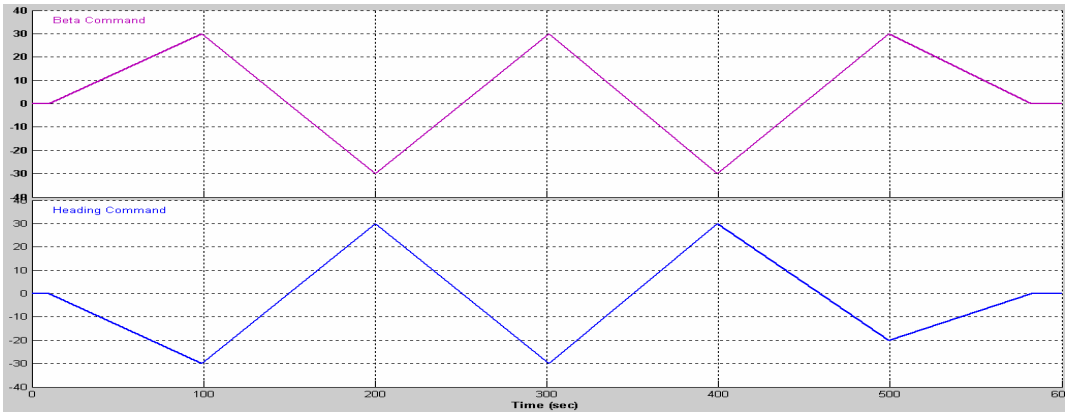

Figure 23. Example Straight Path Beta and Heading Commands.

If however, the β and ψ commands are not equal and opposite, the path can change as shown in Figure 24.

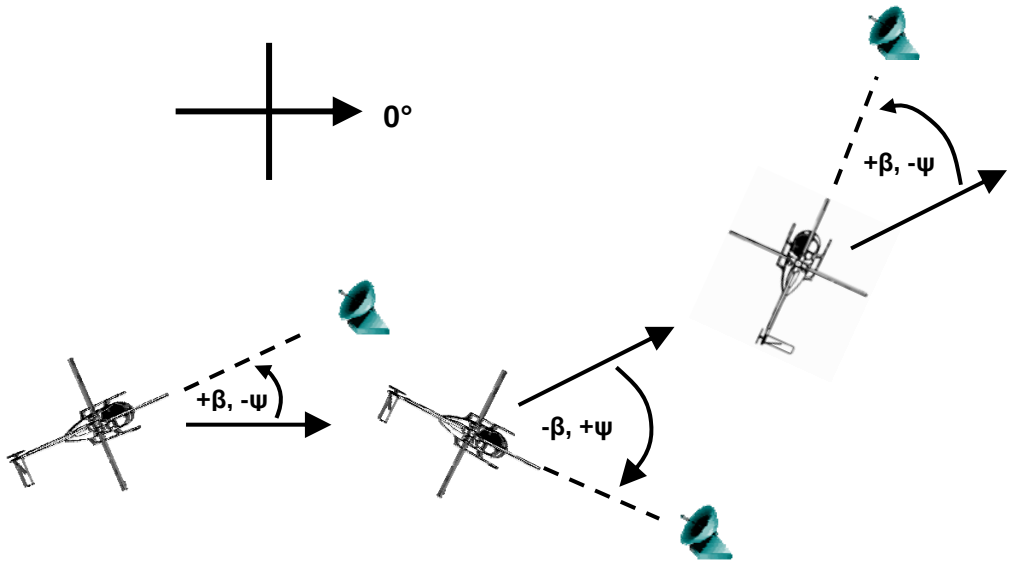

Figure 24. Changing β and ψ Angles, Changing Trajectory.

Thus, route trajectory can be controlled, not by commanding heading angle, ψ, like traditional guidance systems, but by commanding sideslip angle, β. This is a new concept that this author could not find published research on. Any path optimization commands get closed around the sideslip angle loop, and the orientation optimization commands get closed around the heading angle loop. This is a departure from conventional navigation systems that command heading to control the vehicle's route. A generic controller outlining this idea is presented in the "Conclusions" section of this work, Figure 36.

Optimized Trajectory and Altitude, no Sideslip

What is now sought is a set of optimized beta and heading angle commands that will result in no radar exposure, or the least amount of it, in a representative threat

environment. Figure 25 shows a representative hostile radar environment with an associated radar cross section outline around the UAV. The actual radar cross section of the OH-6A helicopter will be left for follow-on research. The assumption made here is that the actual UAV RCS falls within the diamond shaped RCS depicted in the figures. The diamond shape was chosen because of the actual RCS plot of the A-7 Corsair in Figure 3 which can be characterized as a diamond shape. With no change in the UAV's orientation, flying with no sideslip, as conventional piloted air vehicles fly today, the vehicle is exposed over a large portion of the 10 minute route depicted in Figure 25.

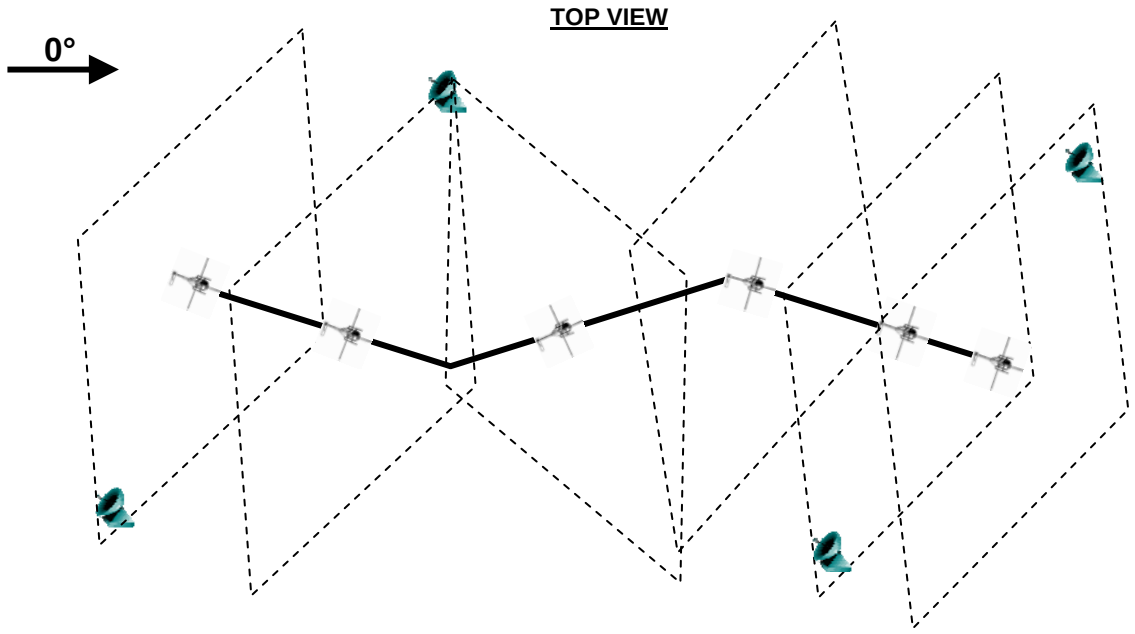

Figure 25. Example Radar Cross Section Exposure, no Sideslip Angle Changes.

If the vehicle is allowed to change orientation along the route, RCS exposure can be reduced significantly, even eliminated completely for the radar environment depicted in Figure 25. The altitude, heading, and sideslip commands that the flight controller would need to execute during the 10 minute route depicted is shown in Figure 26. This

route includes an 800 ft obstacle that the vehicle must traverse. In this way, the aircraft flies coordinated turns along the route with no sideslip, the way piloted aircraft fly today.

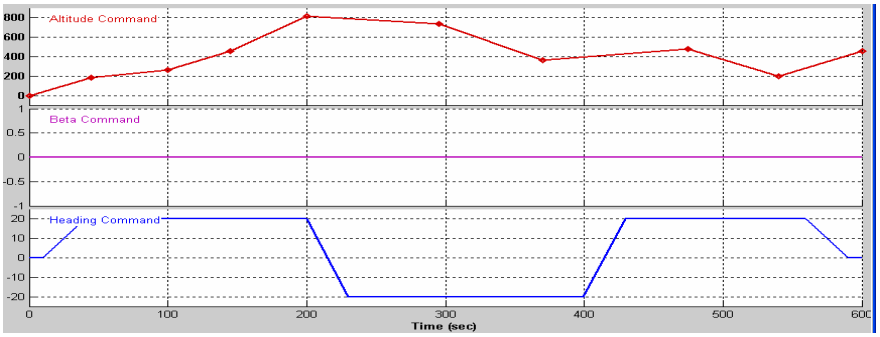

Figure 26. Altitude, Sideslip, and Heading Commands to Fly Route Depicted in Figure 25.

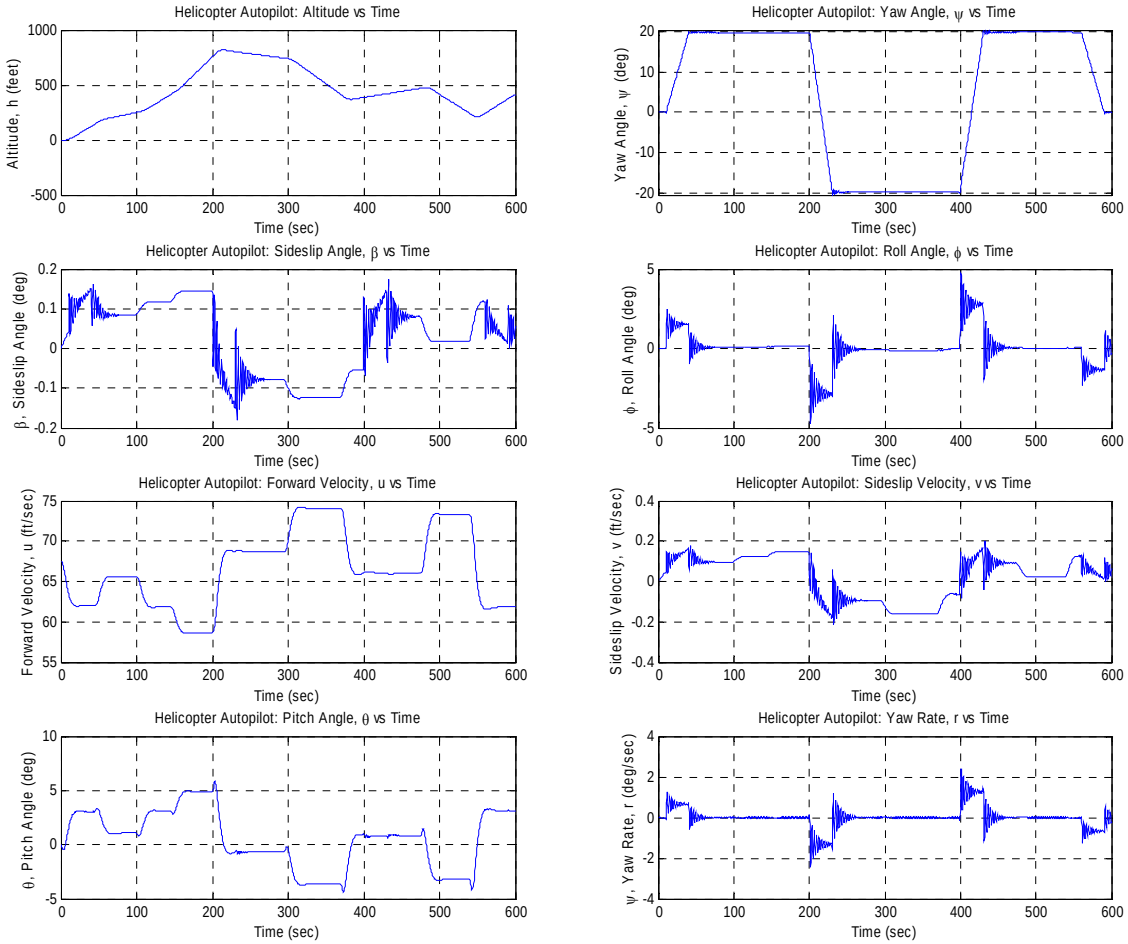

Figure 27. Aircraft Response to Commands in Figure 26, No Sideslip.

Optimized Trajectory and Altitude, with Sideslip

If the flight controller is able to change the orientation of the vehicle along the route due to known or sensed threat radar, then the aircraft's RCS exposure can be reduced substantially, and maybe even eliminated. Figure 28 shows how the UAV's RCS exposure changes if it is allowed to change its heading while still flying the same planned route.

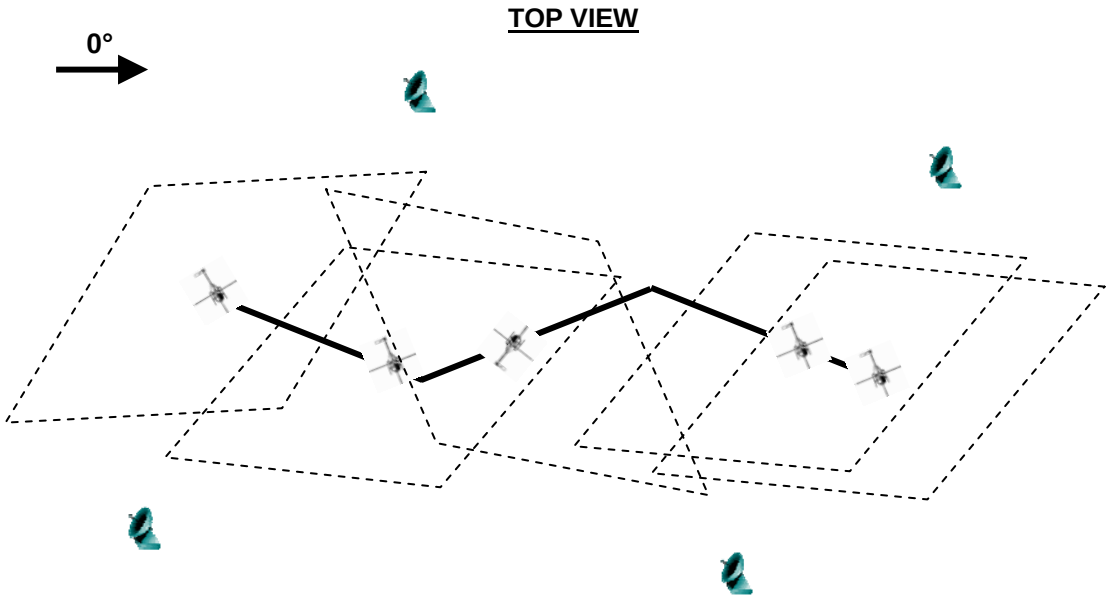

Figure 28. Example Radar Cross-Section Exposure, with Sideslip Angle Changes.

It's important to note the changes in the relationships between the heading and sideslip angles as the route changes. While the route remains straight, the relationship between the two angles ψ and β remains equal and opposite, as stated previously. However, when the path changes direction, the beta command will change to command a change in the vehicles route. The heading angle, ψ, may or may not change, depending

on the threat condition. Figure 29 portrays the relationships between the two angles along the three segments of the route.

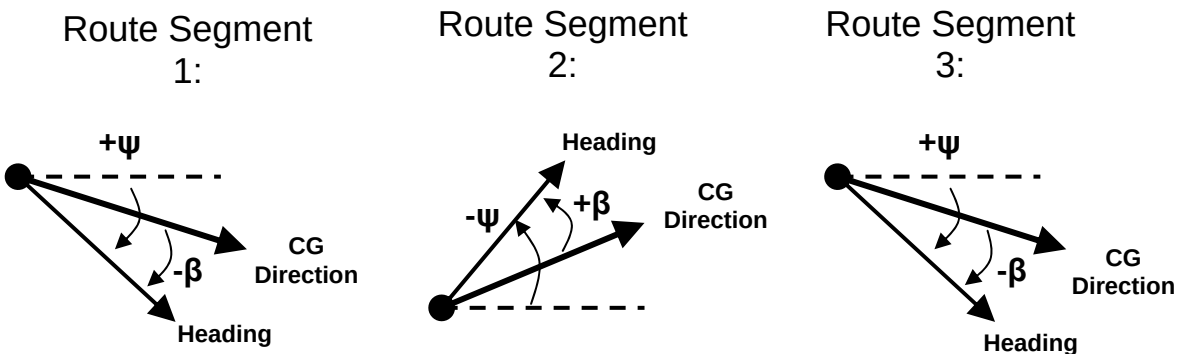

Figure 29. Changing Beta and Psi Angles as Route Changes.

Figure 30 shows representative beta and heading angle commands needed to fly the orientation and route shown in Figure 28. The flight controller is given 30 seconds to make the 60 degree beta angle changes and 100 degree heading changes.

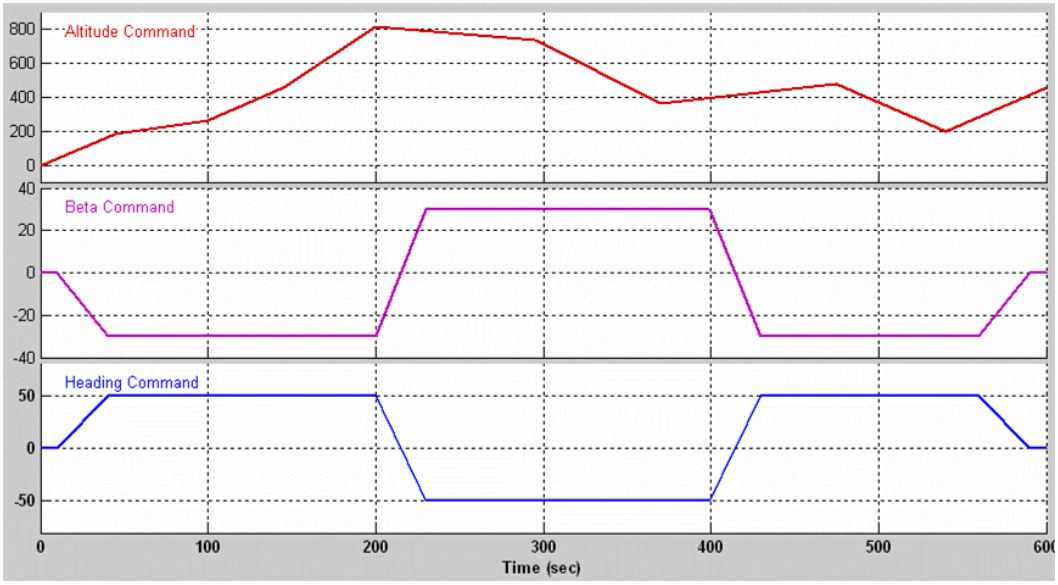

Figure 30. Altitude, Beta and Psi Commands for Mission Depicted in Figure 28.

The aircraft response to the commands shown in Figure 30 is shown in Figure 31.

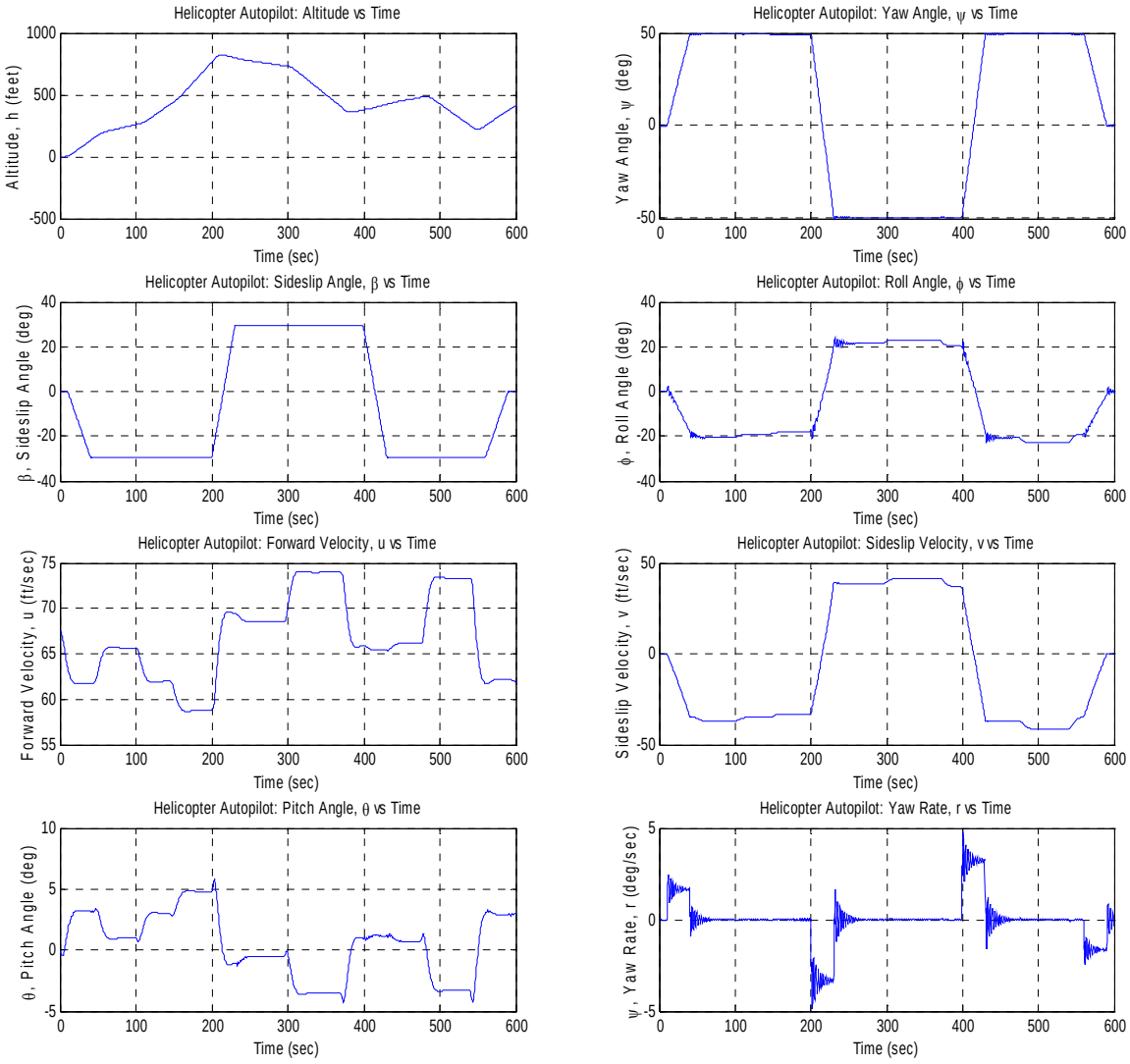

Figure 31. Aircraft Response to Altitude, Beta, and Psi Commands in Figure 30.

As can be seen from these results, the controller tracks the altitude, sideslip and heading commands very well.

The final flight controller is shown in Figure 32. The diagrams to the controller's sub-components are located in Appendix C.

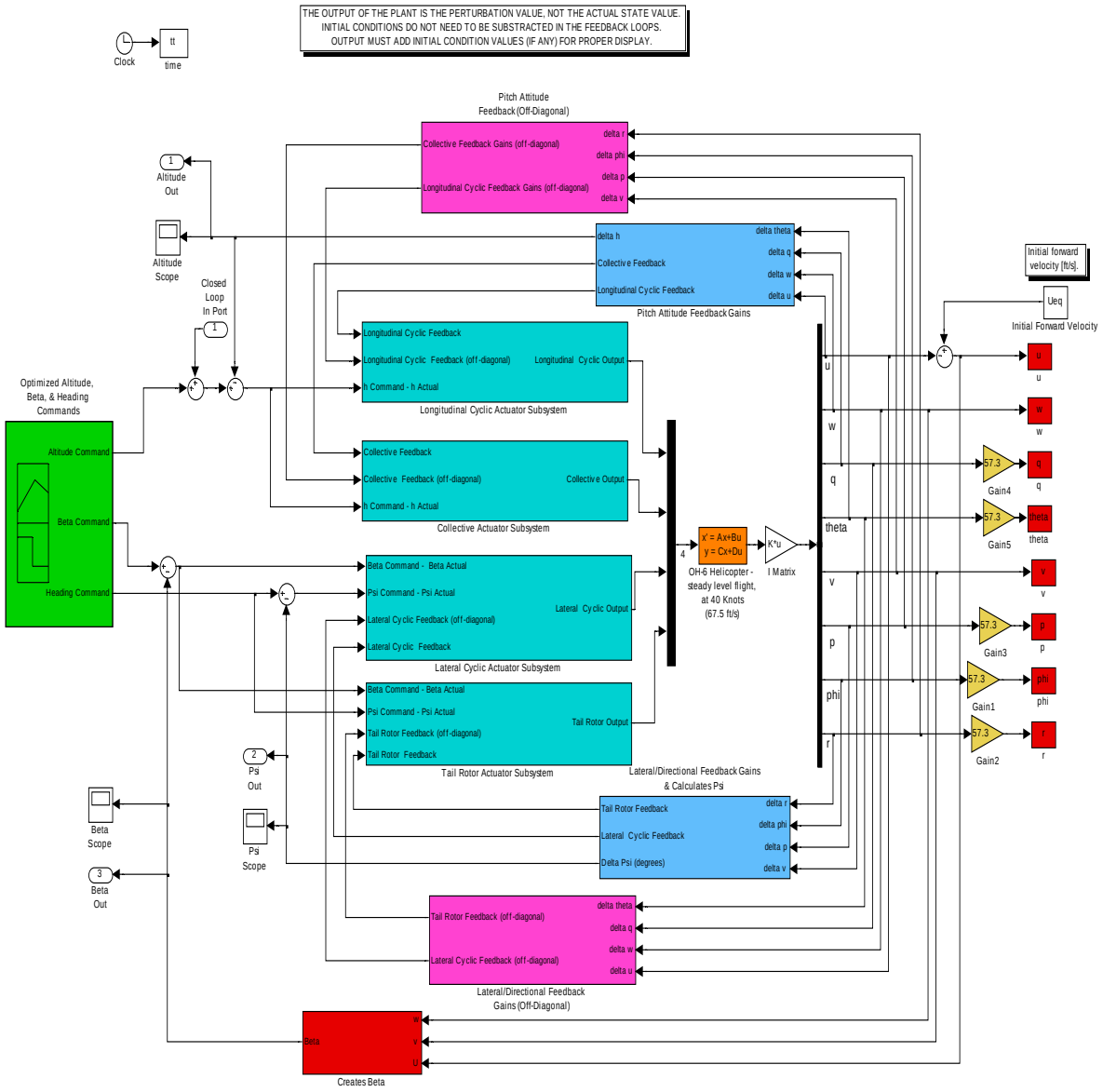

Figure 32. Final Flight Controller Diagram. Sub-Components in Appendix C.

RCS Exposure Comparison Results

The portions of the route where the aircraft's radar cross section is exposed to radar is shown in Figure 33 and is marked by a solid line along the route. The exposed time along the route amounts to 2/3rds of the route, or 6 minutes and 40 seconds of the 10 minute total flight in this example.

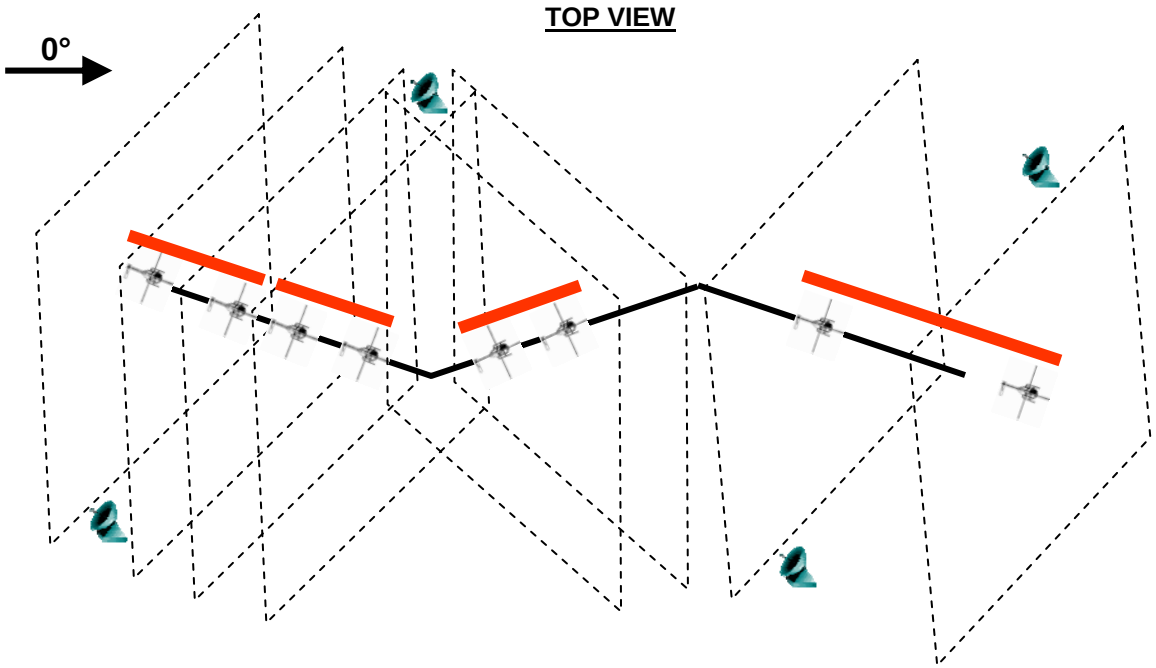

Figure 33. Aircraft RCS Exposure along the Route, no Beta Feedback.

Table 25. Radar Cross Section Exposure with no Beta Feedback (40 knots).

Total Flight Time (min)	10:00
Exposed RCS Along Route (min)	6:40

As shown previously, the exposure time along the same route with beta feedback is 0:00.

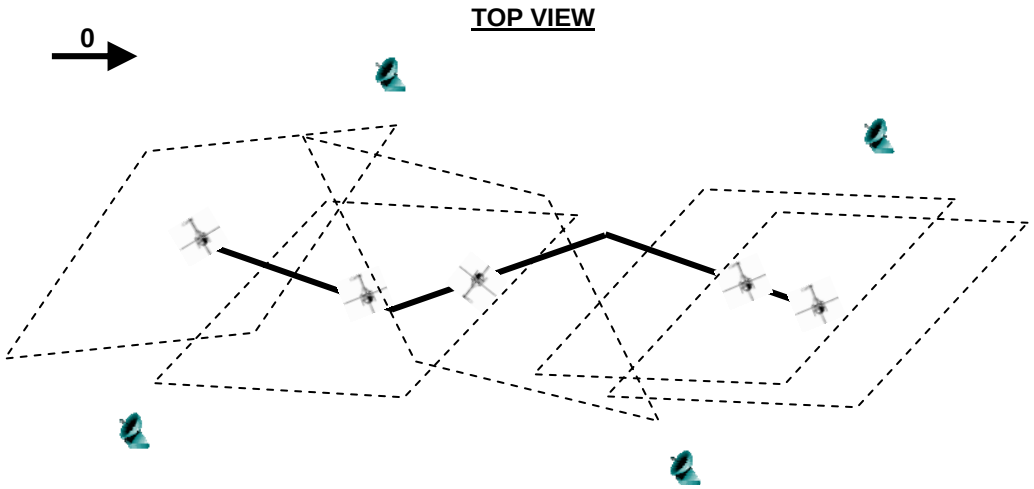

Figure 34. Aircraft RCS Exposure with Beta Feedback.

Table 26. Radar Cross Section Exposure with Beta Feedback (40 knots).

Total Flight Time (min)	10:00
Exposed RCS Along Route with Beta Feedback (min)	0:00

If, however, the UAV is allowed to fly at a faster speed for ingress and egress, the time along the route is significantly reduced. Traveling at 100 knots, with no sideslip angles used, the vehicle traverses the same route in 4 minutes. The cost of using the sideslip angle then is airspeed. The faster the UAV travels, the less sideslip it is able to use because of helicopter sideward flight limits that guarantee directional control authority.

Table 27. Radar Cross Section Exposure with no Beta Feedback (100 knots).

Total Flight Time (min)	4:00
Exposed RCS Along Route (min)	2:40

Beta Feedback Cost

The type of beta feedback controller described in this work would be limited to the maximum sideward flight velocity of the air vehicle it was built around. For most helicopters, maximum sideward flight is limited by tail rotor authority, or the ability of the tail rotor to produce enough thrust to keep the aircraft oriented in the direction it is commanded. Most light helicopters today have sideward flight limits of between 35-40 knots. If, for instance, the helicopter model was trimmed around 100 knots instead of 40 knots as was chosen in this work, the sideward flight state v, would have to be monitored

until enough sideslip angle caused a sufficient amount of sideward velocity to reach the aircraft's maximum limit.

Figure 35 shows how sideslip velocity increases as beta increases. When beta is 90 degrees for example, sideslip velocity is at its maximum, or equal to the velocity of the aircraft CG. This in effect, becomes the cost of utilizing beta angle feedback. As beta angle is increased, the aircraft's CG velocity is limited to its sideward flight limit. Thus, an aircraft traveling at high speeds would have to slow down prior to utilizing an orientation change to minimize radar exposure, or the amount of beta angle used would be limited to a performance chart similar to Figure 35.

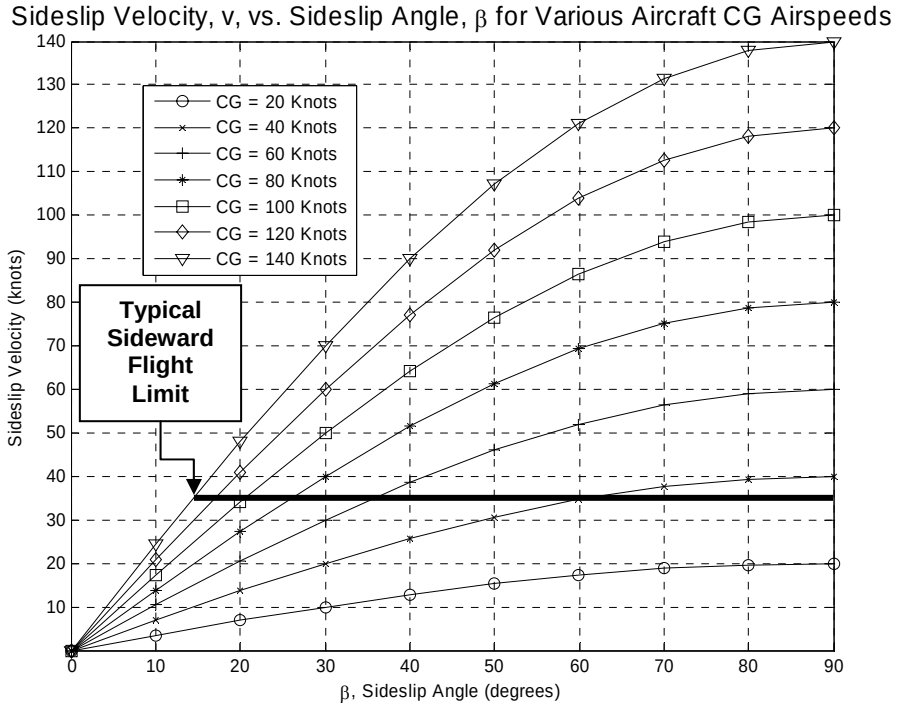

Figure 35. Sideslip Velocity, v, Increase as Sideslip Angle, β, Increases

For example, a UAV traveling at 100 knots, with a 35 knot sideward flight limit, would have a beta angle limit of 20 degrees.

Controller Simulation Limitation due to Linear Helicopter Model

As has been stated, the helicopter model developed for this work is a linear model trimmed at 40 knots, sea level, at 95 degrees F. The linear model is only valid for small perturbations around the trim point. Therefore, large commands in beta would necessarily produce a helicopter response in the simulation that would not be representative of the actual aircraft. A non-linear model of the aircraft dynamics would be necessary for this type of simulation. For this reason, beta commands for this work were kept to less than 30 degrees.

VI. Conclusions and Recommendations

Conclusions of Research

This study has accomplished several key objectives:

1) A linear aircraft dynamics model was created for a helicopter that is in close proximity to the size of several rotorcraft UAVs currently in development.

2) A complete rotorcraft flight controller model was created with four control inputs that include full state feedback, and altitude, heading, and beta angle command feedback loops. Eigenstructure assignment was successfully implemented to calculate the gains necessary to shape the response of the helicopter into desired response modes.

3) A new way of commanding a UAV route was introduced. Instead of commanding heading, as is typical for all current flight controllers, this study investigates the feasibility of utilizing the aircraft's beta state as a means of commanding an optimal trajectory, while the heading command is utilized to orient the aircraft in a way that minimizes its RCS exposure to threat radar. Figure 36 shows how a path optimization algorithm can be used to command beta angle, and an orientation optimization algorithm can be used to command heading for an autonomous rotary winged UAV.

4) It was shown that an air vehicle's RCS can be reduced significantly with changes in vehicle orientation. The range at which threat radar can detect an air vehicle is related to the 4^{th} root of the air vehicle's RCS, so small changes in the aircraft RCS can result in large differences in the range at which an air vehicle can be detected. These orientation changes can help to reduce the vehicle's RCS exposure, and potentially even eliminate it, within the limits of the optimized route allowing it to do so.

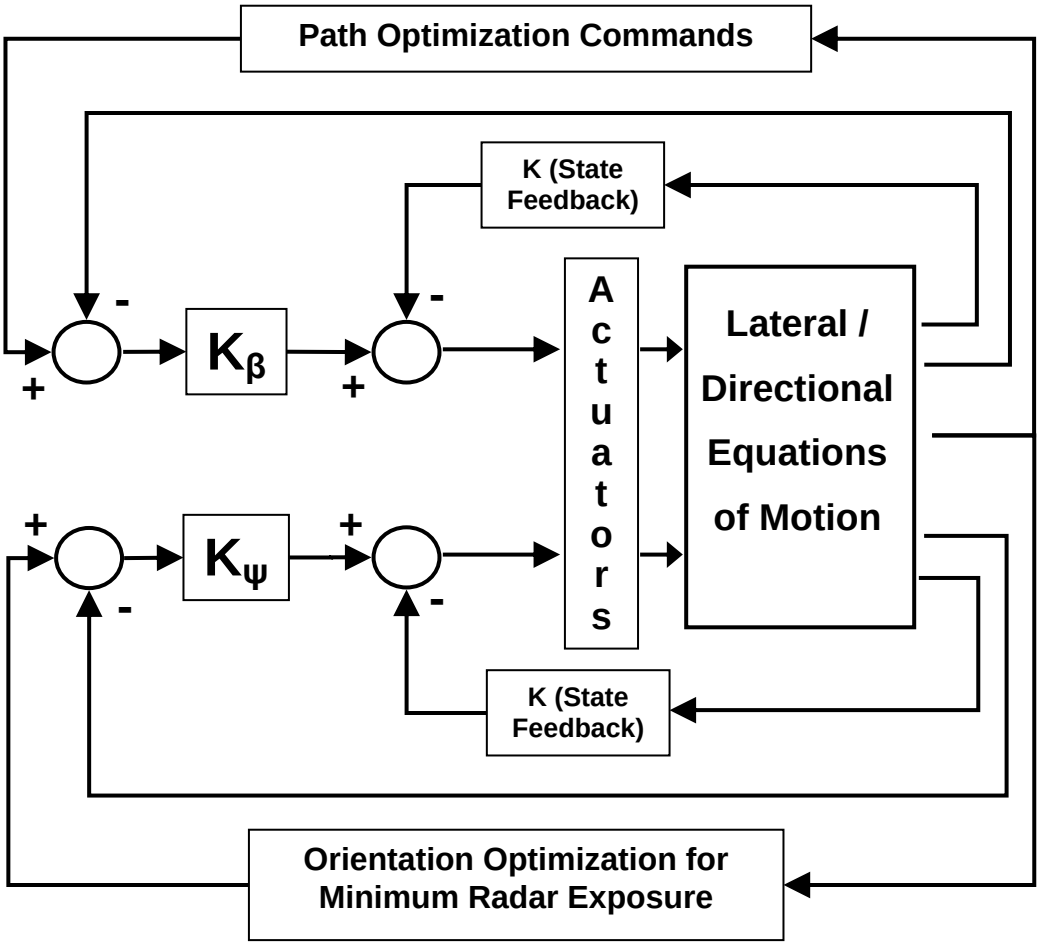

Figure 36. Proposed Lateral Controller for Radar Cross Section Minimization.

Significance of Research

This study is significant in the fact that it adds another variable to the low-observable aircraft equation. For many years, only structural solutions were sought to make aircraft low-observable. While the structural solutions are certainly important, control engineers can contribute to low-observable aircraft through aircraft orientation changes. The contribution that orientation changes can make to low-observable aircraft should not be understated. Pitch, roll and yaw changes can have dramatic effects on an aircraft's RCS.

Helicopters have the unique ability to fly sideward and even backward within structural and directional control limits. Sideslip angle feedback can potentially be of most benefit to them because of this unique capability. Doing so can make these aircraft more survivable, and give them greater chance to successfully accomplish their assigned mission. This can lead to valuable and time-critical intelligence that could give our tactical ground forces the 'picture' they need to successfully prosecute their battles. As the Department of Defense becomes more dependent on UAVs to perform these dangerous yet valuable reconnaissance, security, and attack missions, the success of these UAVs could mean the difference between life and death of our Soldiers.

Recommendations for Future Research

The following were identified during the course of this research as candidates for continued research.

Actuator Dynamics in the Beta Feedback Controller Model.

The controller model that includes beta angle feedback in this work does not include actuator dynamics. All of the other controller models in this study do include actuator dynamics. The response of the beta feedback controller with the actuator dynamics included was initially not good. Given the focus and the scope of this research, including the actuator dynamics in the controller model was deemed unnecessary for demonstrating the concepts of this work. With this work providing the basis and direction for other follow-on work, actuator dynamics should be included in future simulations. During the course of this research, many references were found that listed

the actuator models in their work. These include Garrard and Liebst (27:26) and Walker (28:783).

JANRAD Updates/Fixes.

During the course of this study, some problems with the JANRAD software program were encountered. These made using JANRAD cumbersome initially. The problems encountered include the following:

1) In order to run the Stability and Control module, you cannot start entering helicopter data from a blank input screen. You must modify an existing input file. The JANRAD data files created for this work were OH_6_40.mat and OH_6_40_in.mat and are included on the CD included with this work that contain all of the JANRAD files.

2) In the Stability and Control Module, the JANRAD software has a GUI button that says "SAVE INPUT FILES" that does not work. The Stability and Control data input file must be modified at the base Matlab program, and then loaded into JANRAD.

3) Other airfoil lookup data tables should be loaded into the JANRAD software. Currently there are only a few airfoils to choose from, and this limits JANRAD's applicability.

4) The Stability and Control module GUI is not clear on what values should be entered in its input screens. For example, the GUI prompts the user to input the aircraft "station" location for the vertical fin and horizontal stabilizer. What are intended to be entered here are locations of the vertical fin and horizontal stabilizer's aerodynamic centers. Moreover, the aircraft "station" points are not what are wanted. The moment arms from the aircraft CG is what should be entered in those entry points.

Non-linear Aircraft Model.

In this work, a linear model is developed for the helicopter model. For a more accurate representation of the aircraft dynamics, a nonlinear model of the aircraft dynamics should be developed, especially if large beta angle commands are intended for the vehicle. For this reason, the beta commands given in this work did not exceed 30 degrees from trim.

Actual OH-6A Radar Cross-Section.

In this work, the RCS diagram of the OH-6A was assumed, and assumed to be in the shape of a diamond as depicted in Figure 34. While the actual RCS of an aircraft changes constantly during flight, a more accurate RCS snapshot should be found and integrated into the body of this work.

Path and Orientation Optimization Algorithm that Commands Sideslip Angle and Heading Angle.

Having shown that the closed loop path/route optimization would command sideslip angle and not heading, an algorithm must be developed that would be able to perform this calculation. In other words, having a known route with waypoints that have been optimized to conduct a mission, and knowing the threat radar environment from on-board sensors in the air vehicle, an algorithm must be developed that commands the set of beta and heading angles to achieve the route and orientation desired.

Pitch and Roll Contributions to RCS Reduction.

While this study focused on heading changes as a means to reduce a vehicle's radar cross section, the contributions that pitch and roll have on a helicopter's RCS reduction should also be explored.

Appendix A - Calculation of the Vertical Fin Aerodynamic Center

The Vertical fin Aerodynamic Center was calculated with the aid of a web based aerodynamic surface calculator, "Planform- Analysis Version 1.8" (29). First, the dimensions for the upper vertical fin were entered, the results of which are shown in Figure 37.

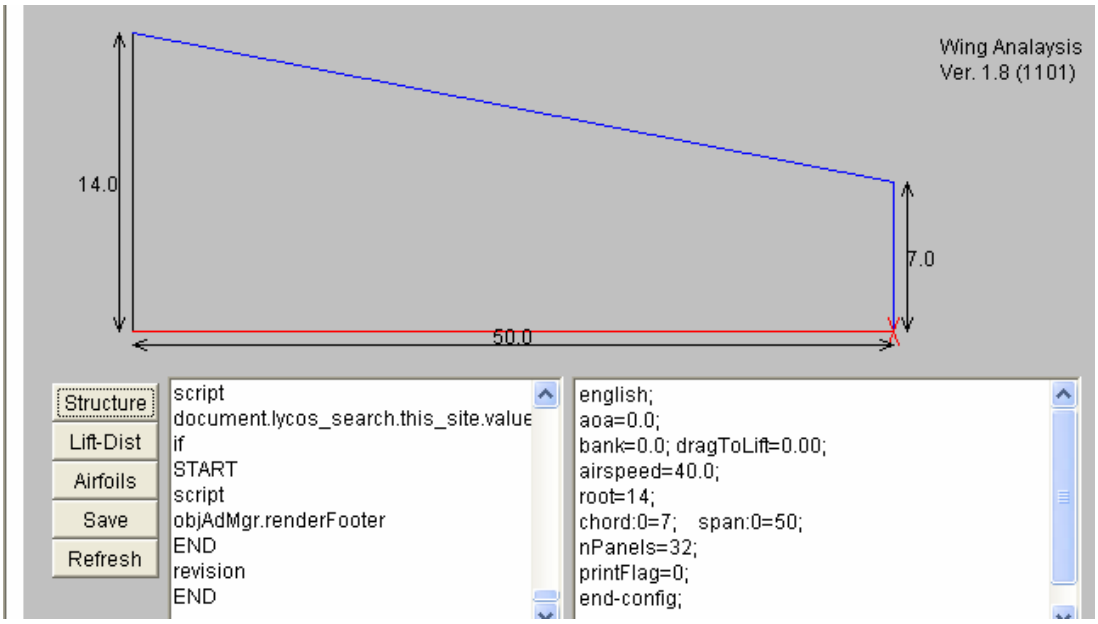

Figure 37. Upper Vertical Fin Planform.

The aerodynamic center (AC) and mean aerodynamic chord (M.A.C.) of this part of the total structure was then calculated and is shown in Figure 38.

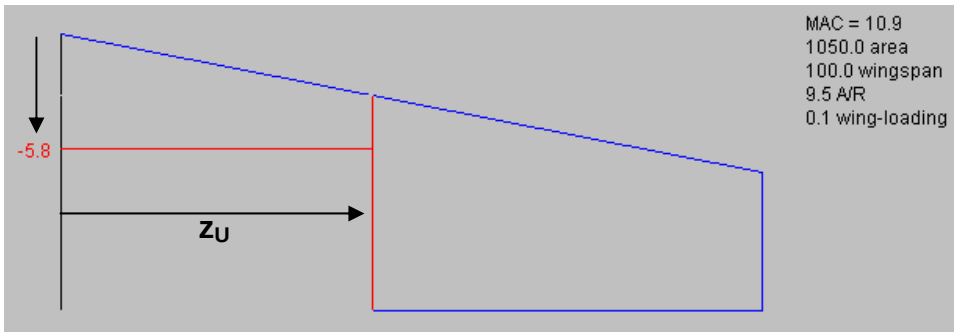

Figure 38. Aerodynamic Center of the Upper Vertical Fin.

The same was done for the lower vertical fin.

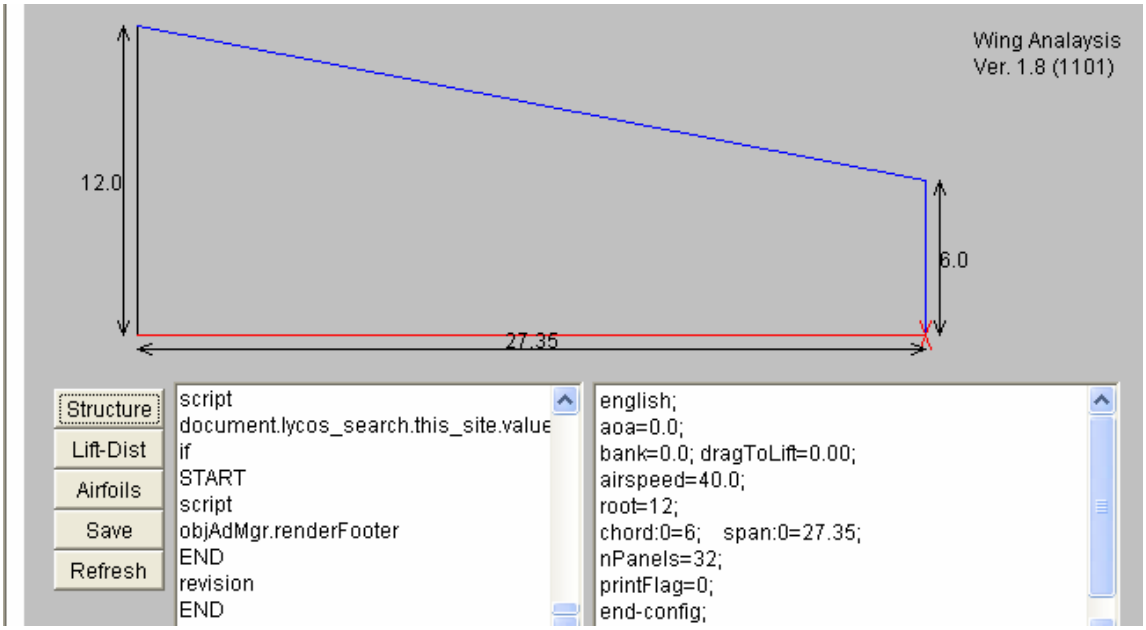

Figure 39. Lower Vertical Fin Planform.

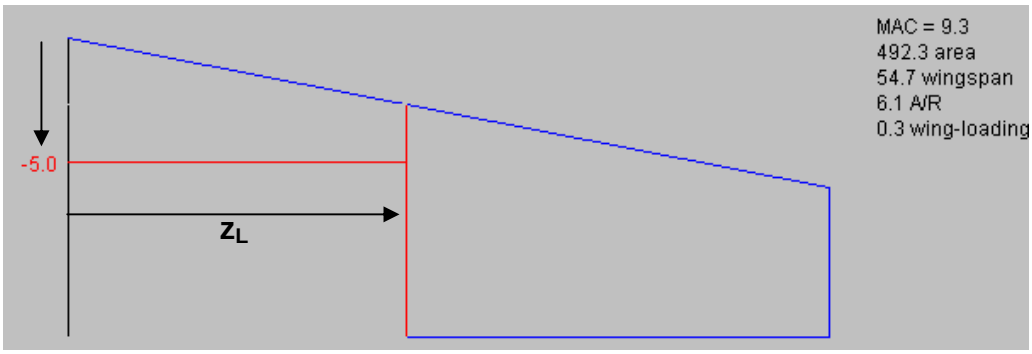

Figure 40. Aerodynamic Center of the Lower Vertical Fin.

Z_U and z_L were found by knowing that the planform areas on either side of the M.A.C. are equal. For the upper vertical fin, the following equation was derived:

$$\frac{z_U}{2}(c_{tu}+c_{ru}) = \frac{50-z_u}{2}(c_{tl}+c_{rl}) \qquad (35)$$

where:

$c_{tu} \equiv$ tip chord of the upper half of the upper vertical fin (in)

$c_{ru} \equiv$ root chord of the upper half of the upper vertical fin (in)
$c_{tl} \equiv$ tip chord of the lower half of the upper vertical fin (in)
$c_{rl} \equiv$ root chord of the lower half of the upper vertical fin (in)

Performing this calculation with the values from Figure 10 resulted in the following, which is shown in Figure 11:

$$\begin{aligned} z_u &= 20.9" \\ z_l &= -11.43" \end{aligned} \tag{36}$$

Finding the location of the aerodynamic center for the entire vertical fin structure was found knowing that the upper vertical fin is twice as large as the lower vertical fin. The following relationship was developed:

$$z = z_u \frac{2}{3} + z_l \frac{1}{3} \tag{37}$$

This yields, $z = 10.12"$. The total height above the aircraft reference line is 54.26” + 10.12” = 64.38”. The aircraft center of gravity (cg) is located at stations (101.85, 0, 49.6) in the x, y, and z locations respectively. The vertical fin aerodynamic center is located at stations (280.65, 0, 64.38) in the x, y, and z directions respectively. Therefore, the moment arms from the aircraft cg are 178.8” or 14.9’ in the x-direction, and 14.78” or 1.23’ above the cg in the z direction.

Appendix B - JANRAD Input Screens

Page 1 input.

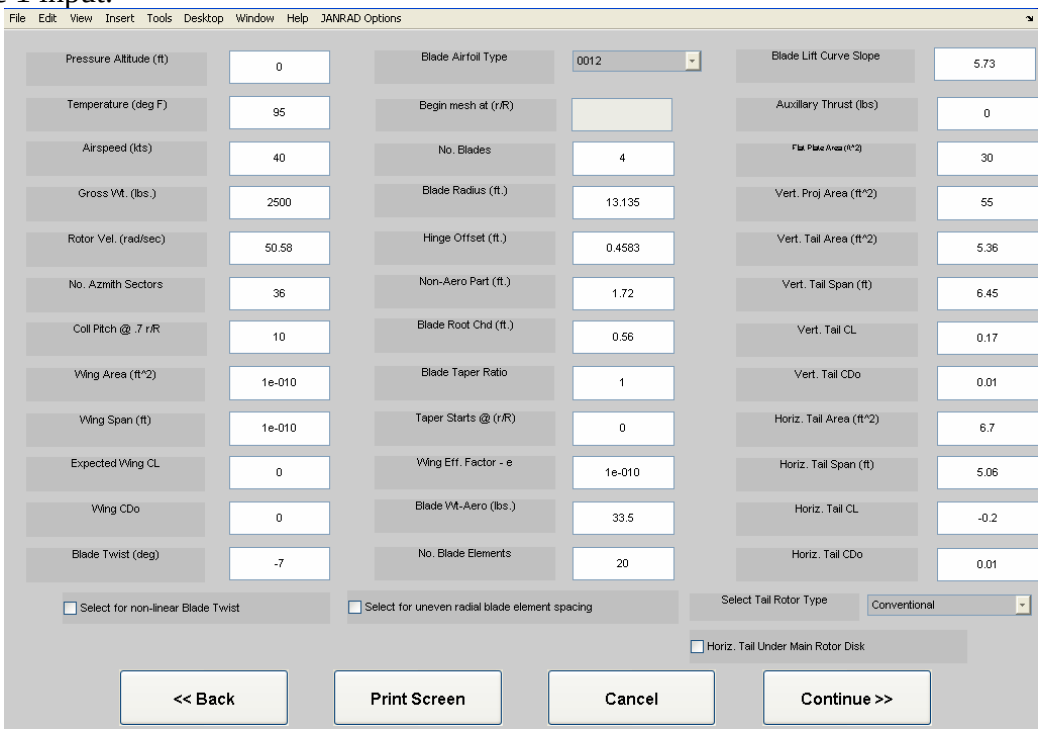

Page 2 input.

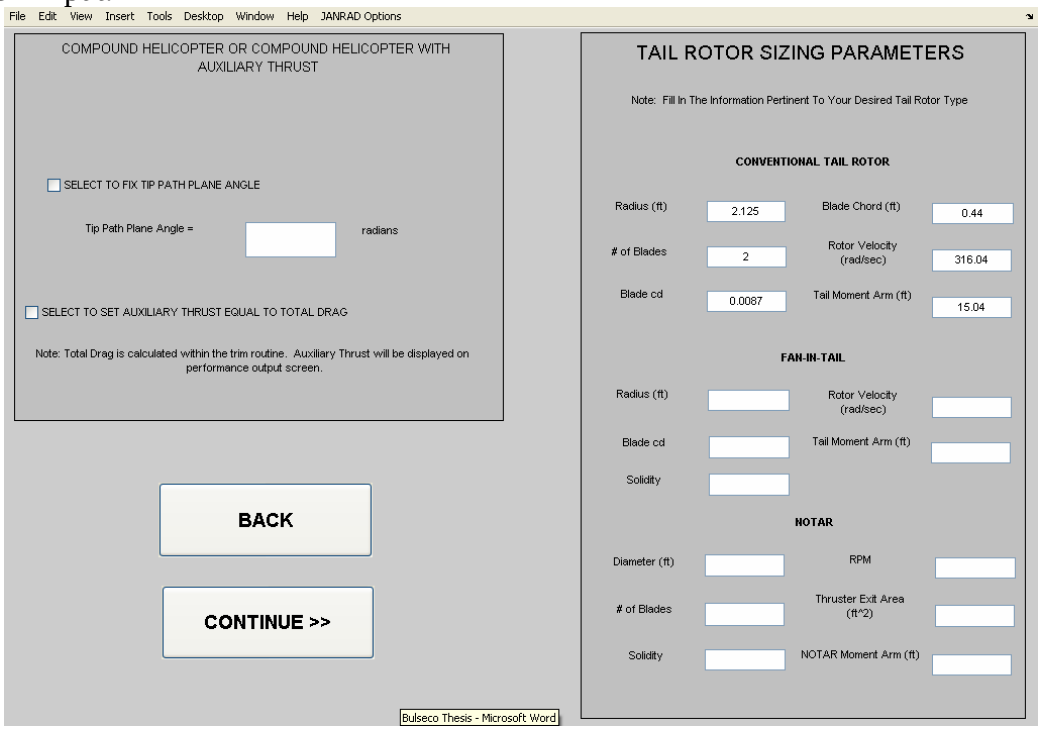

Performance Output Parameters.

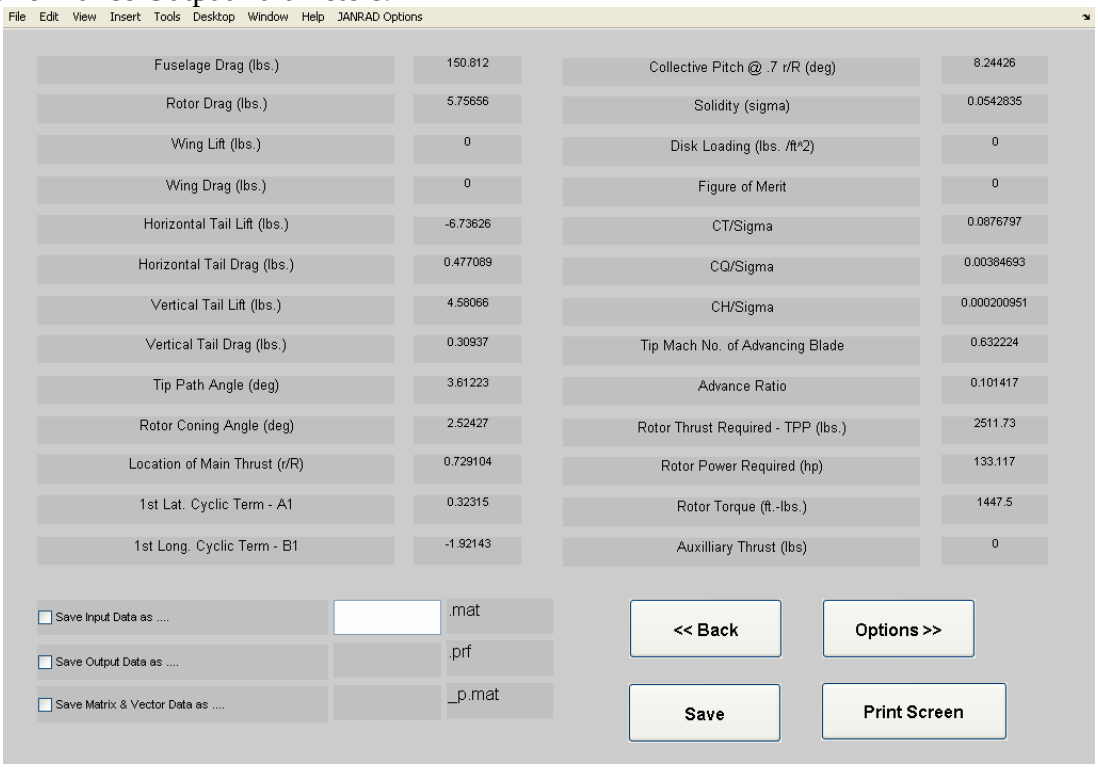

Page 3 input.

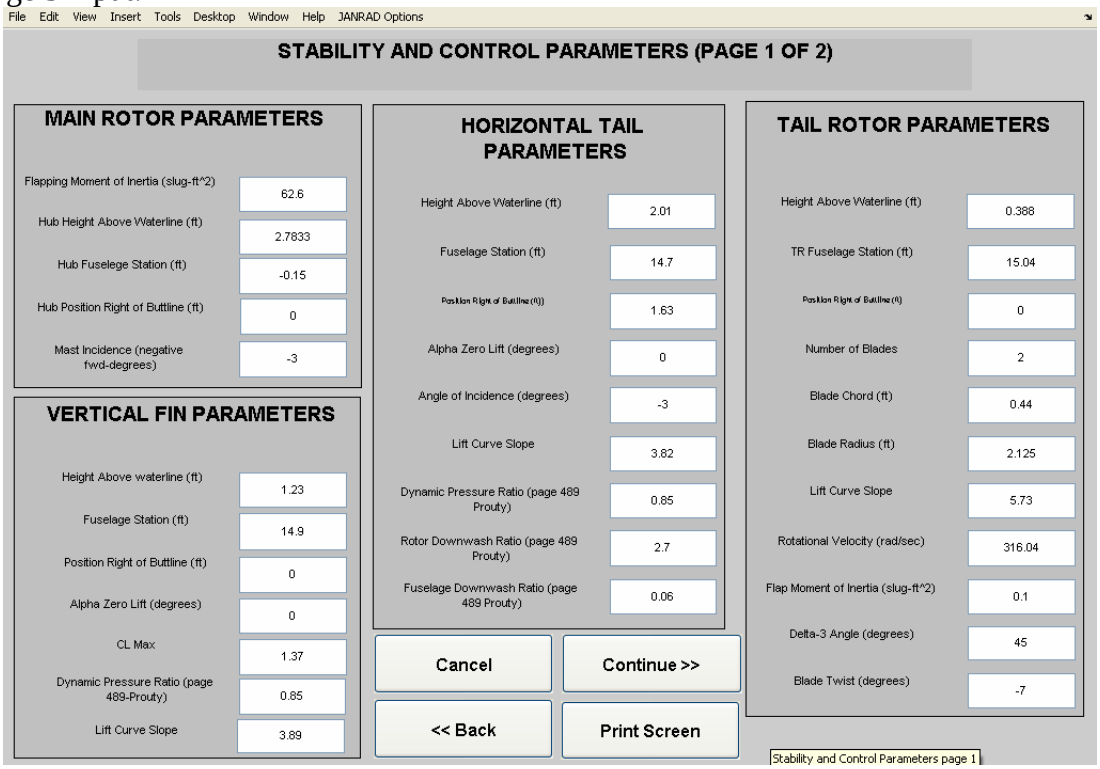

Page 4 input.

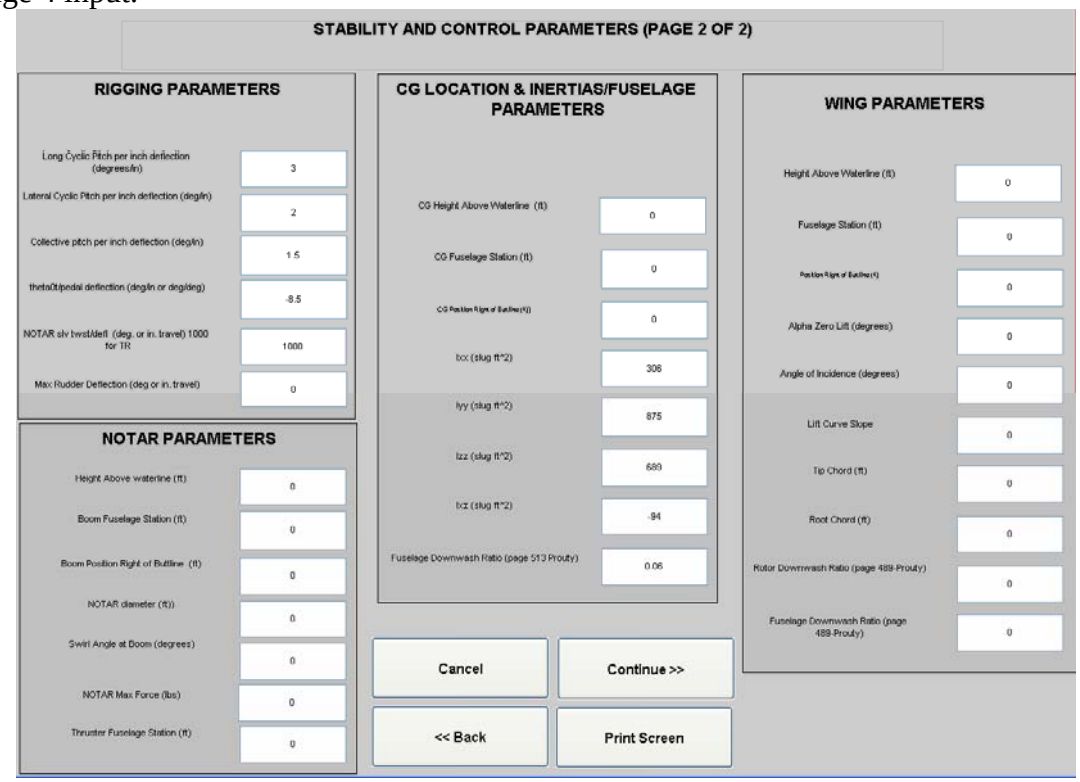

State space output.

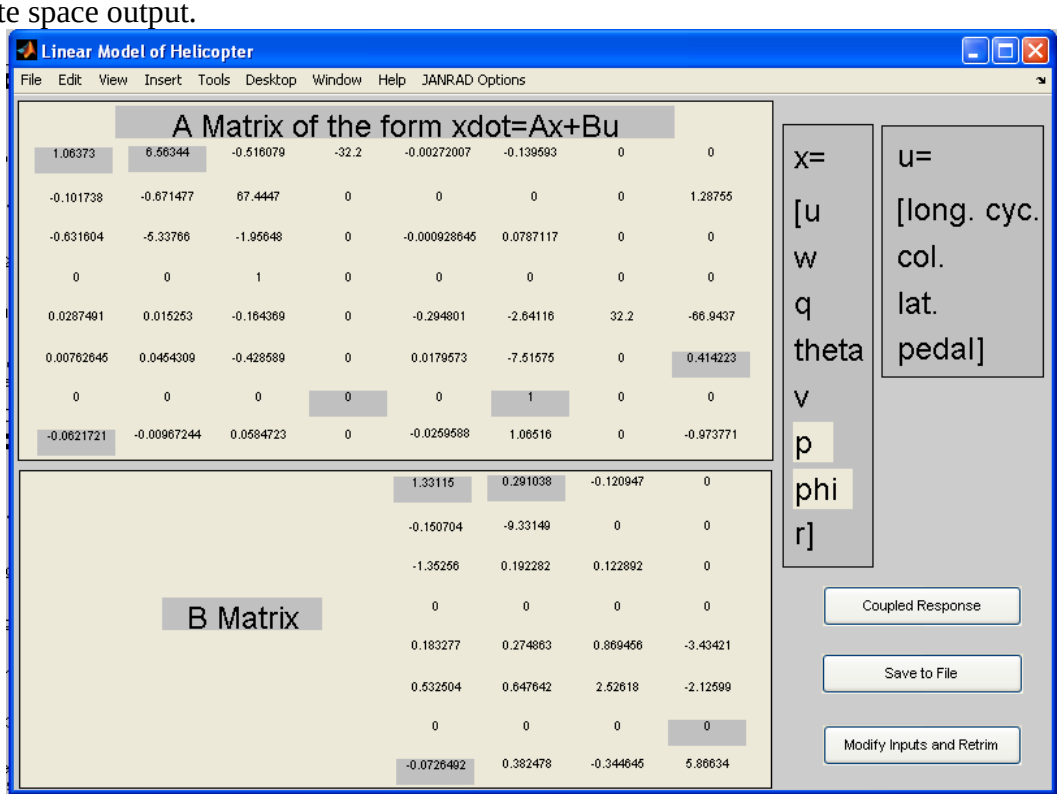

Appendix C – Simulink Diagrams of Final Controller Sub-components

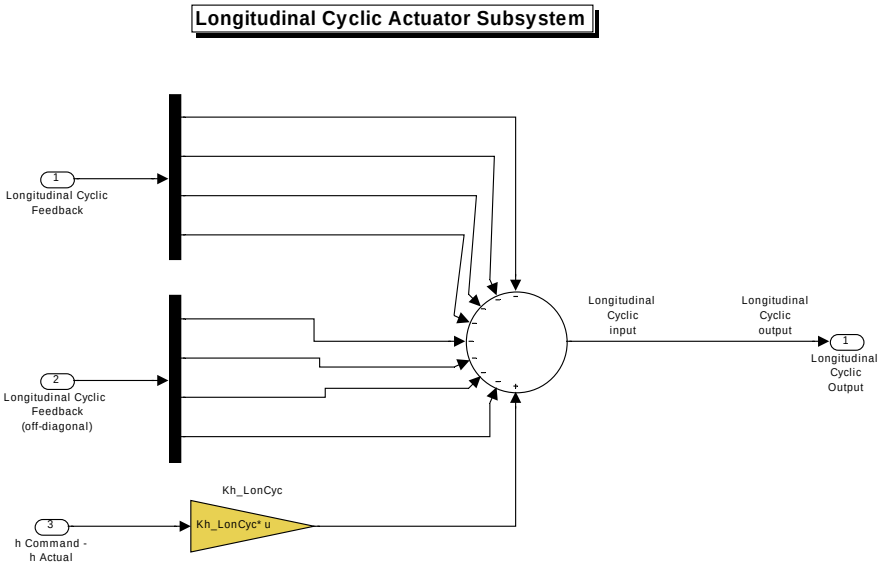

Figure 41. Longitudinal Cyclic Input Diagram.

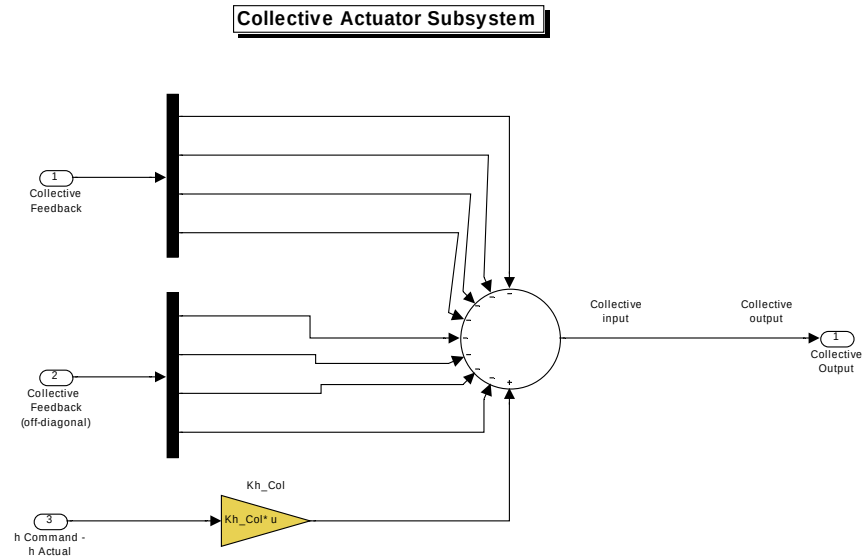

Figure 42. Collective Input Diagram.

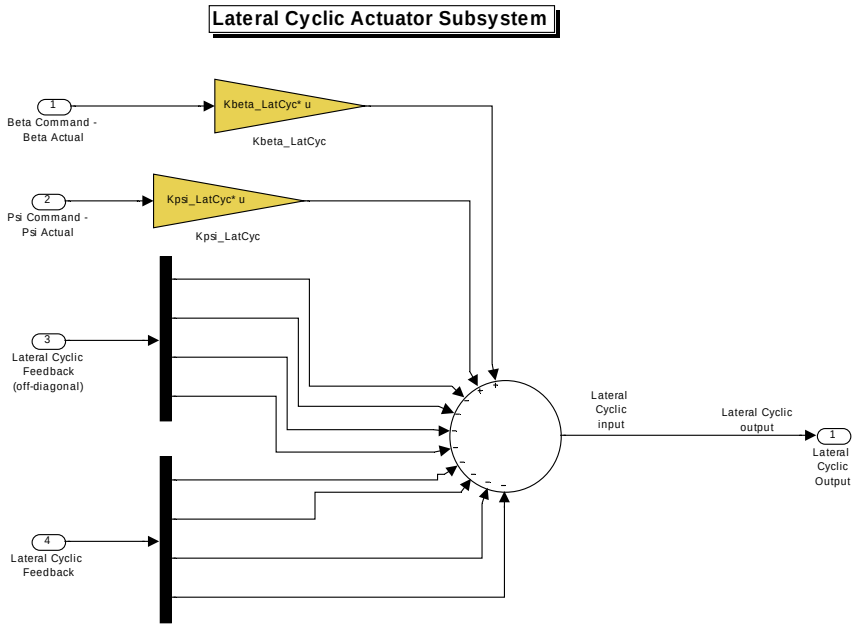

Figure 43. Lateral Cyclic Input Diagram.

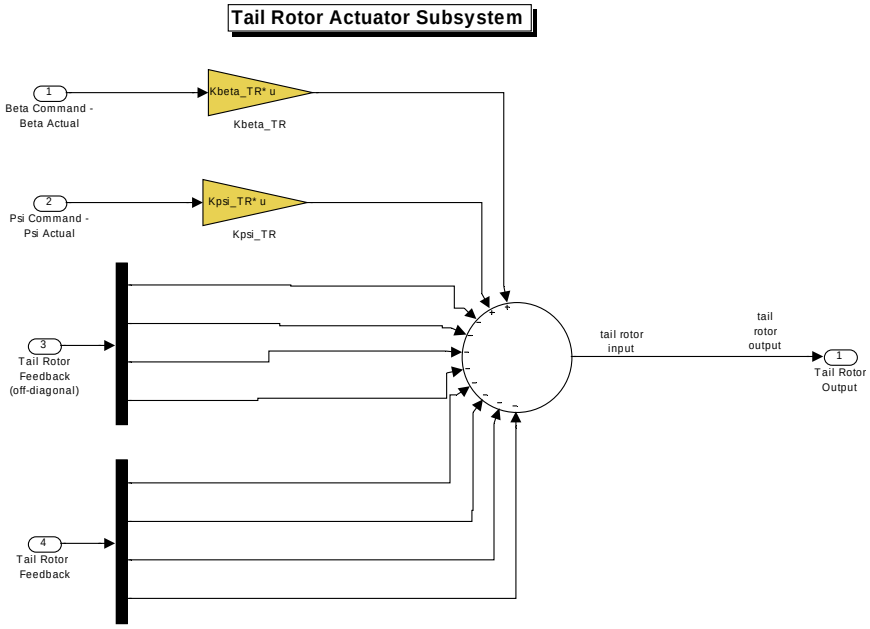

Figure 44. Tail Rotor Input Diagram.

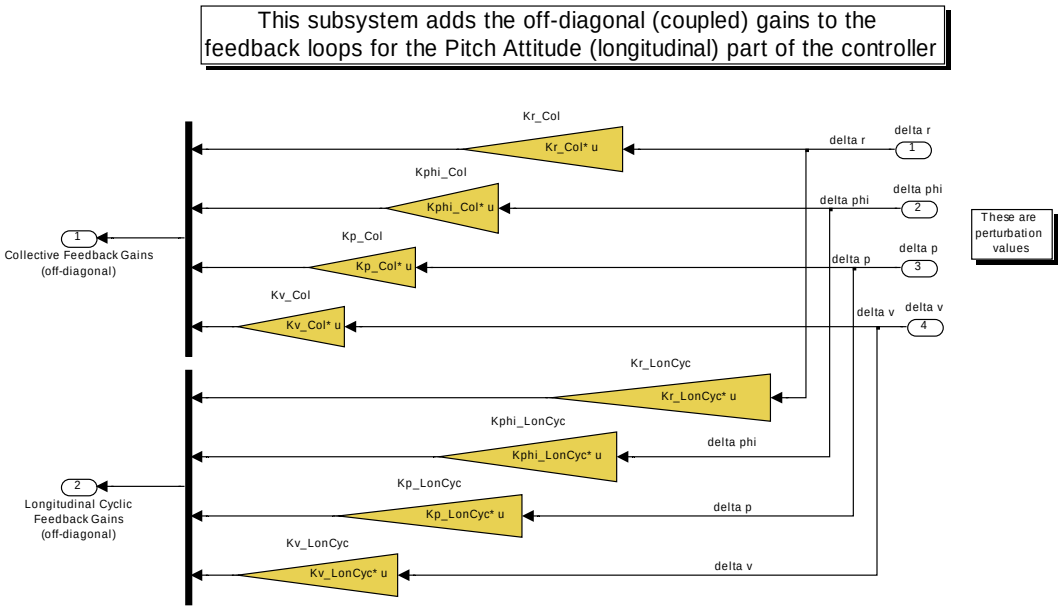

Figure 45. Coupled (Off-Diagonal) Gains to the Longitudinal Motion Controller Diagram.

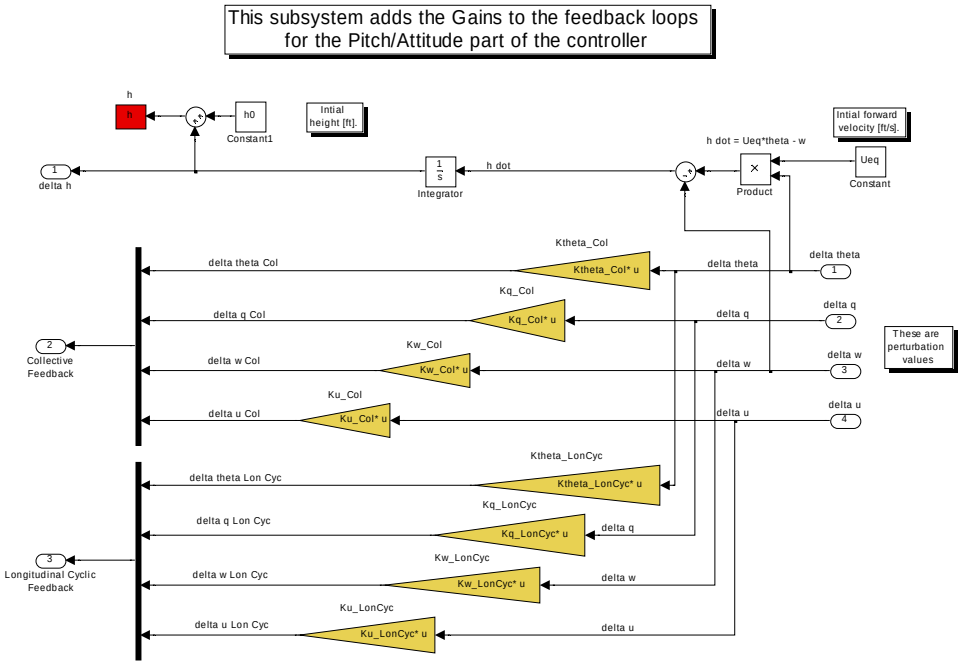

Figure 46. Longitudinal Motion Controller Gain Diagram.

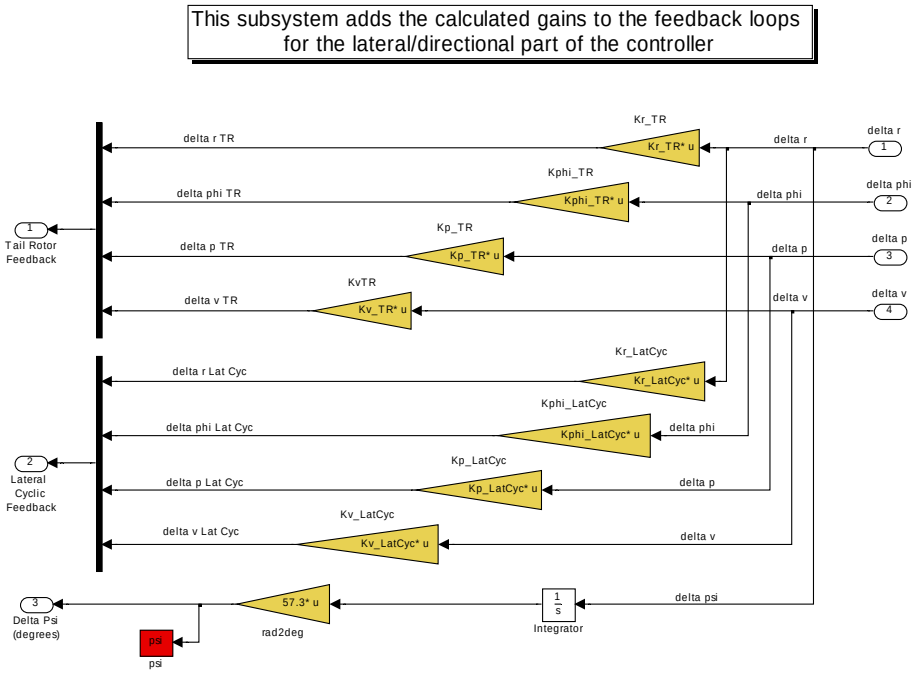

Figure 47. Lateral Motion Controller Gain Diagram.

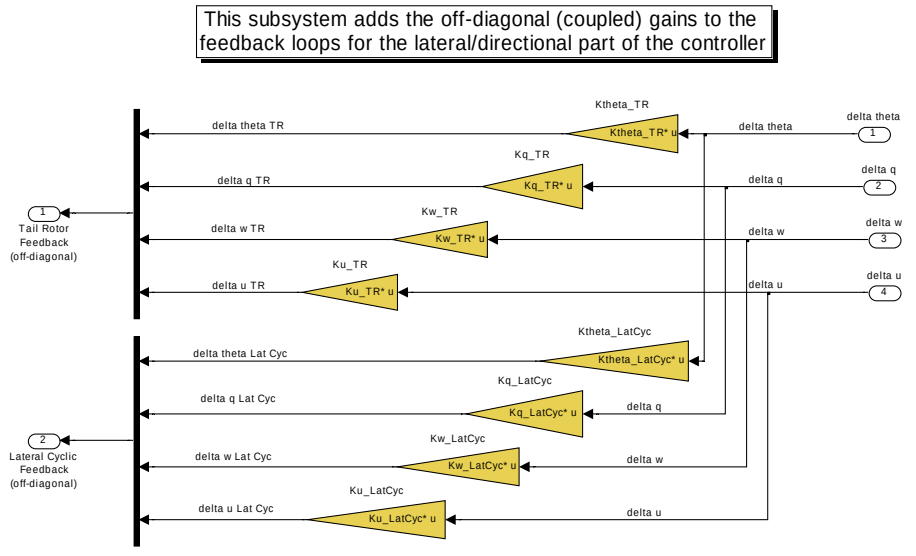

Figure 48. Coupled (Off-Diagonal) Gains to the Lateral Motion Controller Diagram.

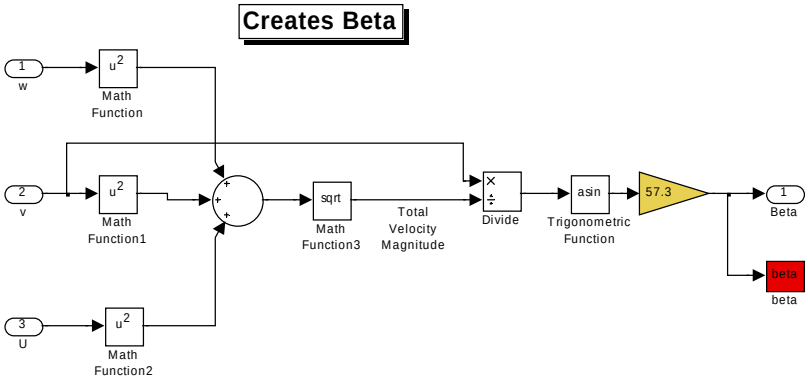

Figure 49. Beta Sub-Component Diagram.

Appendix D – Thesis10_execute.m

Thesis10_execute.m (flight controller executable file).

```
% MAJ Jon Bulseco - Thesis - Jan 2005
% thesis10_execute.m
% Helicopter heading hold/coordinated turn autopilot with altitude, heading,
% and beta feedback.  With optimized heading and beta trajectory that
% minimizes the radar cross section of an unmanned OH-6 in a threat environment

%-------------------------------------------------------------------------

z = 1; % 1 initializes, 2 runs the simulations, 3 plots the graphs

if z == 1

    clear; clc; format loose;

    %Define Variables
    g = 32.174;     % gravity [ft/s^2]
    Ueq = 67.5;     % initial forward velocity equilibrium value [ft/s].
                    % Value used by JANRAD to develop stability matrices.
    h0 = 0;         % initial height [ft]

    % COUPLED 8X8 MATRIX
    % STATES = [u w q theta v p phi r]^T  u,v,w are in [ft/s], all angles are in [rad]

% 40 Knot Model
    A_mdl = [1.06373    6.56344     -0.516079   -32.2   -0.00272007     -0.139593  0
0;
             -0.101738   -0.671477   67.4447     0       0               0           0
1.28755;
             -0.631604   -5.33766    -1.95648    0       -0.000928645    0.0787117   0
0;
             0           0           1           0       0               0           0
0;
             0.0287491   0.015253    -0.164369   0       -0.294801       -2.64116    32.2
-66.9437;
             0.00762645  0.0454309   -0.428589   0       0.0179573       -7.51575    0
0.414223;
             0           0           0           0       0               1           0
0;
             -0.0621721  -0.00967244 0.0584723   0       -0.0259588      1.06516     0
-0.973771];

    B_mdl = [1.33115    0.291038    -0.120947   0;
             -0.150704   -9.33149    0           0;
             -1.35256    0.192282    0.122892    0;
             0           0           0           0;
             0.183277    0.274863    0.869456    -3.43421;
             0.532504    0.647642    2.52618     -2.12599;
             0           0           0           0;
             -0.0726492  0.382478    -0.344645   5.86634];

    C_mdl = eye(8);

    D_mdl = zeros(8,4);

    %-------------------------------------------------------------------

    % EIGENSTRUCTURE ASSIGNMENT
    % Assign the eigenstructure for the full coupled 8X8 matrix

% Desired Closed Loop Eigenvalues
    LD = [-3.5;              % Roll Mode
          -2.9;              % Pitching Oscillation Mode
```

```
          -0.802 + 0.388j;    % Dutch Roll Mode
          -0.802 - 0.388j;
          -0.801 + 0.387j;    % Forward Speed Mode
          -0.801 - 0.387j;
          -1.0;               % Heave Mode
          -1.5];              % Yaw Mode

% Desired Closed Loop EIGENVECTORS

%                   Pitch       Dutch           Forward
%          Roll     Oscill      Roll            Speed                               Heave
Yaw
%          Mode     Mode        Mode            Mode                                Mode
Mode
    VD =  [0        0           0       0       1-1j            1+1j            0
0;      %[u]
          0        0           0       0       0               0               1
0;      %[w]
          0        1           0       0       -0.801-0.387j   -0.801+0.387j   0
0;      %[q]
          0        -0.3448     0       0       0.801+0.387j    0.801-0.387j    0
0;      %[theta]
          0        0           1+1j    1-1j    0               0               0
0;      %[v]
          1        0           0       0       0               0               0
0;      %[p]
          -.2857   0           0       0       0               0               0
0;      %[phi]
          0        0           0       0       0               0               0
1.5];   %[r]


    disp('Open Loop Eigenstructure')
    [v,d] = eig(A_mdl)

    disp('Eigenstructure Assignment Closed Loop Gains')
    K = LIEBSTPL(A_mdl,B_mdl,C_mdl,LD,VD)

    % Check 8X8 A_mdl eigenvalues with new gains calculated
    disp('Closed Loop Eigenstructure')
    [v,d] = eig(A_mdl - B_mdl * K * C_mdl)

    Ku_LonCyc = K(1,1); Kw_LonCyc = K(1,2); Kq_LonCyc = K(1,3); Ktheta_LonCyc = K(1,4);
    Ku_Col = K(2,1); Kw_Col = K(2,2); Kq_Col = K(2,3); Ktheta_Col = K(2,4);

    % Off Diagonal Longitudinal Gains
    Kv_LonCyc = K(1,5); Kp_LonCyc = K(1,6); Kphi_LonCyc = K(1,7); Kr_LonCyc = K(1,8);
    Kv_Col = K(2,5); Kp_Col = K(2,6); Kphi_Col = K(2,7); Kr_Col = K(2,8);

    % Altitude Command Gains
    % The following gaines were found through an FMINCON optimization
    % routine

    Kh_LonCyc = 0.0072;
    Kh_Col = -0.0016;

    Kv_LatCyc = K(3,5); Kp_LatCyc = K(3,6); Kphi_LatCyc = K(3,7); Kr_LatCyc = K(3,8);
    Kv_TR = K(4,5); Kp_TR = K(4,6); Kphi_TR = K(4,7); Kr_TR = K(4,8);

    % Off Diagonal Lateral Directional Gains
    Ku_LatCyc = K(3,1); Kw_LatCyc = K(3,2); Kq_LatCyc = K(3,3); Ktheta_LatCyc = K(3,4);
    Ku_TR = K(4,1); Kw_TR = K(4,2); Kq_TR = K(4,3); Ktheta_TR = K(4,4);

    % Yaw Command Gains
    % The following gaines were found through an FMINCON optimization
    % routine

    Kpsi_LatCyc = 0.5;
```

```
    Kpsi_TR = -2.6789e-004;

    % Beta Command Gains
    % The following gaines were found through an FMINCON optimization
    % routine

    Kbeta_LatCyc = 1.372;
    Kbeta_TR = -0.0782;

    %-------------------------------------------------------------------

    % Initial Conditions
    % *** THE STATE SPACE MATRIX OUTPUT FROM JANRAD ALONE OUTPUTS THE
    % PERTURBATION VALUES, NOT THE ACTUAL VALUES.  OUTPUTS MUST HAVE THE
    % INITIAL CONDITIONS ADDED TO THEM. THE INITIAL CONDITIONS FOR THE
    % STATE SPACE MATRIX MUST ALWAYS BE ZERO.  CHANGE THE VARIABLE OUTPUTS
    % TO INCLUDE THE INITIAL CONDITIONS. ***

    %    [u   w   q theta v   p   phi r]^T   u,v,w are in [ft/s], all angles are in [rad]
    x0 = [0   0   0 0     0   0   0   0];

    %-------------------------------------------------------------------

    disp('Initialization done.');

end

z = 0;

if z == 2

    % Extract the linear model system to determine Kh with a Root Locus
    [A,B,C,D] = linmod('thesis9_mdl');
    sys = ss(A,B,C,D);

    % Evaluate Closed Loop Eigenvalues
    [v,d] = eig(A)

%         figure (1), clf, rlocus(sys)
%         grid on
%         title('Root Locus of the Pitch Attitude System, Varying Kh')
%         axis([-10 1 -20 20])

end

z = 3;

if z == 3

    %-----------------------------------------------------------
    sim thesis10_mdl
    %-----------------------------------------------------------

    clf;

    figure(1)
    subplot 421, plot(tt,h)
    title('Helicopter Autopilot: Altitude vs Time')
    xlabel('Time (sec)')
    ylabel('Altitude, h (feet)')
    grid on
    %axis([0 tt(length(tt)) 0 260]);

    subplot 422, plot(tt,psi)
    title('Helicopter Autopilot: Yaw Angle, \psi vs Time')
    xlabel('Time (sec)')
    ylabel('Yaw Angle, \psi (deg)')
    grid on
```

```
    axis([0 tt(length(tt)) min(psi) max(psi)]);

    subplot 423, plot(tt,beta)
    title('Helicopter Autopilot: Sideslip Angle, \beta vs Time')
    xlabel('Time (sec)')
    ylabel('\beta, Sideslip Angle (deg)')
    grid on

    subplot 424, plot(tt,phi)
    title('Helicopter Autopilot: Roll Angle, \phi vs Time')
    xlabel('Time (sec)')
    ylabel('\phi, Roll Angle (deg)')
    grid on

    subplot 425, plot(tt,u)
    title('Helicopter Autopilot: Forward Velocity, u vs Time')
    xlabel('Time (sec)')
    ylabel('Forward Velocity, u (ft/sec)')
    grid on

    subplot 426, plot(tt,v)
    title('Helicopter Autopilot: Sideslip Velocity, v vs Time')
    xlabel('Time (sec)')
    ylabel('Sideslip Velocity, v (ft/sec)')
    grid on

%     subplot 423, plot(tt,w)
%     title('Helicopter Autopilot: Upward Velocity, w vs Time')
%     xlabel('Time (sec)')
%     ylabel('Upward Velocity, w (ft/sec)')
%     grid on

    subplot 427, plot(tt,theta)
    title('Helicopter Autopilot: Pitch Angle, \theta vs Time')
    xlabel('Time (sec)')
    ylabel('\theta, Pitch Angle (deg)')
    grid on

%     subplot 425, plot(tt,p)
%     title('Helicopter Autopilot: Roll Rate, p vs Time')
%     xlabel('Time (sec)')
%     ylabel('Roll Rate, p (deg/sec)')
%     grid on
%
%     subplot 426, plot(tt,q)
%     title('Helicopter Autopilot: Pitch Rate, q vs Time')
%     xlabel('Time (sec)')
%     ylabel('Pitch Rate, q (deg/sec)')
%     grid on

    subplot 428, plot(tt,r)
    title('Helicopter Autopilot: Yaw Rate, r vs Time')
    xlabel('Time (sec)')
    ylabel('\psi, Yaw Rate, r (deg/sec)')
    grid on

end
```

Appendix E – Thesis8_optimize_call.m

The m file utilizes the Matlab FMINCON command to optimize the altitude, heading, and sideslip angle feedback gains.

```
% thesis8_optimize_call  --  This optimization routine optimizes the following
% variables: Kh_LonCyc, Kh_Col, Kpsi_LatCyc, Kpsi_TR, Kbeta_LatCyc, Kbeta_TR
% in the thesis8_mdl
% MAJ Jon Bulseco - Thesis - Jan 05

clc; clear all

disp('MAJ Jon Bulseco - Thesis')
disp(' ')
disp('Design Optimization of the Altitude Gain for a Helicopter Heading Hold-Coordinated
Turn Controller with Altitude Feedback');
disp(' ')

%-------------------------------------------------------------------------
%-------------------------------------------------------------------------
% Linear model definition

    clear; clc; format loose;

    %Define Variables
    g = 32.174;     % gravity [ft/s^2]
    Ueq = 67.5;     % initial forward velocity equilibrium value [ft/s].
                    % Value used by JANRAD to develop stability matrices.
    h0 = 0;         % initial height [ft]

    % COUPLED 8X8 MATRIX
    % STATES = [u w q theta v p phi r]^T  u,v,w are in [ft/s], all angles are in [rad]

% 40 Knot Model
    A_mdl = [1.06373    6.56344     -0.516079   -32.2   -0.00272007     -0.139593  0
0;
             -0.101738   -0.671477   67.4447     0       0               0           0
1.28755;
             -0.631604   -5.33766    -1.95648    0       -0.000928645    0.0787117   0
0;
             0           0           1           0       0               0           0
0;
             0.0287491   0.015253    -0.164369   0       -0.294801       -2.64116    32.2
-66.9437;
             0.00762645  0.0454309   -0.428589   0       0.0179573       -7.51575    0
0.414223;
             0           0           0           0       0               1           0
0;
             -0.0621721  -0.00967244 0.0584723   0       -0.0259588      1.06516     0
-0.973771];

    B_mdl = [1.33115    0.291038    -0.120947   0;
             -0.150704   -9.33149    0           0;
             -1.35256    0.192282    0.122892    0;
             0           0           0           0;
             0.183277    0.274863    0.869456    -3.43421;
             0.532504    0.647642    2.52618     -2.12599;
             0           0           0           0;
             -0.0726492  0.382478    -0.344645   5.86634];

    C_mdl = eye(8);

    D_mdl = zeros(8,4);
```

```
    %-------------------------------------------------------------------

    % EIGENSTRUCTURE ASSIGNMENT
    % Assign the eigenstructure for the full coupled 8X8 matrix

% Desired Closed Loop Eigenvalues
    LD = [-3.5;               % Roll Mode
          -2.9;               % Pitching Oscillation Mode
          -0.802 + 0.388j;    % Dutch Roll Mode
          -0.802 - 0.388j;
          -0.801 + 0.387j;    % Forward Speed Mode
          -0.801 - 0.387j;
          -1.0;               % Heave Mode
          -1.5];              % Yaw Mode

% Desired Closed Loop EIGENVECTORS

%                   Pitch       Dutch           Forward
%          Roll     Oscill      Roll            Speed                               Heave
Yaw
%          Mode     Mode        Mode            Mode                                Mode
Mode
    VD =  [0        0           0       0       1-1j            1+1j            0
0;      %[u]
          0        0           0       0       0               0               1
0;      %[w]
          0        1           0       0       -0.801-0.387j   -0.801+0.387j   0
0;      %[q]
          0        -0.3448     0       0       0.801+0.387j    0.801-0.387j    0
0;      %[theta]
          0        0           1+1j    1-1j    0               0               0
0;      %[v]
          1        0           0       0       0               0               0
0;      %[p]
          -.2857   0           0       0       0               0               0
0;      %[phi]
          0        0           0       0       0               0               0
1.5];   %[r]


    disp('Eigenstructure Assignment Closed Loop Gains')
    K = LIEBSTPL(A_mdl,B_mdl,C_mdl,LD,VD);

    % Check 8X8 A_mdl eigenvalues with new gains calculated
    disp('Closed Loop Eigenstructure')
    [v,d] = eig(A_mdl - B_mdl * K * C_mdl);

    Ku_LonCyc = K(1,1); Kw_LonCyc = K(1,2); Kq_LonCyc = K(1,3); Ktheta_LonCyc = K(1,4);
    Ku_Col = K(2,1); Kw_Col = K(2,2); Kq_Col = K(2,3); Ktheta_Col = K(2,4);

    % Off Diagonal Longitudinal Gains
    Kv_LonCyc = K(1,5); Kp_LonCyc = K(1,6); Kphi_LonCyc = K(1,7); Kr_LonCyc = K(1,8);
    Kv_Col = K(2,5); Kp_Col = K(2,6); Kphi_Col = K(2,7); Kr_Col = K(2,8);

    Kv_LatCyc = K(3,5); Kp_LatCyc = K(3,6); Kphi_LatCyc = K(3,7); Kr_LatCyc = K(3,8);
    Kv_TR = K(4,5); Kp_TR = K(4,6); Kphi_TR = K(4,7); Kr_TR = K(4,8);

    % Off Diagonal Lateral Directional Gains
    Ku_LatCyc = K(3,1); Kw_LatCyc = K(3,2); Kq_LatCyc = K(3,3); Ktheta_LatCyc = K(3,4);
    Ku_TR = K(4,1); Kw_TR = K(4,2); Kq_TR = K(4,3); Ktheta_TR = K(4,4);

    %-------------------------------------------------------------------
    % Initial Conditions
    % *** THE STATE SPACE MATRIX OUTPUT FROM JANRAD ALONE OUTPUTS THE
    % PERTURBATION VALUES, NOT THE ACTUAL VALUES.  OUTPUTS MUST HAVE THE
    % INITIAL CONDITIONS ADDED TO THEM. THE INITIAL CONDITIONS FOR THE
    % STATE SPACE MATRIX MUST ALWAYS BE ZERO.  CHANGE THE VARIABLE OUTPUTS
    % TO INCLUDE THE INITIAL CONDITIONS. ***
```

```
    %    [u   w   q theta v   p   phi r]^T   u,v,w are in [ft/s], all angles are in [rad]
    x0 = [0   0   0 0     0   0   0   0];

    %-----------------------------------------------------------------
    disp('Initialization done.');
%-----------------------------------------------------------------

% GLOBAL variable definitions
% global psi_command
global g

% other variable definitions
h_command = 250;    % 250 ft altitude command
psi_command = -20;   % degree heading command
beta_command = 20;   % degree sideslip command

g = 32.174;         % gravity [ft/s^2]

%-------------------------------------------------------------------------
% SET INITIAL GUESSES FOR DESIGN VARIABLES

% Altitude command gains
%   Kh_LonCyc = -0.01;
%   Kh_Col = -0.005;

%    Kh_LonCyc = -0.0352;
%    Kh_Col = -0.024;

    Kh_LonCyc = 0.0072;
    Kh_Col = -0.0016;

% Yaw Command Gains
    % The following gaines were found through an optimization routine that
    % utilized FMINCON to optimize 2 cost variables: overshoot and final tracking

%   Kpsi_LatCyc = 0;
%   Kpsi_TR = 0;

%    Kpsi_LatCyc = 0.15;
%    Kpsi_TR = -0.0009;

    Kpsi_LatCyc = 0.5;
    Kpsi_TR = -2.6789e-004;


% Beta Command Gains
    % The following gaines were found through an optimization routine that
    % utilized FMINCON to optimize 2 cost variables: overshoot and final tracking

%   Kbeta_LatCyc = 0;
%   Kbeta_TR = 0;

%    Kbeta_LatCyc = 0.18;
%    Kbeta_TR = -0.04;

    Kbeta_LatCyc = 1.372;
    Kbeta_TR = -0.0782;

% Put ICs in a vector
init = [Kh_LonCyc, Kh_Col, Kpsi_LatCyc, Kpsi_TR,...
    Kbeta_LatCyc, Kbeta_TR];

% define linear inequality constraints
Aineq=[];
Bineq=[];

% define linear equality constraints
```

```
 % don't have any for this problem, so set to empty
Aeq=[];
Beq=[];

% define lower bounds for Design Variables
 % Note: these constraints could be treated as linear constraints (defined
 % above) or defined in a constraint function (see below), but
 % algorithm treats them more efficiently when specified as limits on DVs

Kh_LonCyc_min = [-0.5];%1e-12];
Kh_Col_min = [-0.5];%1e-12];
Kpsi_LatCyc_min = [-0.5];
Kpsi_TR_min = [-0.5];
Kbeta_LatCyc_min = [-0.5];
Kbeta_TR_min = [-0.5];

DVs_min = [Kh_LonCyc_min, Kh_Col_min, Kpsi_LatCyc_min, Kpsi_TR_min,...
    Kbeta_LatCyc_min, Kbeta_TR_min];

% define upper bounds for Design Variables

Kh_LonCyc_max = [0.5]; %-1e-12];
Kh_Col_max = [0.5];
Kpsi_LatCyc_max = [1.5];
Kpsi_TR_max = [0.5];
Kbeta_LatCyc_max = [1.5];
Kbeta_TR_max = [0.5];

DVs_max = [Kh_LonCyc_max, Kh_Col_max, Kpsi_LatCyc_max, Kpsi_TR_max,...
    Kbeta_LatCyc_max, Kbeta_TR_max];

% define nonlinear constraints (equality and inequality)
  % NOTE: these are (must be) defined in a function, define the function
  % name here (set to empty if no nonlinear constraints)
% nlc_filename='filename';
nlc_filename=[];

% set optimization algorithm options
% SEE ">>help optimset" in Matlab for more info
% options to be used by the optimization algorithm

options = optimset('LargeScale','off','Display','iter','MaxFunEvals',1000,...
    'TolX',.0001,'TolFun',.0001);

% define objective function
  % NOTE: the objective function is (must be) defined in a function, define
  % the function name here
objfun_filename='thesis8_cost';

thesis8_mdl  %call the simulink model

[DVs,Cost_optimal,exitflag,Algorithm_data]=fmincon(objfun_filename, init, Aineq,
Bineq,...
    Aeq, Beq, DVs_min, DVs_max, nlc_filename, options, ...
    h_command, psi_command, beta_command);

% Display Results of optimization

Kh_LonCyc = DVs(1)
Kh_Col = DVs(2)
Kpsi_LatCyc = DVs(3)
Kpsi_TR = DVs(4)
Kbeta_LatCyc = DVs(5)
Kbeta_TR = DVs(6)

Cost_optimal
exitflag
Algorithm_data
```

Appendix F – Thesis8_cost.m

This m file is the cost function that is minimized in the thesis8_optimize_call.m file.

```
function cost = thesis8_cost(DVs, h_command, psi_command, beta_command)

% MAJ Jon Bulseco - Thesis - Jan 05
% Track the output of thesis8_mdl (a linear based heading hold - coordinated
% turn autopilot with altitude feedback) to a commanded altitude command
% and psi command.

% GLOBAL variable definitions
global g

% "extract" DVs so can see what we're working with

Kh_LonCyc = DVs(1);
Kh_Col = DVs(2);
Kpsi_LatCyc = DVs(3);
Kpsi_TR = DVs(4);
Kbeta_LatCyc = DVs(5);
Kbeta_TR = DVs(6);

options = simset('solver','ode45','SrcWorkspace','Current');

[tout,xout,yout] = sim('thesis8_mdl',[0 30], options);

n = length(yout(:,1));

i = find(tout > 20);    % indices of the last 10 seconds of the tout vector
% Cost associated with the SLOPE of the last 10 seconds of the psi output

j = find(tout > 10);    % indices of the last 20 seconds of the tout vector

%yout
%return

% ALTITUDE HOLD
% Max difference from command penalty
cost1 = abs(max(yout(:,1) - h_command));
W1 = 2;     % weight assigned to this performance metric
%5

% Final Track Penalty
cost2 = abs(yout(n,1) - h_command);
W2 = 1;     % weight assigned to this performance metric
%5
%-------------------------------------------------------

% PSI COMMAND
% Max difference from command
cost3 = max(abs(yout(:,2)) - psi_command);
W3 = 2;    % weight assigned to this performance metric
%50

% Final Track Penalty
cost4 = abs(yout(n,2) - psi_command);
W4 = 3;    % weight assigned to this performance metric
%20

% Slope/non-convergence penalty
cost5 = max(abs(yout(i,2)./tout(i)));
W5 = 2.5;
%20
%-------------------------------------------------------
```

```
% BETA COMMAND
% Max difference from command
cost6 = max(abs(yout(:,3) - beta_command));
W6 = 2;     % weight assigned to this performance metric
%30

% Final Track Penalty
cost7 = abs(yout(n,3) - beta_command);
W7 = 5;    % weight assigned to this performance metric
%20

% Slope/non-convergence penalty
cost8 = max(abs(yout(i,3)./tout(i)));
W8 = 3;
%10
%-------------------------------------------------------

% Total Cost Function: FMINCON tries to minimize this penalty function.
% The higher the weighting on each part of the cost function , the more
% the optimization routine tries to reduce that cost.

cost = W1*cost1 + W2*cost2 + W3*cost3 + W4*cost4 + W5*cost5 +...
    W6*cost6 + W7*cost7 + W8*cost8;

Kh_LonCyc = DVs(1)
Kh_Col = DVs(2)
Kpsi_LatCyc = DVs(3)
Kpsi_TR = DVs(4)
Kbeta_LatCyc = DVs(5)
Kbeta_TR = DVs(6)
```

Appendix G – Liebstpl.m

This m file performs the eigenstructure assignment procedure and shapes the aircraft eigenstructure into desired response modes.

```
function k=liebstpl(a,b,c,ld,vd)
%
% LIEBSTPL K = liebstpl(A,B,C,LD,VD) computes the feedback gain matrix K such that
%the eigenvalues of A-B*K*C are those specified in LD.  The desired
%Corresponding eigenvectors are given in VD one vector per column.  For both LD
%and VD any complex eigenvalues/eigenvectors must appear in consecutive pairs.  If there
%is only one control input then only eigenvalues can be placed and the user need not
%input VD. If fullstate feedback is desired then input the identity matrix for C.  The
%rules for eigenplacement in this routine are:
%If n = # of states   m = # of control inputs  r = # of measurement outputs
%then
%1)  # of poles that must be placed = length(LD) = r
%2)  portions of eigenvectors can be placed if m > 1

[l,n]=size(c);
[n,m]=size(b);
j=sqrt(-1);
if (nargin==4)
vd=[];
for i=1:l
vd=[vd ld(i)*ones(n,1)];
end
end
v=[];
w=[];
for i=1:l
lam=ld(i);
la=lam*eye(n)-a;

% Bulseco - Jan 05
% Define P weighting matrix
P = [10     0       0       0       0       0       0       0;      %[u]
     0      8       0       0       0       0       0       0;      %[w]
     0      0       5       0       0       0       0       0;      %[q]
     0      0       0       1       0       0       0       0;      %[theta]
     0      0       0       0       1       0       0       0;      %[v]
     0      0       0       0       0       1       0       0;      %[p]
     0      0       0       0       0       0       1       0;      %[phi]
     0      0       0       0       0       0       0       1];     %[r]

% P = eye(n);

ni=[la -b zeros(n,n);zeros(m,n+m) b';P zeros(n,m) la'];
zi=ni\[zeros(n+m,1);P*vd(:,i)];
v=[v real(zi(1:n,1))];
w=[w real(zi(n+1:n+m,1))];
if(imag(lam)~=0)
v=[v imag(zi(1:n,1))];
w=[w imag(zi(n+1:n+m,1))];
i=i+1;
end
end
k=-w/(c*v);
```

Bibliography

1. Office of the Under Secretary of Defense for Acquisition, Technology, and Logistics. *Defense Science Board Study on Unmanned Aerial Vehicles and Uninhabited Combat Aerial Vehicles.* Washignton: HQ DOD, February 2004.

2. Office of the Secretary of Defense. *Unmanned Aerial Vehicles Roadmap 2002 – 2027.* Washington: HQ DOD, December 2002.

3. Skolnik, Merrill. *Radar Handbook*. New York: McGraw-Hill, Inc., 1990.

4. Ball, Robert F. *The Fundamentals of Aircraft Combat Survivability Analysis and Design*. Blacksburg, VA: AIAA Education Series, 2003.

5. Pendleton, Ryan R. *Use of Unusual Aircraft Orientations to Generate Low Observable Routes*. MS Thesis, AFIT/GAE/ENY/00M-09. Graduate School of Engineering and Management, Air Force Institute of Technology (AU), Wright-Patterson AFB OH, March 2000.

6. McFarland, Michael B., Randy A. Zachery, and Brian K. Taylor. "Motion Planning for Reduced Observability of Autonomous Aerial Vehicles", *Proceedings of the 1999 IEEE International Conference on Control Applications*. 231-235. New York, IEEE Press, 1999.

7. Novy, Michael C. *Air Vehicle Optimal Trajectories for Minimization of Radar Exposure*. MS Thesis, AFIT/GAE/ENY/01M-07. Graduate School of Engineering and Management, Air Force Institute of Technology (AU), Wright-Patterson AFB OH, March 2001.

8. Pachter, Meir and others. "Minimizing Radar Exposure in Air Vehicle Path Planning." *Proceedings of the 41st Israel Annual Conference on Aerospace Sciences*. Feb 2001.

9. Hebert, Jeffrey M. *Air Vehicle Path Planning*. Air Force Institute of Technology (AU), Wright-Patterson AFB OH, November 2001.

10. Misovec, K and others. "Low-Observable Nonlinear Trajectory Generation for Unmanned Air Vehicles," *Proceedings of the IEEE Conference on Decision and Control*, v 3. 3103-3110. New York: IEEE Press, 2003.

11. "OH-6A/HO-6 Cayuse light observation helicopter fact sheet." Redstone Arsenal AL. 27 January 2005 http://www.redstone.army.mil/history/aviation/factsheets/oh6.html.

12. "Rotorcraft Flight Manual for MDHI 500 (369HE/HS/HM) Helicopters." MD Helicopters Inc., Mesa AZ, 13 July 1998.

13. Ouellette, Gregory A. *Modeling the OH-6A Using Flightlab and Helicopter Simulator Considerations*. MS Thesis, Naval Post Graduate School, Monterey CA, March 2002.

14. Harris, John H. *Preliminary Vibration Survey of a Suspended Full Scale OH-6A Helicopter from 0 to 45 HZ*. MS Thesis, Naval Post Graduate School, Monterey CA, March 1996.

15. O'Malley, James A. U.S. Army RDECOM, Redstone Arsenal, AL. Personal Interview with Dr. Don Kunz, Air Force Institute of Technology, Department of Aeronautics and Astronautics, Dec 2004.

16. Prouty, Raymond W. *Helicopter Performance, Stability and Control*. Malabar, FL: Krieger Publishing, 2002.

17. Pampalone, Michael R. *Development, Correlation, and Updating of a Finite Element Model of the OH-6A Helicopter*. MS Thesis, Naval Post Graduate School, Monterey CA, December 1996.

18. "Structural Repair Manual, 500 Series Basic Handbook of Maintenance Instruction Appendix D." MD Helicopters Inc., Mesa AZ, 30 September 1992.

19. Padfield, Gareth D. *Helicopter Flight Dynamics: The Theory and Application of Flying Qualities and Simulation Modeling*. Washington DC: AIAA Education Series, 1996.

20. Nicholson, R.K. Jr. *Computer Code for Interactive Rotorcraft Preliminary Design Using Harmonic Balance Method for Rotor Trim*. MS Thesis, Naval Post Graduate School, Monterey CA, 1993.

21. Wirth, W. M. *Linear Modeling of Rotorcraft for Stability Analysis and Preliminary Design*. MS Thesis, Naval Post Graduate School, Monterey CA, 1993.

22. Eccles, D. M. *A Validation of the Joint Army/Navy Rotorcraft Analysis and Design Software by Comparison with H-34 and UH-60A Flight Test*. MS Thesis, Naval Post Graduate School, Monterey CA, December 1995.

23. Heathorn, David A. *Stability and Control Module for Joint Army/Navy Rotorcraft Analysis and Design (JANRAD) Software and Graphical User Interface (GUI)*. MS Thesis, Naval Post Graduate School, Monterey CA, March 1999.

24. Cooke, Alastair K. and Eric W.H. Fitzpatrick. *Helicopter Test and Evaluation*. Reston VA: AIAA Education Series, 2002.

25. Liebst, Bradley S. and William L. Garrard. "Application of Eigenspace Techniques to Design of Aircraft Control Systems," *Proceedings of the American Control Conference*. 475-480. Boston: IEEE Press, 1985.

26. Andry, A.N. and others. "On Eigenstructure Assignment for Linear Systems," *IEEE Trans. Aerospace and Electronic Systems*. IEEE Press, Sep 1983.

27. Garrard, William L. and Bradley S. Liebst. "Design of a Multivariable Helicopter Flight Control System for Handling Qualities Enhancement," *Journal of the American Helicopter Society*, v 35, n 4. 23-30. Oct 1990.

28. Walker, D.J. "Multivariable Control of the Longitudinal and Lateral Dynamics of a fly-by-wire helicopter," *Control Engineering Practice*, v11. 781-795. 2003.

29. Ciurpita, Greg. "Planform Analysis Version 1.8." 30 January 2005 http://ciurpita.tripod.com/rc/wing/air_db/wing.html.

Vita

Major Jonathan D. Bulseco was born in Honolulu, HI and graduated from South High School, Salt Lake City, Utah in 1987. He then entered the United States Military Academy at West Point, NY. After two years at West Point, Major Bulseco left the academy to serve a two year mission on behalf of his church in Salta, Argentina. He then returned to the academy and graduated with a Bachelor of Science Degree in Mechanical Engineering and was commissioned a Second Lieutenant in 1994.

After graduation, Major Bulseco attended rotary wing flight training at Fort Rucker, Alabama and received his wings in the summer of 1995. His first assignment was as a platoon leader with the Joint Readiness Training Center's Flight Detachment flying the OH-58C. His follow on assignments included being the S3-Air with the Second Armored Cavalry Regiment and Platoon Leader with the 4/2 Aviation Squadron during their deployment to Bosnia-Herzegovina flying the OH-58D Kiowa Warrior.

Upon returning from Bosnia, Major Bulseco attended the Aviation Officer's Advanced Course and Combined Arms Services Staff School. He was then assigned to the 25th Infantry Division, Schofield Barracks, Hawaii were he served as the Aviation Brigade's Battle Captain, and Personnel Officer (S1) for the 3-4 Cavalry Regiment. He then commanded B Troop, 3-4 Cavalry Regiment, with a follow-on command assignment at the Savannah Army Recruiting Company, Savannah, Georgia.

Major Bulseco was selected for the United States Naval Test Pilot School (USNTPS) in 2002 with a graduate degree enroute at the Air Force Institute of Technology (AFIT). He began classes at AFIT in September 2003, will graduate in March 2005, and will attend USNTPS in August 2005.

REPORT DOCUMENTATION PAGE

Form Approved
OMB No. 074-0188

1. REPORT DATE *(DD-MM-YYYY)*	**2. REPORT TYPE**	**3. DATES COVERED** *(From – To)*
21-03-2005	Master's Thesis	Aug 2003 – Mar 2005

4. TITLE AND SUBTITLE

Controlling Sideslip Angle to Reduce the Radar Exposure of a Tactical, Rotary Winged UAV

5a. CONTRACT NUMBER

5b. GRANT NUMBER

5c. PROGRAM ELEMENT NUMBER

6. AUTHOR(S)

Bulseco, Jonathan D., Major, USA

5d. PROJECT NUMBER

5e. TASK NUMBER

5f. WORK UNIT NUMBER

7. PERFORMING ORGANIZATION NAMES(S) AND ADDRESS(S)
Air Force Institute of Technology
Graduate School of Engineering and Management (AFIT/EN)
2950 Hobson Way, Building 640
WPAFB OH 45433-8865

8. PERFORMING ORGANIZATION REPORT NUMBER

AFIT/GAE/ENY/05-M26

9. SPONSORING/MONITORING AGENCY NAME(S) AND ADDRESS(ES)
Dr. Bill Lewis
AMSRD-AMR-AE
Bldg 4488, Rm C-100
Redstone Arsenal, AL 35898-5000
DSN: 897-2350, ext. 9806

10. SPONSOR/MONITOR'S ACRONYM(S)

11. SPONSOR/MONITOR'S REPORT NUMBER(S)

12. DISTRIBUTION/AVAILABILITY STATEMENT

APPROVED FOR PUBLIC RELEASE; DISTRIBUTION UNLIMITED.

13. SUPPLEMENTARY NOTES

14. ABSTRACT
This work investigates another way of contributing to the radar minimization solution for air vehicles in a threat environment. While much research has been conducted on structural solutions to radar exposure minimization, not much work has been done in the area of using control to continuously assess and present the smallest radar cross section of an air vehicle to oncoming threat radar systems by changing the aircraft's orientation. This work looks at the application of sideslip/beta angle feedback control of an unmanned helicopter to minimize radar cross section exposure in a hostile radar environment. A new way of controlling aircraft trajectory is introduced that incorporates both path and orientation optimization feedback; the aircraft's heading is controlled to orient the vehicle in a way that reduces its radar cross section, while sideslip angle is used to control the aircraft's path. A representative hostile environment is created and results show that a substantial reduction in radar cross section exposure can be achieved with beta feedback control. A linear state space model is derived for the OH-6A helicopter with the JANRAD software program. Eigenstructure assignment is used to shape the response of the helicopter into desired response modes. A Matlab based flight control system is developed around the derived helicopter model with altitude, heading, and beta angle command signals that drive four conventional helicopter control inputs.

15. SUBJECT TERMS
Helicopter; Helicopter Stability; Helicopter Flight Control; Helicopter Model; Radar Exposure Minimization; Sideslip Angle; Eigenstructure Assignment; Yaw Control; Path Following; Radar Cross Section (RCS) Reduction; Aircraft Survivability; Flight Control; OH-6A

16. SECURITY CLASSIFICATION OF:			**17. LIMITATION OF ABSTRACT**	**18. NUMBER OF PAGES**	**19a. NAME OF RESPONSIBLE PERSON**
a. REPORT	**b. ABSTRACT**	**c. THIS PAGE**			Dr. Richard G. Cobb, AFIT/ENY
U	**U**	**U**	**UU**	117	**19b. TELEPHONE NUMBER** *(Include area code)* (937) 255-3636, ext 4559 Richard.Cobb@afit.edu

Standard Form 298 (Rev. 8-98)
Prescribed by ANSI Std. Z39-18